

Deliverable 6.2

Performance validation - Results from EV measurements

Prepared by:

Bart Benders, fka

benders@fka.de

Kim Winther, DTI

kwi@dti.dk

Morten Holst, DTI

mhj@dti.dk

Christian Kolf, TÜV NORD Mobilität

ckolf@tuev-nord.de

Date: December 16th, 2014

Version: 1.5

Document Information

Authors

| | Name | Company |
|-----------------|----------------|--------------------|
| Key author | Bart Benders | fka |
| Further authors | Kim Winther | DTI |
| | Morten Holst | DTI |
| | Christian Kolf | TÜV NORD Mobilität |

Distribution

| Dissemination level | | |
|---------------------|---|---|
| PU | Public | x |
| PP | Restricted to other programme participants (including the Commission Services) | |
| RE | Restricted to a group specified by the consortium (including the Commission Services) | |
| CO | Confidential, only for members of the consortium (including the Commission Services) | |

Revision history

| Version | Date | Author | Description |
|---------|----------------------------------|----------------|--------------------------|
| 1.0 | Mai 27 th , 2013 | Bart Benders | Template |
| 1.1 | June 3 rd , 2013 | Morten Holst | First complete draft |
| 1.2 | July 28 th , 2014 | Christian Kolf | Dynamometer measurements |
| 1.3 | November 3 rd , 2014 | Bart Benders | Final Version |
| 1.4 | December 12 th , 2014 | Luis de Prada | Internal review |
| 1.5 | December 16 th , 2014 | Kim Winther | Submission for approval |

Status

| Status | |
|--|---|
| For Information | |
| Draft Version | |
| Final Version (Internal document) | |
| Submission for Approval (deliverable) | x |
| Final Version (deliverable, approved on) | |

Table of Contents

| | | |
|-------|---|----|
| 1 | Executive Summary..... | 13 |
| 2 | Introduction..... | 14 |
| 2.1 | Work package 6 goals and background..... | 14 |
| 2.2 | Alignment between partners | 15 |
| 3 | Performance validation of electric vehicles | 17 |
| 3.1 | State of the art of electric vehicles | 17 |
| 3.1.1 | Main components | 23 |
| 3.1.2 | Layout..... | 26 |
| 3.1.3 | Safety Aspects..... | 29 |
| 3.2 | Hypothesis and their analysis | 37 |
| 3.3 | On road performance validation..... | 38 |
| 3.4 | Climate impact, dynamometer measurements..... | 39 |
| 4 | Analysis of hypothesis, on road performance validation | 40 |
| 4.1 | Test track conditions..... | 40 |
| 4.2 | Vehicles used in the on-road tests..... | 45 |
| 4.3 | Theory in short..... | 46 |
| 4.4 | Hypothesis 1: Range and consumption are mainly dependent on drive pattern..... | 48 |
| 4.4.1 | Steady speed..... | 49 |
| 4.4.2 | Dynamic driving | 51 |
| 4.4.3 | Full acceleration | 54 |
| 4.4.4 | Combinations of dynamic and steady driving..... | 56 |
| 4.4.5 | Aggressive driving | 59 |
| 4.4.6 | Drive train comparison - ICE vs. EV | 62 |
| 4.5 | Hypothesis 2: Range and consumption depend strongly on the use of auxiliaries | 65 |
| 4.6 | Hypothesis 3: SOH is predictable by step response testing..... | 70 |
| 4.7 | Hypothesis 4: Climate has significant impact on battery performance | 71 |
| 4.7.1 | Charging losses..... | 72 |
| 4.8 | Hypothesis 5: Battery performance is almost unaffected by battery charge rate..... | 74 |

| | | |
|----------|---|-----|
| 4.9 | Hypothesis 6: Heating and defrosting capacity is adequate | 76 |
| 4.10 | Hypothesis 7: Regenerative braking adds significantly to vehicle range | 78 |
| 4.11 | Hypothesis 8: Safety functions are maintained in the event of empty battery | 84 |
| 4.12 | Hypothesis 9: Optimum regenerative braking relies on battery and motor parameters | 86 |
| 4.13 | Hypothesis 10: Vehicle performance is almost unaffected by battery SOH..... | 87 |
| 4.13.1 | Vehicle performance compared to conventional ICE vehicles | 91 |
| 4.14 | Hypothesis 11: Propulsion energy is largely unaffected by climate conditions..... | 93 |
| 4.14.1 | The impact of temperature..... | 94 |
| 4.14.2 | The impact of wind | 96 |
| 4.14.3 | The impact of rain..... | 98 |
| 4.14.3.1 | Smoothing the surface | 99 |
| 4.14.3.2 | Increase in air mass due to the presence of rain drops | 100 |
| 4.14.3.3 | Increased cooling of tires | 101 |
| 4.14.3.4 | Auxiliary energy needed to work the wind shield wipers. | 101 |
| 4.14.3.5 | Energy required for water expulsion on surface..... | 102 |
| 4.14.4 | The impact of slope | 103 |
| 4.14.5 | The impact of weight | 104 |
| 5 | Validation and analysis of climatic impact..... | 108 |
| 5.1 | Analysis of influence of temperature and aging on charging efficiency and battery capacity..... | 108 |
| 5.1.1 | Charging behaviour | 108 |
| 5.1.2 | Influence of temperature..... | 110 |
| 5.1.3 | Influence of aging | 113 |
| 5.2 | Analysis of influence of temperature and auxiliary loads on vehicle performance..... | 114 |
| 5.3 | Validation of driving cycles | 117 |
| 5.4 | Validation of CAN data | 119 |
| 5.5 | Validation of SORDS measurements..... | 123 |
| 6 | Technical conclusions..... | 124 |
| 7 | Overall conclusions | 127 |

List of Figures

| | |
|--|----|
| Figure 3.1.1: Renault Twizy ZE..... | 17 |
| Figure 3.1.2: Daimler Smart Fortwo ED | 17 |
| Figure 3.1.3: Mitsubishi i-MiEV | 18 |
| Figure 3.1.4: Renault Fluence ZE | 18 |
| Figure 3.1.5: Nissan Leaf..... | 19 |
| Figure 3.1.6: BMW i3 | 19 |
| Figure 3.1.7: Opel Ampera..... | 20 |
| Figure 3.1.8: Tesla Model S..... | 20 |
| Figure 3.1.9: Example of a topological view of an EV's main components..... | 23 |
| Figure 3.1.10: EV powertrain topologies | 25 |
| Figure 3.1.11: Topological view of a Mitsubishi i-MiEV | 26 |
| Figure 3.1.12: Photographical component view of a Mitsubishi i-MiEV | 27 |
| Figure 3.1.13: Topological view of a Nissan Leaf..... | 28 |
| Figure 3.1.14: Photographical component view of a Nissan Leaf..... | 28 |
| Figure 3.1.15: Topological view of an EV's deformation volume and HV battery pack positioning..... | 30 |
| Figure 3.1.16: Rescue sheet from a Nissan Leaf | 32 |
| Figure 3.1.17: Service plug of a Nissan Leaf | 34 |
| Figure 3.1.18: Touch safe power connectors | 35 |
| Figure 3.1.19: Fuse and Contactor relay in rear battery box | 36 |
| Figure 3.1.20: Wiring below the vehicle | 37 |
| Figure 4.1.1: Illustration of the SORDS scheme on the test track | 40 |
| Figure 4.1.2: Weather conditions during test week in Karup 2013 | 40 |
| Figure 4.1.3: Weather conditions during test week in Karup 2014 | 41 |
| Figure 4.1.4: Test track 2012, Værløse Airfield..... | 42 |
| Figure 4.1.5: Test track 2013 and 2014, Karup Airfield | 42 |
| Figure 4.1.6: Height profile of the test tracks..... | 43 |
| Figure 4.1.7: Start of test track, Værløse 2012 | 43 |
| Figure 4.1.8: Start of test track, Karup 2013 | 44 |

| | |
|---|----|
| Figure 4.1.9: Test track, Karup 2014, the base area | 44 |
| Figure 4.2.1: Overview of the actual EVs used in the on-road tests | 45 |
| Figure 4.2.2: Overview of ICE vehicles used in the on-road tests | 45 |
| Figure 4.4.1: Exemplary NEDC versus SORDS consumption..... | 48 |
| Figure 4.4.2: NEDC versus four repetitions of SORDS shown in speed and time..... | 49 |
| Figure 4.4.3: Energy consumption with a small size EV from driving steady at different target speeds, illustrated by the Mitsubishi i-MiEV | 50 |
| Figure 4.4.4: Energy consumption with a medium size EV from driving steady at different target speeds, illustrated by the Nissan Leaf | 50 |
| Figure 4.4.5: Energy consumption from driving steady with a large size EV at different target speeds, illustrated by the Tesla Model S | 51 |
| Figure 4.4.6: Energy consumption from driving dynamically with a small EV at different target speeds, illustrated by Mitsubishi i-MiEV | 52 |
| Figure 4.4.7: Energy consumption from driving dynamically with a medium size EV at different target speeds, illustrated by the Nissan Leaf | 52 |
| Figure 4.4.8: Energy consumption from driving dynamically with a medium size EV at different target speeds, illustrated by the Fiat Fiorino Micro-Vett | 53 |
| Figure 4.4.9: Energy consumption from driving dynamically with a large size EV at different target speeds, illustrated by the Tesla Model S | 53 |
| Figure 4.4.10: Energy consumption from driving with full acceleration with a small size EV at different speed intervals, illustrated by the Mitsubishi i-MiEV | 55 |
| Figure 4.4.11: Energy consumption from driving with full acceleration with a medium size EV at different speed intervals, illustrated by the Renault Fluence | 55 |
| Figure 4.4.12: Energy consumption from driving with full acceleration with a large size EV at different speed intervals, illustrated by the Tesla Model S | 56 |
| Figure 4.4.13: Total energy consumption and PABE, illustrated by the Nissan Leaf | 57 |
| Figure 4.4.14: Total energy consumption and PABE, illustrated by the Fiat Fiorino Micro-Vett..... | 58 |
| Figure 4.4.15: Total energy consumption and PABE, illustrated by the Tesla Model S..... | 58 |
| Figure 4.4.16: PABE versus speed variance, illustrated by the Renault Fluence ZE | 59 |
| Figure 4.4.17: PABE versus mean absolute acceleration, illustrated by the Renault Fluence ZE | 60 |
| Figure 4.4.18: Speed variance versus speed in different driving styles, illustrated by the Mitsubishi i-MiEV | 60 |
| Figure 4.4.19: Impact of aggressive driving on energy consumption, illustrated by the Mitsubishi i-MiEV | 61 |

| | |
|--|----|
| Figure 4.4.20: Energy consumption during dynamic driving, comparison of all vehicles used in the tests | 63 |
| Figure 4.4.21: SORDS energy consumption comparison (all vehicles used in the test) | 64 |
| Figure 4.5.1: Auxiliary consumption during the day, illustrated by the Renault Fluence ZE | 65 |
| Figure 4.5.2: Auxiliary consumption during the day with no electric heater, illustrated by the Fiat Fiorino Micro-Vett | 66 |
| Figure 4.5.3: Distribution of available auxiliary consumption in different kinds of EVs | 66 |
| Figure 4.5.4: SORDS driving during heating at 3°C ambient temperature, illustrated by the Mitsubishi i-MiEV with a water-borne electric heater..... | 67 |
| Figure 4.5.5: Auxiliary consumption at different driving styles at 2-11°C ambient temperature, illustrated by the Mitsubishi i-MiEV with a water-borne electric heater | 68 |
| Figure 4.5.6: Comparison between auxiliary consumption in several vehicles at steady speeds, illustrated by all EVs used in the on-road tests at given conditions | 68 |
| Figure 4.5.7: Comparison between auxiliary consumption in several vehicles at full acceleration, illustrated by all EVs used in the on-road tests at given conditions | 69 |
| Figure 4.5.8: Comparison between auxiliary consumption in different vehicles at dynamic speeds, illustrated by all EVs used in the on-road tests at given conditions..... | 69 |
| Figure 4.6.1: Exemplary data showing the step response test, illustrated by the Renault Fluence ZE | 70 |
| Figure 4.7.1: Vehicle Performance and Battery Performance as defined in D6.1, Figure 3.1..... | 71 |
| Figure 4.7.2: Total energy delivered of Renault Fluence ZE, Mitsubishi i-MiEV, Citroën C-Zero and results from Waterloo University | 72 |
| Figure 4.7.3: Mode 2 charging efficiency versus temperature..... | 73 |
| Figure 4.7.4: Apparent charging losses estimated from on board SOC indicators at different charging levels, illustrated by the Mitsubishi i-MiEV and the Nissan Leaf | 74 |
| Figure 4.9.1: Heating capacity during SORDS driving, illustrated by the Renault Fluence..... | 76 |
| Figure 4.9.2: Comparison of heating capacity during SORDS driving, illustrated by the Mitsubishi i-MiEV, the Nissan Leaf and the Renault Fluence ZE | 78 |
| Figure 4.10.1: Distribution of energy during SORDS driving (All EVs, including the Opel Ampera in EV mode)..... | 79 |
| Figure 4.10.2: Comparison of total energy drawn from battery in percent of SORDS driving with and without regeneration (All EVs, including the Opel Ampera in EV mode) | 80 |
| Figure 4.10.3: Theoretical maximum kinetic and maximum braking energy compared to measured braking and regeneration energy in EVs with different weights during SORDS 50 km/h..... | 82 |

| | |
|--|-----|
| Figure 4.10.4: Total energy saved during SORDS driving with use of regeneration compared to total theoretical braking energy calculated and total energy drawn from battery, illustrated by all EVs used in the tests, including the Opel Ampera in EV mode. | 82 |
| Figure 4.10.5: Comparison of regeneration power versus instantaneous speed, illustrated by all EVs used in the tests. | 83 |
| Figure 4.10.6: Regeneration comparison of different through-runs of SORDS, illustrated by the Nissan Leaf..... | 84 |
| Figure 4.13.1: Acceleration times at straight line, illustrated by the Mitsubishi i-MiEV and the Fiat Fiorino Micro-Vett | 88 |
| Figure 4.13.2: Acceleration times during straight line testing with the pedal fully depressed, illustrated by the Fiat Fiorino Micro-Vett and the Mitsubishi i-MiEV | 88 |
| Figure 4.13.3: Power curves at straight line acceleration, illustrated by the Mitsubishi i-MiEV and the Fiat Fiorino Micro-Vett..... | 89 |
| Figure 4.13.4: Motor electrical power and torque versus motor RPM at straight line acceleration, illustrated by the Renault Fluence ZE 2013 (mileage: 500 km) and Renault reference curves5 | 89 |
| Figure 4.13.5: Motor electrical power and torque versus motor RPM at straight line acceleration, illustrated by the Renault Fluence ZE 2014 (mileage: 25900 km) and Renault reference curves5..... | 90 |
| Figure 4.13.6: PABE comparison, illustrated by the Mitsubishi i-MiEV..... | 91 |
| Figure 4.13.7: Acceleration times during straight line testing with the throttle pedal fully depressed..... | 92 |
| Figure 4.13.8: Power curves at straight line acceleration..... | 93 |
| Figure 4.14.1: Calculated change in wind resistance versus air pressure at different temperatures with reference to the wind resistance at 24°C and 1000hPa, illustrated by the Nissan Leaf driving SORDS 2014..... | 95 |
| Figure 4.14.2: Tire inflation pressure versus temperature | 95 |
| Figure 4.14.3: Calculated change in rolling resistance versus air temperature at several vehicle weights with reference to the rolling resistance adjusted to 36 psi at 20°C, illustrated by the Mitsubishi i-MiEV, Fiat Fiorino Micro-Vett, Nissan Leaf and Tesla Model S driving SORDS | 96 |
| Figure 4.14.4: SORDS high speed part (1500-3000m) in Værløse 2012, illustrated by the Fiat Fiorino Micro-Vett | 97 |
| Figure 4.14.5: Calculated wind drag at steady speed with possible error margin shown in blue, illustrated by the Tesla model S | 98 |
| Figure 4.14.6: Apparent impact of surface humidity, illustrated by the Mitsubishi i-MiEV (SORDS in Værløse 2012) | 99 |
| Figure 4.14.7: Example of water expulsion from a flooded road (Picture from the Internet) | 102 |

| | |
|---|-----|
| Figure 4.14.8: Potential energy versus slope of road for different vehicle weights, illustrated by the Mitsubishi i-MiEV, Renault Fluence ZE and Tesla Model S | 104 |
| Figure 4.14.9: Total energy drawn from battery versus slope of road for different vehicle weights, illustrated by the Mitsubishi i-MiEV, Renault Fluence ZE and Tesla Model S | 104 |
| Figure 4.14.10: VLFC during dynamic driving from EVs with different weight | 105 |
| Figure 4.14.11: Total measured energy consumption during dynamic driving from EVs with different weight | 105 |
| Figure 4.14.12: Comparison of energy consumption at dynamic driving with the same EV at maximum weight and normal weight, illustrated by the Nissan Leaf | 106 |
| Figure 4.14.13: Change in the energies at maximum weight compared to normal weight, when driving dynamically with the same EV, illustrated by the Nissan Leaf | 107 |
| Figure 5.1.1: Vehicles used on the dynamometer: Mitsubishi i-MiEV, Citroën C-Zero, Renault Twizy | 108 |
| Figure 5.1.2: Exemplary HV-battery current and voltage of Mitsubishi i-MiEV during full charge (s4m10) | 109 |
| Figure 5.1.3: Exemplary HV-battery current and voltage of Citroën C-Zero during full charge (s2m06) | 109 |
| Figure 5.1.4: Total energy during full charge, sorted according to ambient temperature..... | 111 |
| Figure 5.1.5: Mitsubishi i-MiEV on MAHA dynamometer in climate chamber; driving robot in Mitsubishi i-MiEV | 112 |
| Figure 5.1.6: Total energy during full charge, sorted chronological..... | 113 |
| Figure 5.2.1: Range of vehicle starting with full HV-battery..... | 114 |
| Figure 5.2.2: Energy distribution during range measurements (absolute values)..... | 115 |
| Figure 5.2.3: Energy distribution during range measurements (relative values)..... | 116 |
| Figure 5.2.4: Average energy consumption during range tests..... | 117 |
| Figure 5.3.1: Speed and acceleration during three SORDS cycles (s1m09)..... | 119 |
| Figure 5.4.1: Comparison of internal and external measurements of current at HV-battery (NEDC, s4m21) | 120 |
| Figure 5.4.2: Comparison of internal and external measurements of current at HV-battery (SORDS, s4m22)..... | 120 |
| Figure 5.4.3: Comparison of internal and external measurements of current at HV-battery (WLTC2, s4m23) | 121 |
| Figure 5.4.4: Comparison of internal and external measurements of current at HV-battery (full charge, s2m06)..... | 121 |



Figure 5.4.5: Integrated energy stored in HV-battery based on internal and external measurement data (full charge, s2m06)122

List of Tables

| | |
|--|-----|
| Table 3.1: Technical data of several EVs..... | 22 |
| Table 4.1: Weather conditions at test tracks | 41 |
| Table 4.2: Mileages of the vehicles used in the on-road tests – rounded values..... | 46 |
| Table 4.3: Consumed time and gradient during cabin heating and defrosting..... | 77 |
| Table 4.4: Empty battery shutdown sequences, illustrated by the Renault Fluence..... | 85 |
| Table 4.5: Empty battery shutdown sequences, illustrated by the Nissan Leaf | 86 |
| Table 4.6: Empty battery shutdown sequences, illustrated by the Mitsubishi i-MiEV | 86 |
| Table 4.7: Regeneration status after quick charging or at 100% SOC. | 87 |
| Table 5.1: Average energy and duration of a full charging cycle based on environmental temperature | 112 |
| Table 5.2: Average energy and duration of a full charging cycle based on year | 114 |
| Table 5.3: Average values measured by the dynamometer for different driving cycles..... | 117 |
| Table 5.4: Average mechanical energy measured by the dynamometer for different driving cycles | 118 |
| Table 5.5: Average energy consumption during SORDS at different environmental temperatures | 123 |
| Table 5.6: Efficiencies based on the average energy consumptions in Table 5.5 | 123 |

List of Abbreviations

| | |
|-----------|--|
| AC | Alternating Current |
| BMS | Battery Management System |
| CA | Consortium Agreement |
| CAN | Controller Area Network (vehicle bus system that interconnects the control units within a car) |
| CCS | Combined AC/DC-Charging System |
| DC | Direct Current |
| DoW | Description of Work (Annex I of Grant Agreement) |
| ECU | Electronic Control Unit |
| ERG | Emergency Response Guide |
| EU | European Union |
| Euro NCAP | European New Car Assessment Programme |
| EV | Electric Vehicle |
| HV | High Voltage (voltage of at least 30V AC or 50V DC) |
| ICE | Internal Combustion Engine |
| IEC | International Electro technical Commission |
| LV | Low Voltage (voltage of 12V) |
| NEDC | New European Driving Cycle |
| OBD | On Board Diagnosis |
| OEM | Original Equipment Manufacturer |
| PABE | Powertrain And Breaking Efficiency |
| SOC | State Of Charge |
| SOH | State Of Health |
| SORDS | Standardised On-Road Driving Schedule |
| VLFC | Vehicle Limited Fuel Consumption |
| WLTP | Worldwide harmonised Light vehicle Test Procedures |
| WP | Work Package |

1 Executive Summary

The purpose of work package 6 is to validate the performance of EVs under different climatic conditions and use patterns. The validation is done over time so that degradation mechanisms on the vehicles can be discussed. It must be pointed out that the goal is not the comparison of different brands of EVs, but the evaluation of EV technology viability in general. Therefore vehicles of different size and brand are included in the work to assess the impact of several parameters, such as weight in combination with driving style, climatic impact onto different battery types and others.

In order to achieve results that are comparable with real driving experience, the team designed a new procedure named SORDS (Standardised On-Road Driving Schedule) inspired by the UITP-SORT test for city buses. The SORDS represents a fairly dynamic drive pattern, which results in an accelerated depletion of the traction battery. The SORDS cycle is explained in detail in deliverable 6.1¹ as well as in chapter 4 of this report.

To validate the on-road measurements and provide a link to official tests, electric vehicles were also tested on dynamometers. Some of these measurements were performed in a climate chamber at different temperatures to assess the climatic impact. Due to the controlled environment in the laboratory the dynamometer tests can be used as baseline for comparison with on-road tests.

The main results are:

- Range and consumption are mainly dependent on drive pattern. An aggressive driving style, meaning high speeds and fast accelerations/decelerations, will increase the consumption significantly.
- Range and consumption depend strongly on the use of auxiliaries. At heavy urban driving the auxiliaries consume more than 50% of the total power drawn from the battery. When doing high speed highway driving this number is reduced to approximately 25%.
- Climate has significant impact on battery performance. Both power and capacity of the batteries were up to spec in the weather conditions tested. However, in climate chamber at -7°C the charging losses were a significant part of the input energy.
- Battery performance is almost unaffected by battery charge rate. The measurements revealed no performance loss of any importance after fast charging.
- Heating and defrosting capacity is adequate. The time required for reaching convenient cabin temperature within the tested electric vehicles is comparable to traditional vehicles.
- Safety functions are maintained in the event of an empty battery. Even with 0% state of charge the electric vehicles are safe for the driver.
- Vehicle performance is almost unaffected by battery SOH, meaning aging of the battery. Even after four years of use no visible loss of batter capacity had occurred.

Altogether it can be concluded that state to the art electric vehicles offers good consumer convenience, but that the driving range is strongly dependent on user behaviour and climatic conditions. The electric vehicles as of today are safe even with empty battery. And in contrast to some public statements in the past, fast charging does not seem to negatively affect the battery.

¹ Available at <http://www.greenemotion-project.eu/dissemination/deliverables-evaluations-demonstrations.php>

2 Introduction

2.1 Work package 6 goals and background

The purpose of work package 6 is to validate the performance of EVs under different climatic conditions and use patterns. The validation is done over time so that degradation mechanisms on the vehicles can be discussed.

The work package also supplies in depth information about the variations in energy consumption based on highly controlled track and dynamometer testing in different weather conditions. This information is valuable both for scientific but also for educational purposes since it aims at a better understanding of how the EV range and consumption varies with different parameters. The variation in EV range and consumption is *much larger and quite different* from that of vehicles with ICE and therefore investigated in detail in this work package.

Within the Green eMotion WP6 several different vehicles from different OEMs are used. However, the analysis is done in a generic way, because the goal of WP6 is not to benchmark different vehicles, but to make an overall analysis of the performance of electric vehicles. Therefore an EV classification was made as described in section 3.2. One of the biggest hurdles/goals was to develop a testing methodology in which a realistic performance validation of EVs would be possible. The major boundary conditions which have to be covered by the performance validation are: Temperature influence, driver influence (use case/user behaviour/driving behaviour) and technical maturity level of EVs. Therefore a set of technical hypothesis was defined within WP6 and the background of these explained in the Deliverable 6.1² "Methodology of EV measurements". Section 3.1 of this report however shortly explains again the approach with hypothesis as well as the physical testing procedures.

Chapter 3 gives a short summary on the overall methodology which is used in the WP6 and which is explained in detail within the deliverable 6.1. Furthermore chapter 3 describes the functionalities and different layouts of electric vehicles and thus the "state of the art relevant for WP6".

In the next step, in chapter 4, the analysis of the measurement data is performed and scientific answers on the hypotheses are given in a generic, not vehicle specific, way. The content of this chapter results out of the WP6 on road vehicle measurements.

The analysis in chapter 5 describes the dynamometer results which focus significantly on the climate impact on EVs. At the end of the deliverable, conclusions are made and briefly discussed.

² Available at <http://www.greenemotion-project.eu/dissemination/deliverables-evaluations-demonstrations.php>

2.2 Alignment between partners

In the Green eMotion WP6 the following partners are involved:

DTI:

The Danish Technological Institute is an independent, non-profit institution approved as a technological service institute by the Danish Ministry of Science, Technology and Innovation. The two centres of DTI “Renewable Energy and Transport” and “Automotive” act as a national specialist centre at vehicle, driveline and engine level with a large toolbox for EV testing and characterisation (e.g. chassis dynamometers at vehicle and engine level). DTI is among others strongly involved in EV rollout related education/training and in approval activities for EVs in Denmark.

fka:

The Forschungsgesellschaft Kraftfahrwesen Aachen mbH (fka) offers a distinctive spectrum of expertise owing to its extensive setup. fka handles research assignments and advises on projects related to the development of vehicles as well as their components. The key research areas include chassis, body work, drive train, electronics, acoustics and driver assistance systems.

Additionally, fka also engages actively in the strategy and process development for the automotive industry. fka has been involved in the conception and development of innovative drive train technologies for electric and hybrid vehicles as well as the recharging infrastructure for more than 35 years. The first completely indigenously developed hybrid vehicle prototype was presented in the year 1973. Since then, the fka engineers have continually proven their competence in the field of electro mobility in the form of numerous further prototypes, concept studies and consulting services.

TNM-IFM:

The IFM (Institut für Fahrzeugtechnik und Mobilität) of TÜV NORD Mobilität GmbH & Co. KG is an accredited and independent engineering services provider in the automotive sector, which works for industrial companies and government authorities at national, European and worldwide level.

In the three core areas: complete vehicles, systems and components, TNM-IFM monitors and tests technological innovations in the automotive industry, in order to ensure the market success of manufacturers and suppliers, and to contribute to the improvement of vehicle and traffic safety. The TNM-IFM is accredited for testing to national and international standards, and works with many approval authorities at home and abroad.



Additionally the following OEMs are involved in this work package to deliver expertise and knowledge from an OEM perspective to complete the portfolio of technical WP6 members:

- BMW
- Daimler
- Nissan
- Renault

For lending vehicles for the hypothesis testing we thank:

- Opel Denmark (Opel Ampera)
- Sixt (Nissan Leaf)
- NBE (Tesla Model S)

3 Performance validation of electric vehicles

3.1 State of the art of electric vehicles

Within the Green eMotion project, several vehicles were used during different testing phases. The analysis of the data is done as described in section 3.1 and the testing was done as described in sections 3.1.1 and 3.1.2. In this section several EVs are detailed examined.

To make a generic analysis approach, the EVs have been categorised regarding several parameters and divided into three groups – mini, small, medium and large.

Renault's Twizy Zero Emission, as depicted in Figure 3.1.1, is a Euro NCAP classed quad cycle out of 2011 with rear wheel drive. Its lithium ion HV battery has a capacity of 6.5 kWh at a voltage of 60 V with



Figure 3.1.1: Renault Twizy ZE

an empty vehicle weight of 562 kg. The electric engine has a maximal power of 13 kW, a maximal engine torque of 57 Nm and a maximal speed of 80 km/h reaching a range of 100 km in the NEDC. Renault's Twizy ZE is categorised as mini vehicle. Based on its extremely low size and weight this vehicle is built for urban traffic and short ranges only. This mini categorised vehicle is not suited for motorways due to its engine speed limit and its low battery capacity. The EV can be configured for charging at domestic electrical sockets or Type 2 Mennekes slots; Renault is not giving its customers the opportunity of both. Due to one at the vehicle fixed charging cable with Type 2 Mennekes or electrical socket plug, customers have to choose at the purchase. Fast recharging times of 3.5 hours for a full charge and low average consumption are optimising this EV for low distance solo commuters inside of cities, it is not suitable for Nordic climate/winter driving.

The electric engine has a maximal power of 13 kW, a maximal engine torque of 57 Nm and a maximal speed of 80 km/h reaching a range of 100 km in the NEDC. Renault's Twizy ZE is categorised as mini vehicle. Based on its extremely low size and weight this vehicle is built for urban traffic and short ranges only. This mini categorised vehicle is not suited for motorways due to its engine speed limit and its low battery capacity. The EV can be configured for charging at domestic electrical sockets or Type 2 Mennekes slots; Renault is not giving its customers the opportunity of both. Due to one at the vehicle fixed charging cable with Type 2 Mennekes or electrical socket plug, customers have to choose at the purchase. Fast recharging times of 3.5 hours for a full charge and low average consumption are optimising this EV for low distance solo commuters inside of cities, it is not suitable for Nordic climate/winter driving.

Daimler's Smart Fortwo Electric Drive, as shown in Figure 3.1.2, is a Euro NCAP classed super mini with rear wheel drive, manufactured first in 2012. The HV battery pack has a capacity of 17.6 kWh at 240 V resulting in an empty weight of 900 kg. Its electric engine has a maximal power of 55 kW, a maximal engine torque



Figure 3.1.2: Daimler Smart Fortwo ED

of 130 Nm and a maximal speed of 125 km/h on a NEDC tested maximal range of 145 km. Daimler's Smart is categorised as small vehicle because of its small size, weight and vehicle payload, but also due to a smaller engine compared to medium categorised vehicles. Beside the driver there is only one further seat (Fortwo – for two passengers). As a small categorised vehicle, motorway driving on short distances is possible by contrast with mini categorised cars. The Smart has a Type 2 Mennekes plug

socket and can be fully AC charged within 7 hours at a standard electrical socket or within 6 hours at a wallbox with 230 V 1-phase 16A on its 3.3 kW on-board charger. An optionally purchasable upgrade of the on-board charger up to 22 kW allows the Smart Fortwo to recharge at optimised wallboxes with 400 V 3-phase at Type 2 Mennekes plug-ins within 1 hour.

The i-MiEV (Mitsubishi innovative Electric Vehicle) from Mitsubishi Motors, shown in Figure 3.1.3, is a 2011 released Euro NCAP classed supermini with rear wheel drive. A lithium ion HV battery pack with a capacity of 16 kWh at a voltage of 330 V causes an empty weight of 1185 kg. With a maximal power of 49 kW, a maximal engine torque of 180 Nm and a maximal speed of 130 km/h, its engine reaches a range of 160 km in the NEDC. It is also categorised as small vehicle based on the vehicle's comparable characteristics and engine to Daimler's Smart Fortwo ED. The Mitsubishi i-MiEV has a Type 1 Yazaki plug socket on its right hand side to recharge at an electrical socket within 8 hours. Although Mitsubishi Motors is not offering wallboxes for optimised charge, the Mitsubishi i-MiEV can be charged at public



Figure 3.1.3: Mitsubishi i-MiEV

recharge at an electrical socket within 8 hours. Although Mitsubishi Motors is not offering wallboxes for optimised charge, the Mitsubishi i-MiEV can be charged at public

Type 2 Mennekes slots with an extra charging cable. On its left hand side, Mitsubishi Motors implemented a CHAdeMO plug-in for DC fast charge up to 50 kW, recharging the EV within 30 min to 80% of the battery's maximal capacity. Overall, these small categorised EVs are ideal for short distance commuters who occasionally need to drive on the motorways.

Renault's Fluence Zero Emission, as seen in Figure 3.1.4, was first manufactured in 2009 and is a Euro NCAP classed small family vehicle with front wheel drive. The HV battery has a capacity of 22 kWh on a 398 V power circuit. The car's empty weight is 1605 kg. The electric engine, with a maximal power of 70 kW and a maximal engine torque of 226 Nm reaches a maximal speed of 135 km/h and a NEDC tested range of 185 km. This EV played a major role in Better Place's battery switching concept. Due to the project's lacking acceptance, the commercially unsuccessful switching system and finally Better Place's insolvency, Renault stopped the Fluence ZE's



Figure 3.1.4: Renault Fluence ZE

production in 2012. Based on its bigger size, weight, vehicle payload and engine, Renault's Fluence ZE is medium categorised. Its HV battery, which is compared to other EVs not attached at the bottom of the vehicle body, but behind the back seats, is rechargeable by the Type 1 Yazaki plug socket. Recharging at electrical sockets requires 12 hours, recharging at wallboxes with Type 2 Mennekes slot requires 9 hours for a complete charge. Due to the idea of a battery switching system, Renault did not add a fast charge possibility.

production in 2012. Based on its bigger size, weight, vehicle payload and engine, Renault's Fluence ZE is medium categorised. Its HV battery, which is compared to other EVs not attached at the bottom of the vehicle body, but behind the back seats, is rechargeable by the Type 1 Yazaki plug socket. Recharging at electrical sockets requires 12 hours, recharging at wallboxes with Type 2 Mennekes slot requires 9 hours for a complete charge. Due to the idea of a battery switching system, Renault did not add a fast charge possibility.

Nissan's Leaf (Leading, Environmentally friendly, Affordable, Family car), as depicted in Figure 3.1.5, is a 2011 released Euro NCAP classed small family vehicle with front wheel drive. The HV battery packs have



Figure 3.1.5: Nissan Leaf

24 kWh capacities and a power circuit of 360 V at an empty car weight of 1505 kg. The engine's maximal power is 80 kW, its maximal torque is 280 Nm and its maximal speed is 145 km/h reaching 175 km range in the NEDC. It is also categorised as medium as a result of comparable characteristics and engine to Renault's Fluence ZE. The Nissan Leaf has a Type 1 Yazaki plug socket for AC charge and a CHAdeMO slot for DC supercharge in its front. It is fully rechargeable at the standard electrical socket within 10 hours or at Nissan's wallbox within 8 hours. The wallbox officially has a Type 3 Scame, but Nissan is also delivering charging cables with Type 2 Mennekes plug-in for the European public charging stations. CHAdeMO charge is refilling the battery's capacities within 30 min up to 80% at 50 kW DC fast charging stations.

The i3 from BMW, shown in Figure 3.1.6, is a 2013 into the market introduced Euro NCAP classed small family vehicle with rear wheel drive. BMW's HV battery pack has a capacity of 18.8 kWh and a voltage of



Figure 3.1.6: BMW i3

360 V. The empty vehicle's weight is 1195 kg. The engine's maximal power is 125 kW, its maximal torque is 250 Nm and its maximal speed is 150 km/h reaching a distance of 190 km in the NEDC. It is medium categorised, although BMW's i3 is comparatively light, its engine and size is comparable to other medium categorised vehicles. BMW implemented CCS Type 2 plug sockets which imply a Type 2 Mennekes slot. It can be AC charged up to 80% within 8 hours at the electrical socket, within 5 hours at a 230 V 1-phase wallbox or within 3 hours at a 400 V 3-phase wallbox using the implied Type 2 Mennekes plug socket. The wallbox itself is also equipped with Type 2 Mennekes slot. In addition, the i3 can be supercharged with DC up to 50 kW by the use of its CCS Type 2 plug-in. Moreover, there is much more comfort compared to mini and small vehicles, so medium categorised vehicles afford its customers the entrainment of more than two passengers. BMW's i3 can be upgraded with a range extender.

Opel's Ampera, as depicted in Figure 3.1.7, is a 2011 released Euro NCAP classed small family vehicle with front wheel drive. The Ampera's battery packs have a capacity of 16 kWh and a voltage of 360 V.



Figure 3.1.7: Opel Ampera

Empty weight of the vehicle is 1732 kg. Opel's engine has a maximal power of 111 kW, its maximal torque is 370 Nm and its maximal speed is 161 km/h reaching distances of up to 80 km in the NEDC. It is also medium categorised. Opel implemented a Type 1 Yazaki slot for the electric charge. The Ampera can be charged at electrical sockets with 6 A within 11 hours or with 10 A within 6 hours. Optimised wallbox charge with 230 V 1-phase AC requires 4 hours. Supercharging is not possible, but Opel serially implemented a range extender reaching ranges above 500 km.

Opel's philosophy is differing from other manufacturers. The electrical capacity is laid out for short distances, e.g. the way to work. For longer distances, the Ampera is running at a gasoline engine.

Tesla's Model S Performance 85 out of 2012, as depicted in Figure 3.1.8, is a Euro NCAP classed executive vehicle with rear wheel drive. It has a HV battery pack with 85 kWh capacities and a voltage of 402 V causing an empty weight of 2129 kg.



Figure 3.1.8: Tesla Model S

Its engine has a maximal power of 310 kW, a maximal torque of 600 Nm and a maximal speed of 210 km/h reaching a range of 502 km in the NEDC. Tesla's Model S is categorised as large vehicle. The Model S is currently unmatched regarding electric engines power, torque, speed and range due to an enormous battery capacity, which is also resulting in much higher weight. Tesla tried to achieve an EV

which convenience can be compared to vehicles with ICE regarding the engines features and its range. Regarding standardisation, Tesla also disregarded any existing plug-ins and created a self-made plug socket for the American market. For the European market, Tesla developed a reinforced Type 2 Mennekes plug socket which matches to Type 2 Mennekes plug-ins at public charging stations, but additionally implies a possibility of DC fast charging. To reduce high charging times, Tesla Motors integrated a possibility of implementing a second 11 kW on-board charger in addition to the single standard 11 kW on-board charger. Altogether, Tesla's Model S can be charged in many different ways. Recharging at domestic electrical sockets requires at least 29 hours for a full battery capacity charge depending on the sockets maximal current, but these standard sockets are not laid out for the use of maximal current on longer time periods. Wallboxes solve this problem. Tesla's wallboxes with 230 V 1-phase AC also require charging times of 29 hours with 3 phase 16 A current, but with a second on-board charger it is reduced to 14 hours at a current of 3 phase 32 A. AC 400 V 3-phase wallbox charge



establish further reduction of the charging time. With these wallboxes, the Model S can be charged within 9 hours with a single on-board charger at 16 A or within 4.5 hours with dual on-board charging at a current of 32 A. The EV's supercharge with a maximum of 120 kW DC recharges the HV battery packs up to 80% within 40 min. Tesla Motors is currently developing a 135 kW charging station.

A detailed overview on the EVs characteristics introduced in this chapter is figured out in Table 3.1. For a better understanding, next sections will give a detailed overview on the functions of EVs and the differences between several vehicles.

| | | Classification | | | | | |
|-----------------|------------------|----------------|-----------------|-------------------|--------------|----------------|--------------------------|
| | | Mini | Small | Medium | Large | | |
| General | Manufacturer | Renault | Daimler AG | Mitsubishi Motors | Renault | Opel | Tesla Motors |
| | Model | Twizy ZE | Smart Fortwo ED | i-MiEV | Fluence ZE | Ampera | Model S Performance 85 |
| Euro NCAP class | NEDC Range | 100km | 145km | 160km | 185km | 80km | 502km |
| | Release | 2011 | 2012 | 2011 | 2009 | 2011 | 2012 |
| Height | Length | 2,335mm | 2,700mm | 3,475mm | 4,748mm | 4,498mm | 4,970mm |
| | Width | 1,381mm | 1,560mm | 1,475mm | 2,041mm | 1,775mm | 2,187mm |
| Empty weight | Height | 1,454mm | 1,570mm | 1,610mm | 1,458mm | 1,578mm | 1,445mm |
| | Vehicle payload | 562kg | 900kg | 1185kg | 1605kg | 1195kg | 2129kg |
| Engine | max. Power | 123kg | 250kg | 265kg | 418kg | 403kg | 461kg |
| | max. Torque | 13kW | 55kW | 49kW | 70kW | 125kW | 310kW |
| Battery | max. Speed | 57Nm | 130Nm | 180Nm | 226Nm | 250Nm | 600Nm |
| | avg. Consumption | 80km/h | 125km/h | 130km/h | 135km/h | 150km/h | 210km/h |
| Charge | Transmission | 6.3kWh/100km | 15.1kWh/100km | 12.5kWh/100km | 14kWh/100km | 12.9kWh/100km | 18.1kWh/100km |
| | Drive axle | automatic | automatic | automatic | automatic | automatic | automatic |
| Battery | Type | rear | rear | rear | front | front | rear |
| | Capacity | Lithium ion | Lithium ion | Lithium ion | Lithium ion | Lithium ion | Lithium ion |
| Charge | Voltage | 6.5kWh | 17.6kWh | 16kWh | 22kWh | 16kWh | 85kWh |
| | Standard Charge | 60V | 240V | 330V | 398V | 360V | 402V |
| Charge | AC 230V 1-phase | 3.5h (100%) | 7h (100%) | 8h (100%) | 12h (100%) | 8h (80%) | 29h (100%) |
| | Wallbox Charge | EV: fix | EV: Type 2 | EV: Type 1 | EV: Type 1 | EV: Type 2 | EV: Tesla self-made |
| Charge | AC 230V 1-phase | Slot: Schuko | Slot: Schuko | Slot: Schuko | Slot: Schuko | Slot: Schuko | Slot: Schuko |
| | Wallbox Charge | 3.5h (100%) | 6h (100%) | - | 9h (100%) | 4h (80%) | 29h (100%) 14h (100%)* |
| Charge | AC 400V 3-phase | EV: fix | EV: Type 2 | - | EV: Type 1 | EV: Type 2 | EV: Tesla self-made |
| | Supercharge DC | Slot: Type 2 | Slot: Type 2 | Slot: Type 2 | Slot: Type 2 | Slot: Type 2 | Slot: Type 2 |
| Charge | AC 400V 3-phase | - | 1h (100%) | - | - | 3h (80%) | 9h (100%) 4.5h (100%)* |
| | Supercharge DC | - | EV: Type 2 | - | - | EV: Type 2 | EV: Tesla self-made |
| Charge | AC 400V 3-phase | Slot: Type 2 | Slot: Type 2 | Slot: Type 2 | Slot: Type 2 | Slot: Type 2 | Slot: Type 2 |
| | Supercharge DC | 30min (80%) | 30min (80%) | EV: CHADEMO | EV: CHADEMO | EV: CCS Type 2 | 40min (80%) |
| Charge | AC 400V 3-phase | EV: CHADEMO | EV: CHADEMO | EV: CHADEMO | EV: CHADEMO | EV: CCS Type 2 | EV: Tesla self-made |
| | Supercharge DC | Slot: fix | Slot: fix | Slot: fix | Slot: fix | Slot: fix | Slot: fix |

* Values imply the use of an additional second on-board charger

Table 3.1: Technical data of several EVs

3.1.1 Main components

Electric vehicles of the 21st century do have a main structure and functionality in common. However, the automotive sector is still inhibited by a lack of international standards, especially regarding battery and charging systems. Reason for this is the overlap of EV technology in automotive, electric and telecommunication standards. For a detailed overview on standardisation in EV technology please see D6.3³ and D7.1⁴.

The main components of electric vehicles are a HV battery pack, at least one electric motor, three electric converters and an already from the conventional vehicles standardised LV battery. The topological view of an electric vehicle in Figure 3.1.9 depicts these components and its main energy consumers in one possible structure.

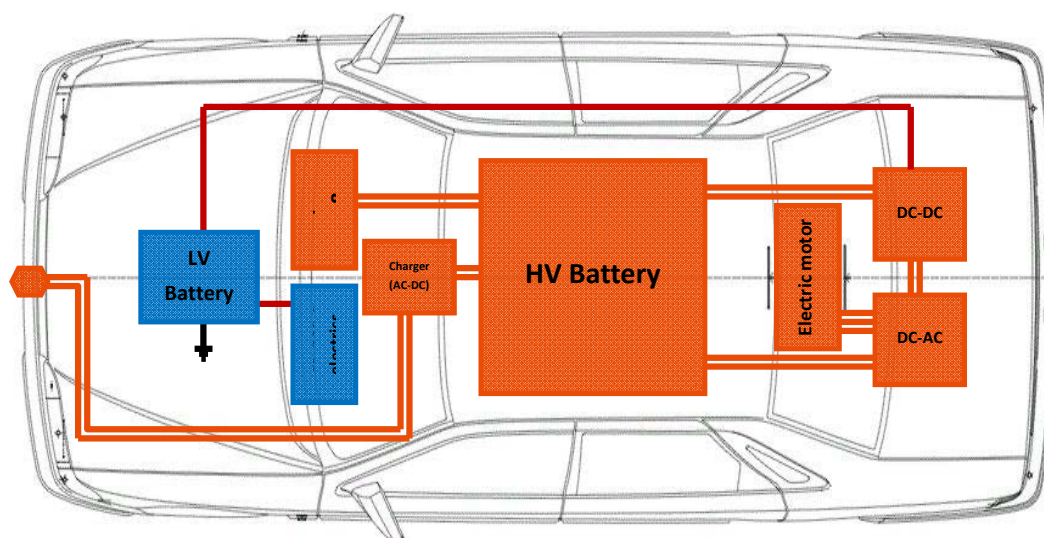


Figure 3.1.9: Example of a topological view of an EV's main components

The HV battery, usually lithium ion accumulators, is the heart of the energy system and the whole vehicle. Because of its weight, it is in almost all constructions fixed at the bottom of the vehicle body to set its balance point as close as possible to the ground. This HV battery pack is gaining its energy via AC or DC charge. In most cases, the HV battery is charged by AC from the standard electrical socket transformed

³ Available spring 2015 at <http://www.greenemotion-project.eu/dissemination/deliverables-evaluations-demonstrations.php>

⁴ Available at <http://www.greenemotion-project.eu/dissemination/deliverables-standards.php>

into DC by the charger, which is one of the electric converters, the AC-DC converter. Due to lower current, this recharging method requires multiple hours, depending on the battery's capacity and charging system. Manufacturer's wall boxes, if offered, are optimising the AC charge for their batteries. In addition, some OEMs implemented a possibility of fast charging via DC in much less time. Some manufacturers also integrated a battery switching system. The energy from the HV battery is also used by the climate compressor and the heating for the air conditioning of the interior vehicle room, but its primary use is to provide the electric engine with power. In every case, the electric engine is consisting of at least one electric motor and another electric converter, the DC-AC converter, also called inverter, which is transforming DC of the HV battery into AC required by the electric motor. The electric motor itself is transforming electric energy into mechanical energy to accelerate. The LV battery, which is standardised on a voltage of 12 V, provides the second power circuit for LV consumers (e.g. dashboard electrics, lights, alarm system, etc.) with power. It is recharged via DC by the HV battery. To transform the HV into LV, the electric vehicle requires another electric converter, a DC-DC converter, which is transforming the voltage from the HV power circuit to 12 V from the second power circuit.

Electric and gasoline vehicles do only have one main difference: the energy system. Conventional vehicles are equipped with combustion engines. Fuel as gasoline or diesel is combusted to get the containing energy. This is a non-reversible chemical reaction. Main remnant of this reaction is carbon dioxide. For a constant feeding of fuel these kind of vehicles have fuel tanks, which are easily refillable. Electric vehicles in contrast have electric engines with an ecologically beneficial possibility of driving without any emissions. These vehicles are gaining their energy from the HV battery, which is unleashing the electric energy in a reversible chemical reaction with no remnants. Both types of vehicles do have a LV battery to power the electrical 12 V consumers and in case of vehicles with ICE to start the engine, but because of the non-existent HV power circuit in vehicles with ICE, there is not any electric converter needed, but an alternator to reload the LV battery while driving.

Compared to vehicles with ICE, EV's simplified gearbox for accelerating is extremely compact. According to its distributions and configurations numerous feasible schemes of powertrain topologies can be achieved. Four types of EV powertrain topologies can be identified as shown in Figure 3.1.10. The central drive powertrain, as shown in Figure 3.1.10 (a), is the most common and predominant topology for both EVs and conventional vehicles. Others are rarely used. Compared to conventional vehicles, the ICE is substituted by an electric motor and the multi-speed gearbox is simplified to a single-stage transmission. The mechanical differential and essential drive shafts are still reserved. Therefore, the chassis layout and configuration do not need to be modified excessively. Some existing EVs such as Nissan's Leaf adopted this topology. However, the central drive powertrain topology is relatively cumbersome. The tight arrangement of the mechanical components makes it difficult to hold battery packs with large capacities, which results in small ranges. In addition, the energy dissipation is relatively large due to mechanical losses.

A distributed configuration, as seen in Figure 3.1.10 (b), allows the independent control of each driving wheel and the engine torque distribution to be determined intelligently and precisely. The vehicle dynamics, steering performance and driving safety can be optimised and improved without additional hardware implementation. Additionally, eliminating mechanical transmission such as the gearbox, the

mechanical differential and redundant drive shafts, may provide significant improvements on weight reduction, and cost savings. This most simple EV powertrain is called the wheel-hub drive without reduction gear. This type of EV powertrain topology has been widely adopted in motorised wheelchairs, electric bicycles and electric scooters. Although the mechanical transmission loss is eliminated, the electric motor works mainly within the non-efficiency region of the low speed and high torque due to the lack of a reduction gear.

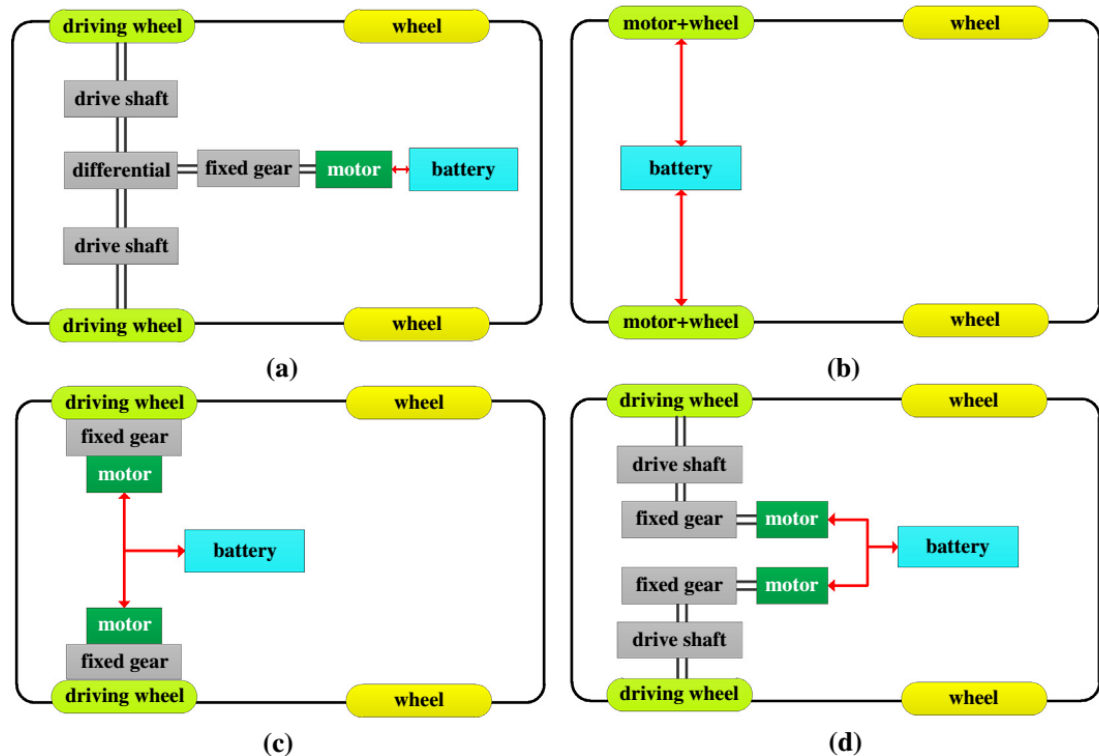


Figure 3.1.10: EV powertrain topologies

The wheel-hub drive with reduction gear powertrain, as depicted in Figure 3.1.10 (c), facilitates the use within higher efficiency and speed region. The electric motor and the reduction gear with constant gear ratio are integrated into a single assembly. The driving wheel connects the drive shaft to the reduction gear. The major shortcoming of those two wheel-hub drive powertrain topologies is that the unsprung mass of the suspension will be increased, which adversely affects the handling and ride, especially during fast oscillating motions over bumps, the wheels will transmit instead of absorbing the oscillations to the chassis.

Figure 3.1.10 (d) depicts the schematic of close-wheel drive powertrain. The electric motor and the reduction gear are also integrated into a single assembly. However, different from the wheel-hub drive powertrain, the close-wheel drive powertrain uses an output shaft of the reduction gear to drive the wheel through the drive shaft assembly containing universal joints. For instance, Mercedes-Benz applies this type of powertrain topology to their SLS AMG E-Cell vehicle. The assembly of electric motors and reduction gears are mounted on the vehicle body above the suspension. Hence, the vehicle's handling

and ride comfort level can be improved remarkably. Since the electric motor is the only engine for accelerating, those proposed EV powertrain topologies can be directly applied.

3.1.2 Layout

Developers of EV technology have chosen different topologies regarding component composition and powertrain engineering for their vehicles as described in the last section. Schematic topologies of the component structure and its linkage may depict the EV's functionality. For the Green eMotion project, the vehicles, as described in the beginning of this chapter, are the most important for validating the performance of EVs. As an example of the research work, two EVs, Nissan's Leaf and Mitsubishi's i-MiEV, are now discussed here.

Mitsubishi's small categorised and NCAP classed supermini Mitsubishi i-MiEV, as seen topological in Figure 3.1.11 and photographical in Figure 3.1.12, is analysed in the first part of this section. The HV battery packs are fixed at the bottom of the vehicle body and provide energy for the electric engine, the HV heating and the climate compressor. The vehicle's electric engine is fixed at the rear axle implementing rear wheel drive and has an automatic transmission. The three power converters are combined in a construction in its rear trunk above the electric engine to simplify the cooling concept. The standardised 12 V battery is in front of the vehicle under the engine hood to provide LV consumers with energy.

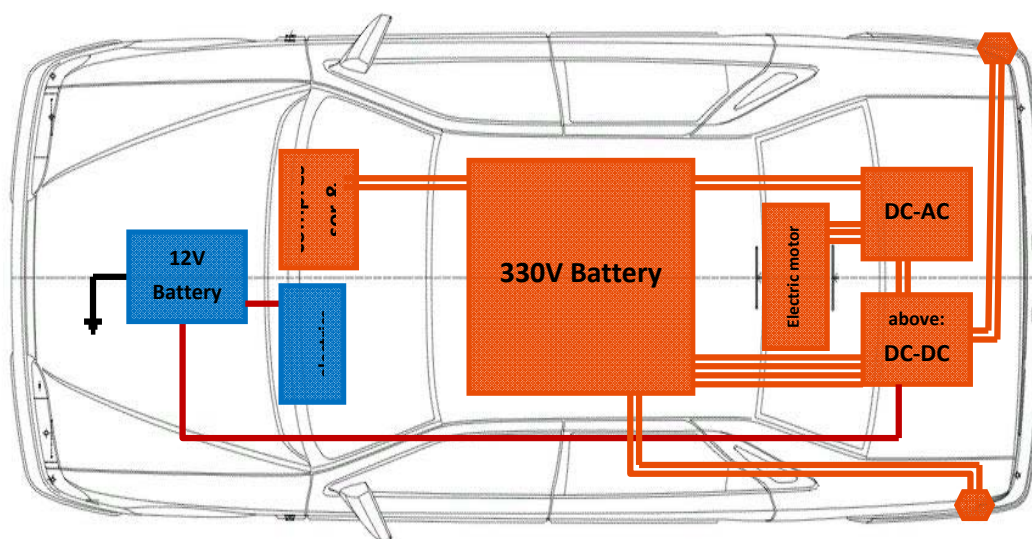


Figure 3.1.11: Topological view of a Mitsubishi i-MiEV

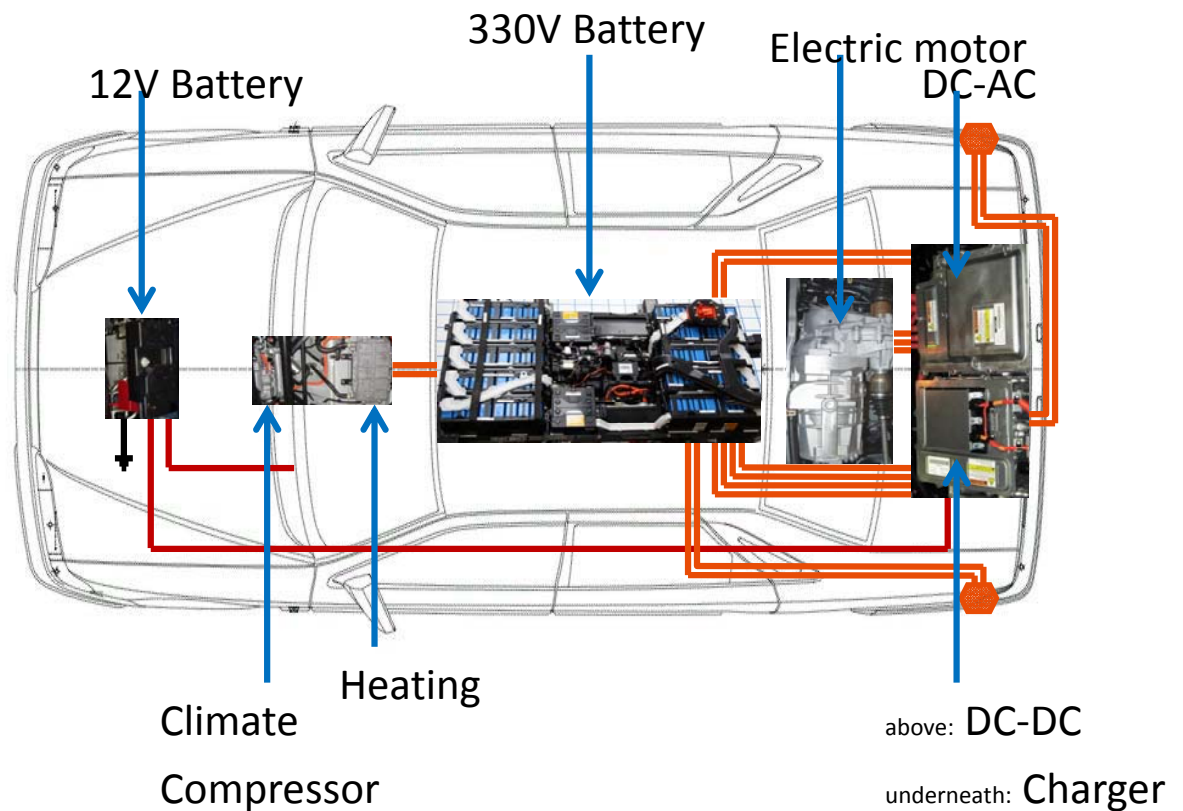


Figure 3.1.12: Photographical component view of a Mitsubishi i-MiEV

A topological view in Figure 3.1.13 and a photographical view in Figure 3.1.14 of Nissan's medium categorised and NCAP classed small family vehicle Nissan Leaf illustrate a completely different component structure comparing to the Mitsubishi i-MiEV. Only the HV battery is also fixed at the bottom of the vehicle body and provides energy for the electric engine, the HV heating and the climate compressor. Nissan's small family EV has front wheel drive with automatic transmission, so the electric engine is right above the front axle. The power inverter for the electric motor is stored under the engine hood next to the LV battery, which provides LV consumers with energy. The charger is right on top of the HV battery and the power converter is stored on top of the rear axles.

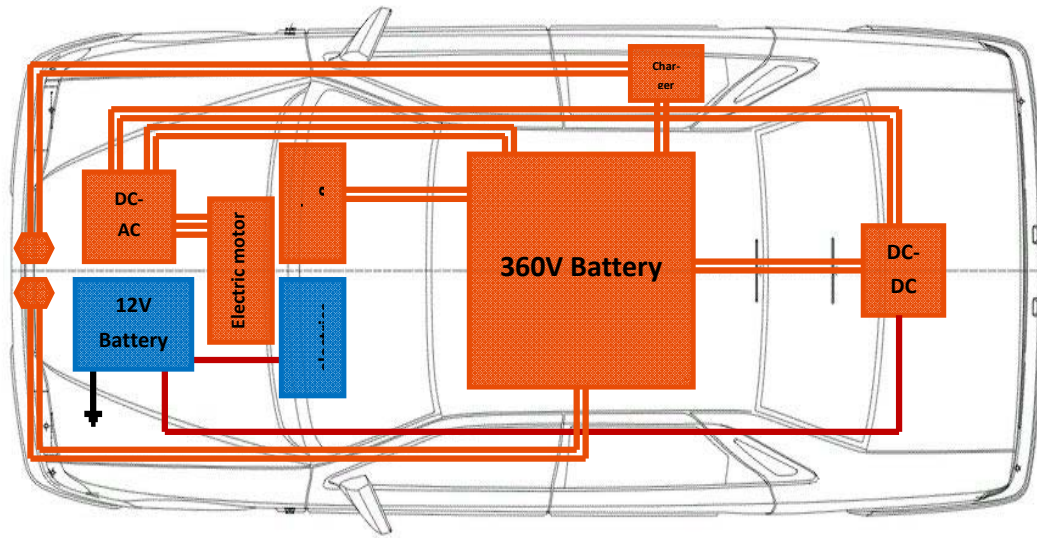


Figure 3.1.13: Topological view of a Nissan Leaf

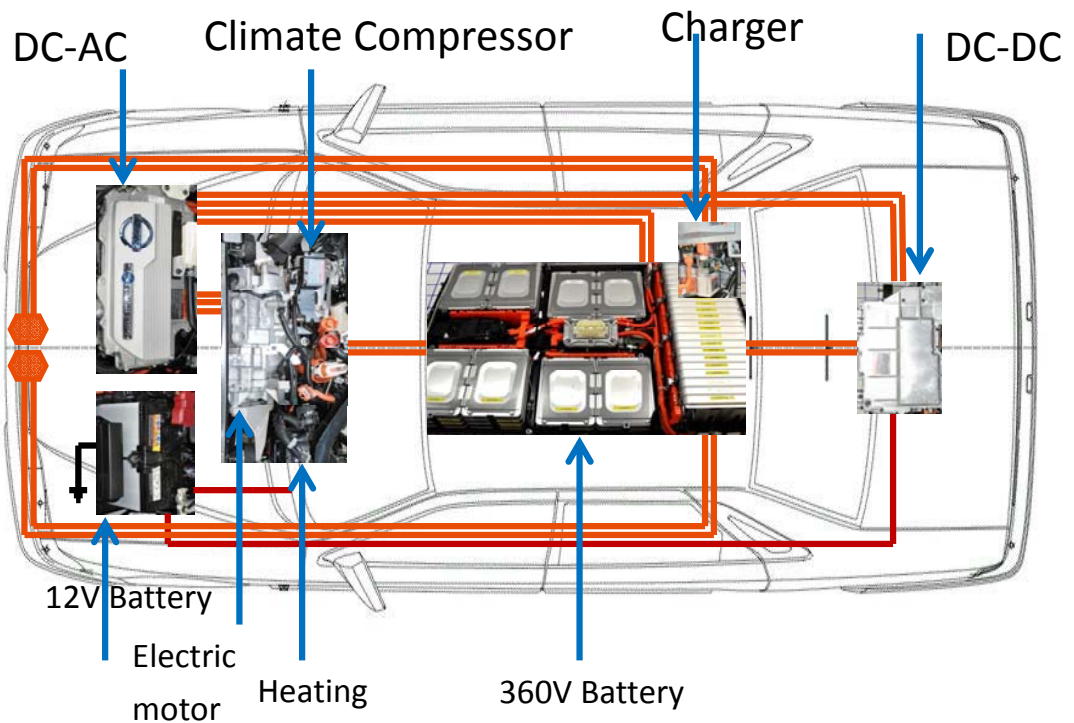


Figure 3.1.14: Photographical component view of a Nissan Leaf

Comparing these two EVs illustrates the manufacturer's possibilities in their strategic power circuit conception. Although, both the small categorised Mitsubishi i-MiEV and medium classified Nissan Leaf have different concepts regarding characteristics like size or weight and the resulting vehicle payload, the electrical engine is based on a nearly identical system, but in an absolutely different component structure and different component efficiency concerted to the vehicles characteristics. The Nissan Leaf's front wheel drive constitutes the only main system difference compared to the Mitsubishi i-MiEV's rear wheel drive. Reason for this completely different component structure, although the EV components are similar, is the independence of EV components. ICEs, in contrast, are massive and splitting the components up is practically only done in sports-oriented, front-engined (transaxle) vehicles like Ferrari, Porsche 944 and Alfa Romeo GTV.

Regarding EVs, the electrical components themselves can be placed everywhere in the car because of lesser size and the lacking need of a collective placement. Reason for this is the mechanical independence of electrical components – electric signals can easily be transmitted by wires. This facilitates the manufacturers not to be forced into standardised construction concepts. Only the HV battery pack's size and weight are significant resulting in a construction in the middle under the vehicle's body. More information for the battery pack's placement is considered in chapter 3.2.3 due to the regulated achievement of safety measures.

Altogether, the types of electrical system components are identical – as the types of mechanical components within a vehicle with ICE are identical. Components' capabilities are customisable and adaptable to the vehicle's characteristics and the manufacturer's intention. As a result, OEMs of EVs are rather uninhibited compared to those of vehicles with ICE regarding strategic conception of the engine's electrical system component structure.

To achieve a better general understanding of EV technology and to examine the functionalities of different OEMs vehicles, the WP6 team analysed all in WP6 used vehicles in this way.

3.1.3 Safety Aspects

Electrical and conventional vehicles must generally achieve the statutory requirements concerning safety. Comparing to vehicles with ICE, EV's electrical system safety, especially the HV components and battery packs safety, is separately regularised by automotive, electrical and telecommunication standards. This wide spectrum of standardisation areas poses a challenge for vehicle manufacturer's engineers. Above all, the IEC standards for electric system safety play a big role for EV technology.

Electric system safety:

In order to avoid injuries, HV components of EVs must be protected against direct and indirect contact. Direct contact is a person's direct contact (e.g. with his hands) into HV components. Indirect contact is the contact of HV components to other electricity conducting components (e.g. the vehicle's body). To avoid direct contact by persons in or outside the vehicle, the removal of protective devices and the access to

electrical equipment shall only be possible with tools or keys. Avoiding indirect contact means obviating the contact between electric equipment and any other component by adequate isolation.

Regarding the electric system safety in detail, environmental and deadly consequences are to be minimised concerning prevention of electric discharging and igniting. The HV battery, as the most critical component of EV's, must be protected against electrical, mechanical and chemical damage. To prevent an electric discharge, deformation of the HV battery packs must be avoided. Therefore, deformation volume is considered at the front, the rear and at the middle of the sides, shown in Figure 3.1.15, to eliminate the probability of the battery packs to get distorted. Collisions hitting the vehicle body from other positions would just turn the car around its centre of gravity and can be neglected. Reason for this high security level is the probability of igniting or explosion of the HV battery packs. Damage on HV battery packs, e.g. in case of short circuit or deformation, is critical due to the high concentrated chemical energy becoming free. Because of the battery pack's chemical reaction not being able to transform this released energy so fast, it is reacting thermal causing self-ignition of the battery. Furthermore, as it may not be possible to prevent damage on any HV component, there must be an automatic separation of the battery packs from the whole electric system in case of accident.

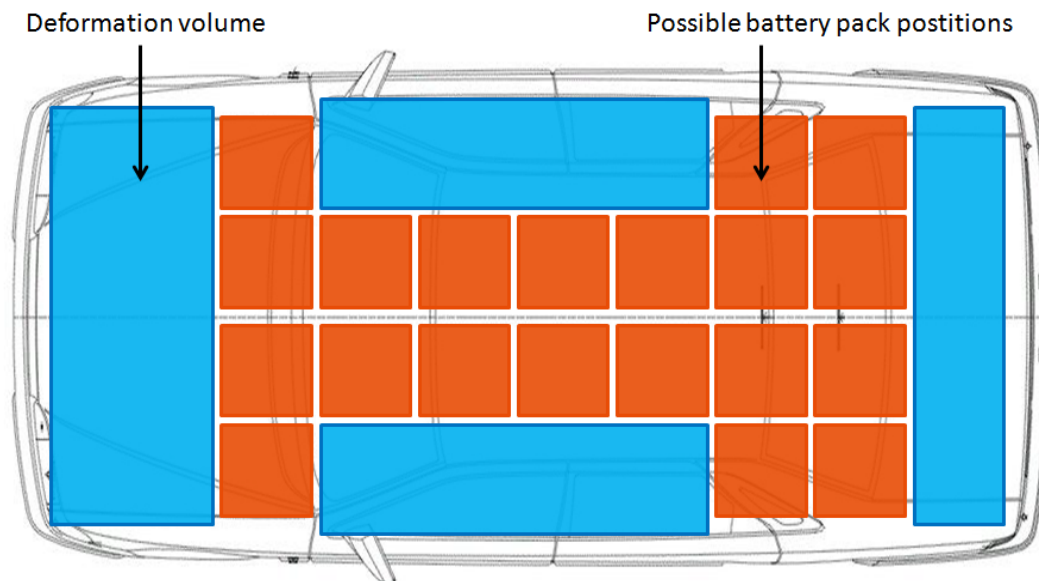


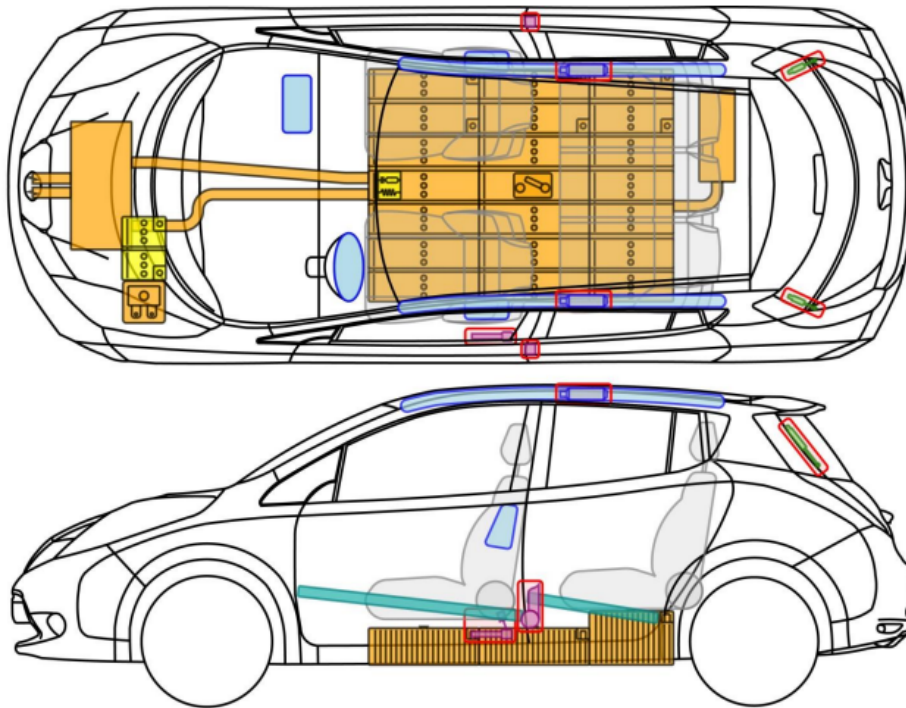
Figure 3.1.15: Topological view of an EV's deformation volume and HV battery pack positioning

Crash safety:

To improve the chances of being rescued while stuck into the vehicle in case of accident, rescue sheets, as depicted above in Figure 3.1.16, showing the main electrical components and the almost indestructible structural reinforcements, should be placed onto the driver's sun visor with an indication for rescue workers at the bottom left corner of the windscreen. Due to the fact that collisions from the side hitting the vehicle in the middle are the most dangerous for the passengers, structural reinforcements at the vehicle's side, also demonstrated in Figure 3.1.16 e.g. on a Nissan Leaf, prevent bigger deformation of the vehicle.

Regarding crash safety, especially electric system safety of next generation EVs, the following elements must be balanced: Positioning of safety related high-voltage components, deformation volume, crash performance, structural rigidity, vehicle weight and costs.

Positioning of safety related HV components becomes important, insofar as neither the battery packs nor any other high-voltage component should get damaged. Although there must be an emergency separation of the battery and high isolation resistances, residual voltages on HV components may not be completely diverted due to component damage. Based on minor energy density, the battery packs require more space than combustion engines of conventional vehicles so that deformation volume is auxiliary getting smaller. Smaller deformation volume causes the crash performance to get worse as the negative acceleration affecting on the passengers is getting bigger with less deformation distance in case of crash. The protective covering materials of the high-voltage components and the high priced stiffer materials to guarantee stability on smaller deformation volume adulterate the vehicles structural rigidity and increase the vehicles weight and its primary costs. In addition, raising the vehicles weight results in minor range.



Rescue Sheet standard translation (English)

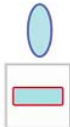














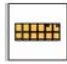

| | | | | | | | |
|---|--------------------------|---|--------------------------------|---|----------------------------------|---|-------------------------------|
|  | Airbag |  | Structural reinforcements |  | Control unit |  | Gas generator |
|  | Gas filled spring device |  | Battery |  | Active rollover protection |  | Seat belt tensioner |
|  | Seat belt tensioner |  | Fuel tank |  | Gas tank (NGT/LPG) |  | Safety valve (NGT/LPG system) |
|  | High-voltage components |  | High-voltage wire / components |  | High-voltage disconnection point |  | High-voltage battery |
|  | Mechanical sensor | | | | | | |

Figure 3.1.16: Rescue sheet from a Nissan Leaf

Functional safety:

The EV's functional system must ensure a reliable and safe performance of the vehicle. Due to an electric vehicle in several cases being completely silent, a system activation warning shall prevent unintentional activating of the traction circuit while standing still. Any movement of the EV during start-up because of excessive torque, overcurrent or fierce acceleration must be eliminated. Unintentional acceleration due to failures in electronic components must be prevented as a minor current deviation in small electric control components can cause massive differences in engine currents. The components must be isolated galvanic and against the infiltration or condensation of water. Electromagnetic interferences from the outside or between the components themselves must be avoided. Over speed protection of the electric motor must regulate revolution limits. Regenerative braking must not result in battery overcharge and the brake system's function must be top priority in all circumstances, especially, its function must be guaranteed and the driver must be warned early in case of the HV battery packs running low.

Charging safety:

While the vehicle's charging process is running, safety measures assure the impossibility of electrocution implying off-board, on-board and partially on-board charging systems. All charges must be protected against overcharge to sustain the battery's health. Off-board battery charging becomes interesting because of its possibility to rapidly charge EVs. Due to its dimension, implementing these kinds of chargers into the vehicle generally is neither possible nor efficient. On-board charging systems usually require a standard electrical socket, public loading stations and/or manufacturer's wall boxes. During both, off-board and on-board charge, the EV's body must be connected to the ground to avoid dangerous situation in case of fault. Partially on-board charging systems based on inductive energy transfer, does not have any electrical contact between the energy network and the EV itself. Besides of the absence of mechanical risks due to not required cables, the electrical safety is mainly very high because of the non-existent electrical slots. In all cases, the charging process itself must be regulated, insofar as the electrical system starts the charge with lower currents growing to a maximal charging speed with high currents and reducing the current when the battery is reaching its maximal SOC. In order to avoid internal voltages, the system must assure an equal loading status of all attached battery cells during charge and discharge. The battery charging system safety must also prevent battery overcharge.

To ensure safety to the user itself, but also to sustain the battery's SOH, the plug connector must be tied during the whole charging process and cannot be pulled out. Therefore, the electrical system is locking the plug-in mechanically while the system is charging. In addition, the HV battery packs must always be separated from the plug socket if the plug-in is removed. The electric circuit of the loading process is closed with inserted connector only.

Maintenance:

The EV's maintenance must be separated according to the person's technical know-how.

1. First-line maintenance includes only minor matters which can be performed by the ordinary user as a not trained electrician, in most cases by the owner itself. This user must be protected against all risks of direct contact. Owners should be introduced into that kind of issues they are in position to solve on their own by the purchasers. For safe and especially energy-efficient driving, EV's

owners should be trained - the electric engine's characteristics are quite different to those from ICEs. Discipline considering battery charging and efficient driving style is essential.

2. Second-line maintenance by workshops includes minor electrical and complete mechanical service. Servicemen have to be trained thoroughly for safe maintenance action if servicing EVs. HV batteries have to be disconnected before any intervention is done. Therefore, service plugs, as depicted in Figure 3.1.17, are installed to afford manual separation of the HV battery packs from the remaining electrical components.
3. Third-line maintenance, focusing major electrical repairs, is to be done by trained personnel only. EV's should be subjected to routine maintenance at regular service intervals to test electrical, functional and battery charging system safety.

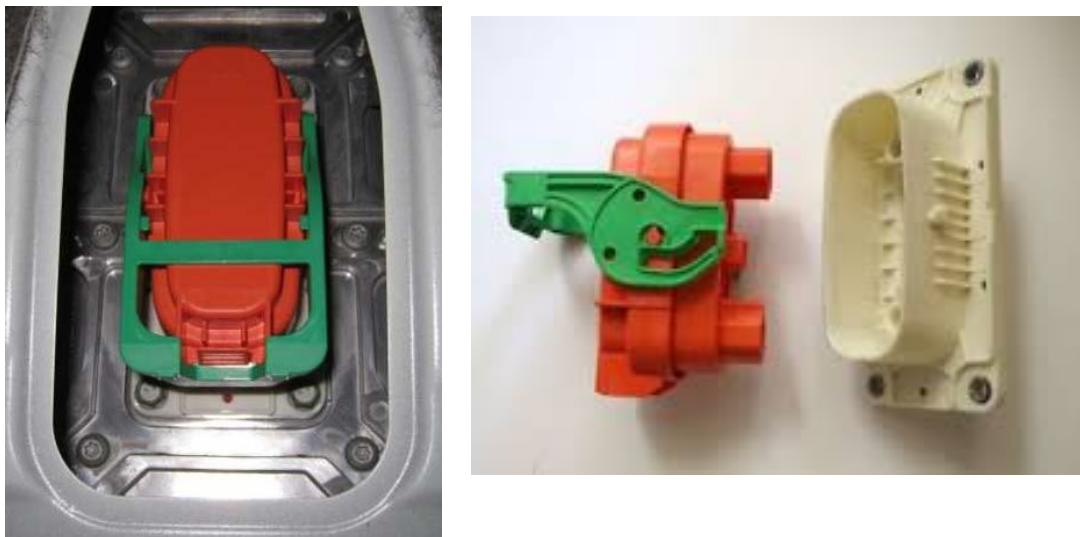


Figure 3.1.17: Service plug of a Nissan Leaf

Service plugs or service disconnect plugs, as depicted in Figure 3.1.17, have to be installed in every HV system as a manual disconnecting possibility of the HV battery packs. With a service plug pulled out, the HV power circuit is separated from the HV battery packs. As a result, all HV components except the battery packs itself are freed from electric voltage. The position of the service plug and the explanation on how to safely disconnect the HV battery is provided in the Emergency Response Guide (ERG). In case of the Nissan Leaf, the service disconnect plug is located under the carpet behind the centre console.

The modern EVs are also equipped with a so-called interlock system, which is a simple safety feature integrated into the HV system. In principle no battery can be turned off, but the battery can be separated from the remaining HV power circuit, which is exactly the purpose of the interlock system.

With respect to the safety assessments, the Nissan Leaf description represents the majority of the EVs used in the on-road tests, as they did all have similar safety features installed. Only the converted EVs, two converted Fiat Fiorino, had room for improvements in the safety area. Actually, these two EVs are in broad outlines alike in their conversions and therefore, only the Fiat Fiorino Enerblu is used in the description below.

In the Fiat Fiorino converted from ICE to EV by Enerblu, the structure of the retrofitted electrical system is to a great extent easily assessed for inspection compared to factory produced EVs. Therefore, this vehicle presents the opportunity to point out a number of features, which increases the safety level as well as a number of less appealing features.

The traction battery is divided into two and located in aluminium enclosures underneath the vehicle. It is worth mentioning the problems that a full metallic aluminium box presents from the EMC viewpoint. Aluminium is fully permeable, magnetically speaking, which is one of the reasons why this solution for the battery casing is not accepted among carmakers. There's the secondary problem of deformability in the event of a crash, especially in a steel intensive car.

All sense wires running from the battery cells are equipped with automatic fuses, very near to the cell terminals; this protects the sense wires, which otherwise would melt if shorted and could be a risk of fire. The power connectors located on the battery boxes are touch-safe and each battery box contains a contactor relay, which ensures that the power terminals are live only when the battery is active; while the ignition or the charger is on, these features can be seen in Figure 3.1.18 and Figure 3.1.3. Furthermore, by locating a contactor in each of the battery packs connected in series, redundancy is established, meaning that the battery current can be interrupted by the BMS, even if one of the contactors fails to open.



Figure 3.1.18: Touch safe power connectors

The BMS monitors, as expected, individual cell voltages and battery current. During functional test of the vehicle it has been found that the BMS do not interrupt the battery current at cell under voltage, before the battery current has hit 0 A. This prevents that the driver experiences sudden loss of traction power while driving, but increases the risk of deep discharge of the battery.



Figure 3.1.19: Fuse and Contactor relay in rear battery box

The wiring between the retrofitted main system components is performed in flexible black conduit. This protects the wires from sharp edges etc. However, a clear indication of conduits containing high voltage wires would be desirable. This could be obtained through the use of orange conduit for the high voltage part of the electrical system, as seen in modern EVs. Furthermore, the wiring below the vehicle is running in conduit in the left side of the transmission tunnel, this cabling could preferably have been performed less exposed. Please see Figure 3.1.20.



Figure 3.1.20: Wiring below the vehicle

3.2 Hypothesis and their analysis

In order to make a statement on the performance of EVs on the market, a total of eleven hypotheses were formulated in cooperation with vehicle manufacturers. The test program was then designed to deliver an answer to each of the eleven hypotheses:

1. Range and consumption are mainly dependent on drive pattern
2. Range and consumption depend strongly on the use of auxiliaries
3. SOH is predictable by step response testing
4. Climate has significant impact on battery performance
5. Battery performance is almost unaffected by battery charge rate
6. Heating and defrosting capacity is adequate
7. Regenerative braking adds significantly to vehicle range
8. Safety functions are maintained in the event of an empty battery
9. Optimum regenerative braking relies on battery and motor parameters
10. Vehicle Performance is almost unaffected by battery SOH
11. Propulsion energy is largely unaffected by climate conditions

There are a number of good reasons for choosing exactly those hypotheses. The main objectives are:

- Consumer understanding of why vehicle range is not constant
- Consumer understanding of the impact of auxiliaries usage
- A scientific contribution to the understanding of battery SOH
- Consumer understanding on how the driver should act to obtain better range
- Demonstration that driving performance does not die out like in simple battery toys
- Public assurance that independent tests are possible
- Demonstration of adequate winter performance of the OEM vehicles
- Demonstration that quick charging is safe for the vehicle
- Validation of the SOH estimated by vehicle OBD
- Demonstration of adequate winter comfort of the OEM vehicles
- Consumer understanding that traction power is independent of heating power etc.
- Possibly a simplified approach to SOH assessment
- Validation of basic safety functions in the OEM vehicles
- Demonstration of the regenerative braking ability of OEM vehicles in various conditions
- Consumer understanding of the quality difference between OEM and retrofit vehicles
- Consumer understanding of the possibilities and limitations of regenerative braking
- Consumer understanding of the benefits of regenerative braking
- Understanding of climatic influences and life expectancy

All together this report leads to a better understanding and debunking of myths, leading to less fear of the EV technology.

3.3 On road performance validation

Since there is no official test cycle to be used on the road for passenger vehicles, but only the NEDC, which due to its complexity only can be driven on a test bench (dynamometer), the team designed a new procedure named SORDS (Standardised On-Road Driving Schedule) inspired by the UITP-SORT test for city buses. The SORDS represents a fairly dynamic drive pattern, which results in an accelerated depletion of the traction battery. The SORDS cycle is explained in detail in deliverable 6.1⁵ as well as in chapter 4.

The first part of the schedule consists of start-stop sequences, representing swift urban driving, whereas the last part is a highly demanding highway stint at speeds up to 130 km/h ending up with a firm deceleration, putting especially high stress on the regenerative braking system. The length of the

⁵ Available at <http://www.greenemotion-project.eu/dissemination/deliverables-evaluations-demonstrations.php>

schedule is 3000 m. The expected mean duration is 243 sec and the average effective speed is 44.44 km/h. This includes four pauses of 10 sec each.

3.4 Climate impact, dynamometer measurements

To validate the on-road measurements and provide a link to official tests, electric vehicles were also tested on dynamometers. Some of these measurements were performed in a climate chamber at different temperatures to assess the climatic impact. Due to the controlled environment in the laboratory the dynamometer tests can be used as baseline for comparison with on-road tests. As such they are complementary to the on-road SORDS tests performed by the partners in WP6.

Both of the methods of measurement (CAN logging and power analysers) explained in chapter 4 were used during the dynamometer tests. Different climatic environments, cycles (SORDS and NEDC), and settings for the auxiliary systems were used during the tests as explained in the next chapter.

4 Analysis of hypothesis, on road performance validation

This chapter describes the on road testing and especially the results from this testing. The background of the procedures and analysis can be taken from the deliverable 6.1.

4.1 Test track conditions

Two test locations have been used for the on road climate testing in the field, the airfields of Værløse and Karup in Denmark. The test tracks are equally 1500 m long at the two locations. The driving scheme for both tracks is shown in Figure 4.1.1.

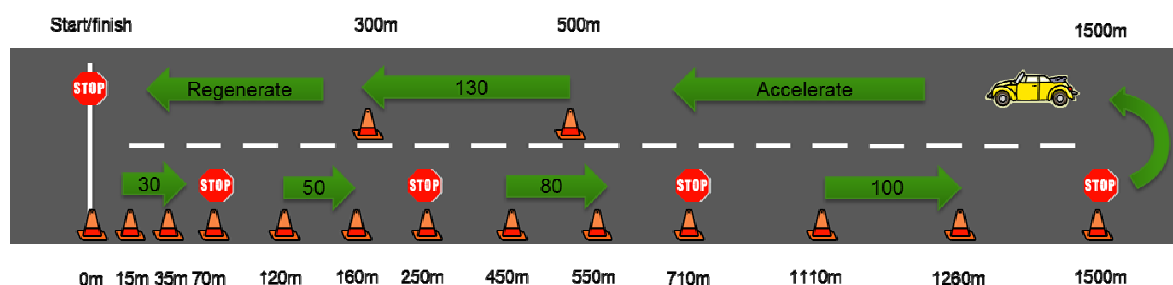


Figure 4.1.1: Illustration of the SORDS scheme on the test track

In order to make a precise and realistic analysis, weather conditions as well as height, direction, speed etc. were monitored via GPS-communication. Detailed weather information on air temperature and wind conditions were collected from the airport in Karup as well as from the Danish Meteorological Institute in 2013 and 2014. These are shown in Figure 4.1.2 and Figure 4.1.3.

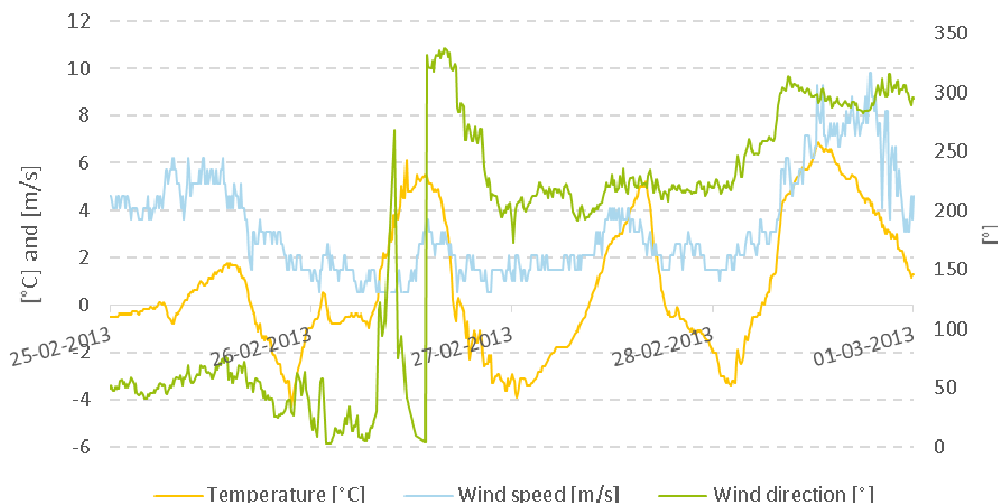


Figure 4.1.2: Weather conditions during test week in Karup 2013

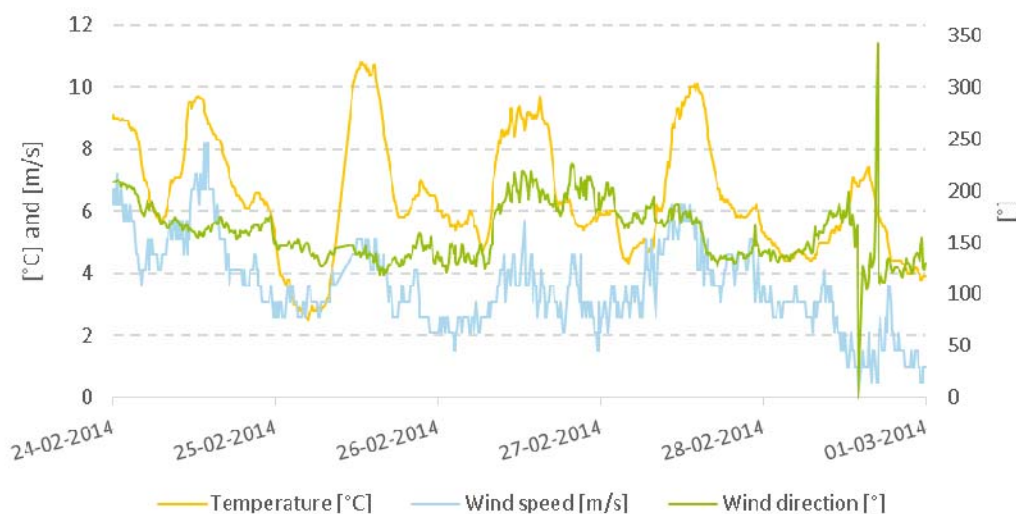


Figure 4.1.3: Weather conditions during test week in Karup 2014

A generic overview on the weather conditions is given in Table 4.1.

| Location | | Værløse | Karup | Karup |
|-------------------------|-----|--|---|---|
| Weather station | | Viborg | Karup | Karup |
| Year / week | | 2012 / 10 | 2013 / 9 | 2014 / 9 |
| Period | | 5 th -9 th March | 25 th -28 th February | 24 th -27 th February |
| Mean air temperature | °C | 3.9 | 1.3 | 5.9 |
| Normal air temperature | °C | 1.4 | 0.0 | 0.0 |
| Maximum air temperature | °C | 8.2 | 7.3 | 10.9 |
| Minimum air temperature | °C | -0.6 | -4.5 | 2.4 |
| Precipitation sum week | mm | 11.0 | 0.6 | 10.5 |
| Mean wind speed | m/s | 5.8 | 3.9 | 3.3 |
| Maximum wind speed | m/s | 17.1 | 17.0 | 12.9 |
| Wind direction | | SE-W | N-SW | S-SE |
| Sun hours week | h | 13 | 20 | 28 |
| Humidity | % | 80-95 | 85-100 | 80-90 |
| Pressure | hPa | 1015-1030 | 1025-1035 | 1005-1015 |

Table 4.1: Weather conditions at test tracks

Værløse Airfield is located in the north-eastern Zealand near Copenhagen. The test track was located at the actual runway, a perfect straight line, see Figure 4.1.4. The airfield has not been in operation since 2004, but in 2013 the airfield was opened to the public and therefore the test track was moved to Karup Airfield instead.



Figure 4.1.4: Test track 2012, Værløse Airfield

Karup Airfield is operated as a military facility located in the middle of Jutland between the cities of Viborg, Herning and Silkeborg. The test track was established on the old taxi way, because the runway is still in operation as an airport for military and domestic flights. Figure 4.1.5 displays the test track from an air perspective.



Figure 4.1.5: Test track 2013 and 2014, Karup Airfield

For a proper and comparable analysis, a detailed analysis of the tracks regarding the height profile had to be done. As shown in Figure 4.1.6, the test track in Karup was more flat than in Værløse. Both test tracks had a slope in the start and flattened out in 500 m to 800 m. In Karup, the test track was slightly curved in the far end.

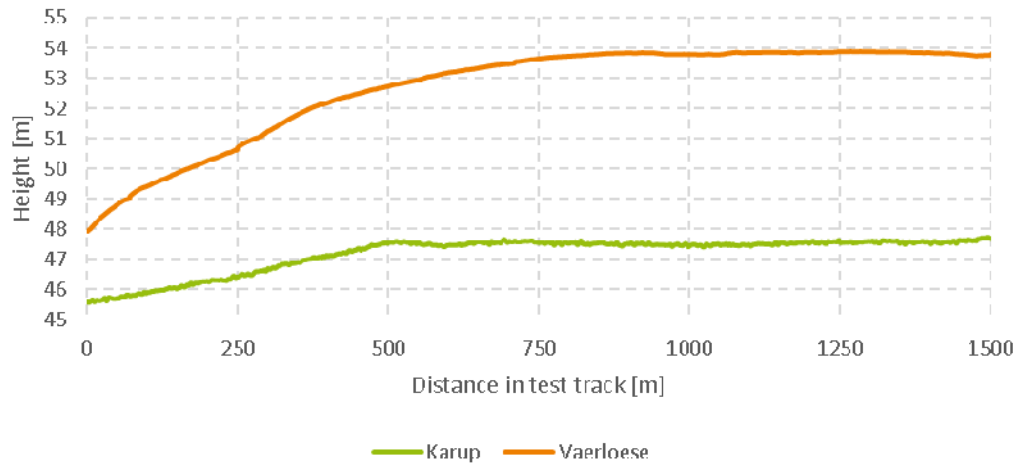


Figure 4.1.6: Height profile of the test tracks

An overall impression of the test tracks is given in Figure 4.1.7 and Figure 4.1.8.



Figure 4.1.7: Start of test track, Værløse 2012



Figure 4.1.8: Start of test track, Karup 2013

The equipment and basic infrastructure equipment (base camp and BAT Mobile) for doing the measurements, as described in detail in D6.1, are shown in Figure 4.1.9.



Figure 4.1.9: Test track, Karup 2014, the base area

4.2 Vehicles used in the on-road tests

The used vehicles for the on road EV performance validation are shown Figure 4.2.1. For evaluating the differences between EV technology and ICE technology in addition also the vehicles in Figure 4.2.2 were used (one rental car, and two private cars (diesel and gasoline)).



Opel Ampera - Plug-in hybrid



Fiat Fiorino Micro-Vett – Converted EV



Renault Fluence ZE



Nissan Leaf



Mitsubishi i-MiEV



Tesla Model S

Figure 4.2.1: Overview of the actual EVs used in the on-road tests



Volkswagen Touran - Diesel



Ford C-max - Diesel



Mazda 6 - Gasoline

Figure 4.2.2: Overview of ICE vehicles used in the on-road tests

All the vehicles used in the on-road tests, including their mileage and model year, are shown in Table 4.2.

| EVs | Model year | Mileage 2012 | Mileage 2013 | Mileage 2014 |
|-------------------------|------------|--------------|--------------|--------------|
| Mitsubishi i-MiEV | 2010 | 3,600 km | 7,700 km | 11,400 km |
| Nissan Leaf #1 | 2011 | - | 50 km | - |
| Nissan Leaf #2 | 2011 | - | - | 3,300 km |
| Renault Fluence ZE #1 | 2012 | - | 500 km | - |
| Renault Fluence ZE #2 | 2012 | - | - | 25,900 km |
| Opel Ampera #1 | 2012 | - | 17,500 km | - |
| Opel Ampera #2 | 2012 | - | - | 2,600 km |
| Fiat Fiorino Micro-Vett | 2009 | 8,000 km | 12,100 km | - |
| Fiat Fiorino Enerblu | 2010 | - | - | 14,000 km |
| Tesla Model S 85P | 2013 | - | - | 7,500 km |
| ICE vehicles | | | | |
| Volkswagen Touran | 2004 | - | - | 273,000 km |
| Mazda 6 | 2008 | 91,000 | 105,000 km | 119,000 |
| Ford C-max | 2012 | - | ~30,000 km | - |

Table 4.2: Mileages of the vehicles used in the on-road tests – rounded values

4.3 Theory in short

To sum up the methodology used to calculate the energy balance, the influencing factors are briefly explained here. For a more detailed explanation see D6.1.

The term VLFC is defined as the minimum theoretical energy consumption over a given distance (kWh/100km) or the shaft power (kW) necessary to rotate the wheels at any given moment. It consists of four factors, which have to be neutralised for the vehicle to move. These factors are wind resistance, rolling resistance, potential energy and kinetic energy.

Wind resistance originates from the air molecules, which have to be pushed aside, when the vehicle is driven forward. The air has a certain density depending on its temperature. Vehicle's specific aerodynamics exerts influence on the wind resistance, especially the vehicle's frontal area.

Rolling resistance is caused by the deformation of the tires onto the road surface. The tires contribute a constant resistance for the specific vehicle because the tires and the mass of the vehicle are constant. The test areas' road surfaces are relatively uniform resulting in almost constant values.

To move any vehicle, it needs to be supplied with energy. In case of acceleration, kinetic energy is gained in the mass of the vehicle simply by the fact that it is moving. When the propulsion of the vehicle stops, the accumulated kinetic energy is released by prolonging the ongoing movement. The moving vehicle can gain potential energy by travelling uphill and release it again when moving downhill.

Please note that the accumulated kinetic energy, when accelerating a vehicle up in speed, is not lost, it is stored for later use. Therefore, the total energy consumption should be filtered for kinetic energy to see the true consumption during acceleration through the following expression:

$$\begin{aligned} \text{Acceleration consumption} \\ = \text{Total energy consumption} - \text{kinetic energy accumulated} \end{aligned} \quad (1)$$

In addition to the VLFC, a vehicle always has some auxiliary consumption or idle consumption. While heaters in vehicles with ICE are contributed by the thermal energy loss of the motor, energy for EV's heating processes must be supplied by the battery. Auxiliary energy for powering head lights, ventilation, air-conditioning, etc., is needed in both types of vehicles.

In addition to the above mentioned, every vehicle has an energy loss in the powertrain. This loss of energy is primarily influenced by the characteristics of the gear box, the differential drive, the ball bearings, etc., and cannot be avoided.

The last important part of the energy balance is the energy used for braking. To stop a moving vehicle the kinetic and/or potential energy need to be transferred to something else. It is possible to drive in freewheel clutch until the vehicle stops by the influence of resistance factors, but typically, the stopping process involves friction braking, which dissipates the energy as heat in the brake discs. In EVs, it is possible to regenerate a large part of the braking energy as electrical energy via the recuperation of the electric motor.

The True Powertrain And Braking Efficiency (True PABE) is defined as the electro-mechanical efficiency, which includes energy lost in the braking system but excludes the auxiliary consumption in the EV case:

$$\text{True PABE} = \frac{\text{VLFC}}{\text{Total energy consumption} - \text{auxiliary consumption}} \quad (2)$$

For the calculation of the maximal available energy, which can theoretically be regenerated during the braking process of constant deceleration in each SORDS section, this will be further explained in the formulas (9) to (16) on page 80.

As a matter of statistics, all the drive tests in this report have been repeated three to five times. Based on these data, mean value and variance have been calculated to approximate the true values. Variances are expected due to the human factor of the driver of the vehicles and the fact that different drivers were driving throughout the tests. The calculated variance is shown when possible.

4.4 Hypothesis 1: Range and consumption are mainly dependent on drive pattern

Figure 4.4.1 illustrates the difference between the NEDC and the SORDS cycle. The SORDS is an outdoor on-road test in the natural climate conditions for the time of testing, where the NEDC is performed in a controlled laboratory facility – the vehicle is fixated on a dynamometer in an acclimatised (warm) room.

Therefore, when going from the NEDC to the SORDS, the extra consumption from the natural conditions need to be added on top. Natural conditions such as the influence from the present road surface, wind, increased air density and need for heating due to low ambient temperature, increased vehicle speed (etc.).

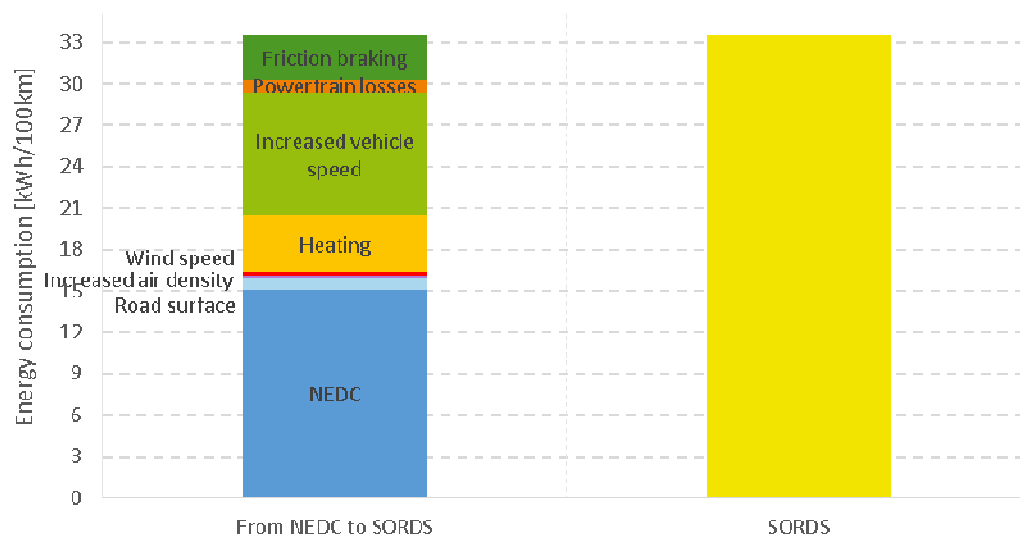


Figure 4.4.1: Exemplary NEDC versus SORDS consumption

The predominant factors which separate NEDC from SORDS are:

- Difference in speed
- Heating
- Aggressive braking

Figure 4.4.2 compares the NEDC and the SORDS in speed and time. The SORDS is more aggressive than the NEDC, because of the larger variation in speed. The SORDS has higher top and mean speed and harder braking.

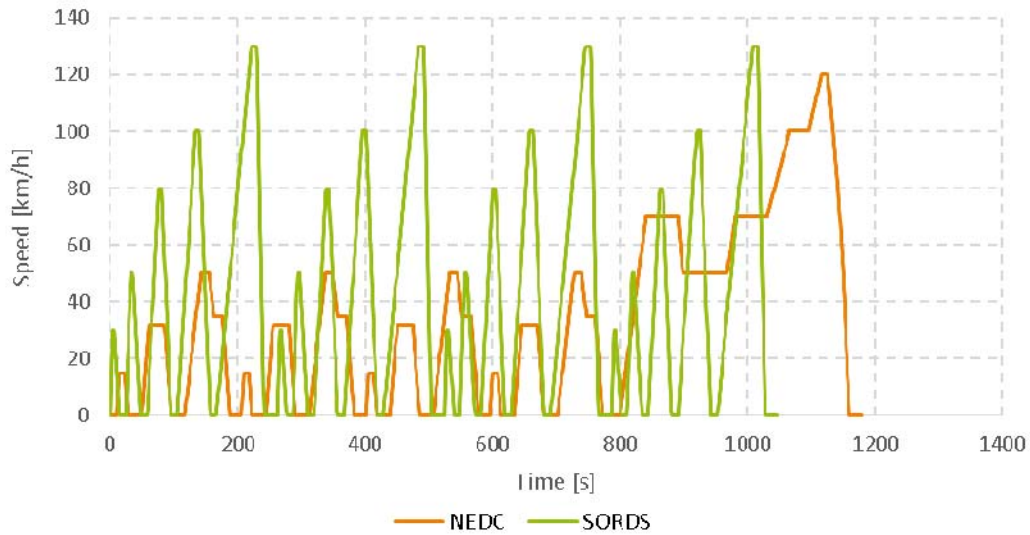


Figure 4.4.2: NEDC versus four repetitions of SORDS shown in speed and time

4.4.1 Steady speed

According to the laws of physics - the higher the vehicle's speed, the higher the influence of wind resistance.

The rolling resistance will be almost constant, because neither the tires nor the road, nor mass of the vehicle changes during the test. Rolling resistance does not depend on the drive pattern.

The auxiliary consumption depends on comforts and safety equipment (like climatic control, lighting, etc.), hence it is not directly depending on the drive pattern.

During low speeds, the auxiliary consumption represents a very big percentage of the total consumption, but the percentage of the auxiliary consumption will decrease with higher speed, as known from the idle consumption in vehicles with ICE.

The steady speed test was performed simply by driving with steady speed (constant) throughout the test track. Due to the test track having small variations in height, the testing of each target speed was repeated in both directions to compensate for the general slope of the track. While driving at steady speed, no kinetic energy should be gained. Any energy gain is resulting from imperfections or the slope. The effective wind resistance is also included in the graphs.

In addition, neither regeneration nor braking energy should exist while driving at steady speed.

Summing the bars horizontally in the graphs in the followed sections give the total DC consumption from battery in the given situation.

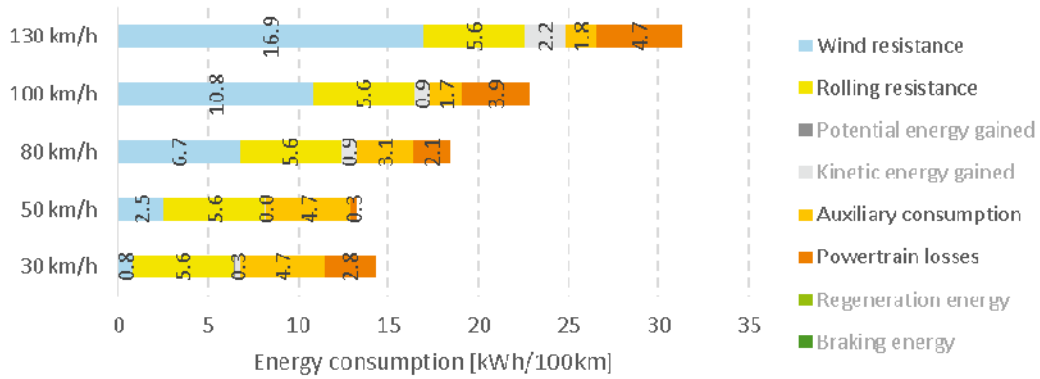


Figure 4.4.3: Energy consumption with a small size EV from driving steady at different target speeds, illustrated by the Mitsubishi i-MiEV

At high speeds, the wind resistance is relatively high for small sized EVs, as depicted in Figure 4.4.3, because of its relatively large frontal area. Low rolling resistances are based on its small tires and light weight resulting in minor needed amounts of total energy.

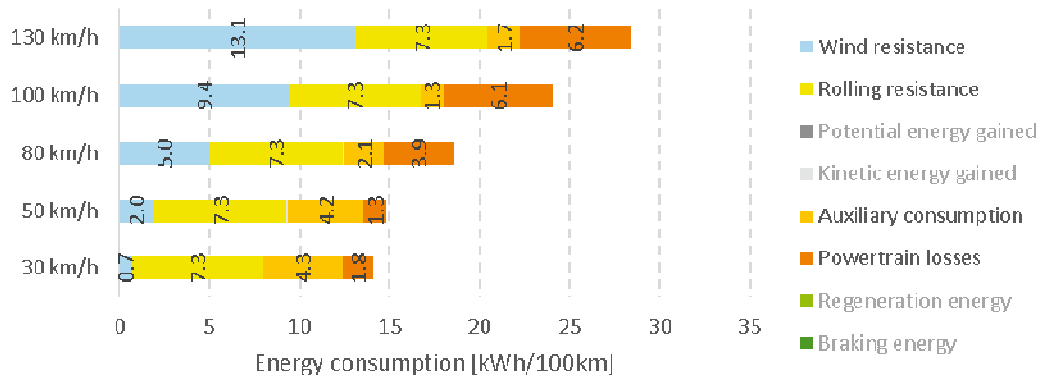


Figure 4.4.4: Energy consumption with a medium size EV from driving steady at different target speeds, illustrated by the Nissan Leaf

However, at highway speeds the larger, more aerodynamic vehicle consumes less. The small difference due to auxiliary consumption cannot be attributed directly to the vehicle. However, heat pump, LED lighting etc. can.

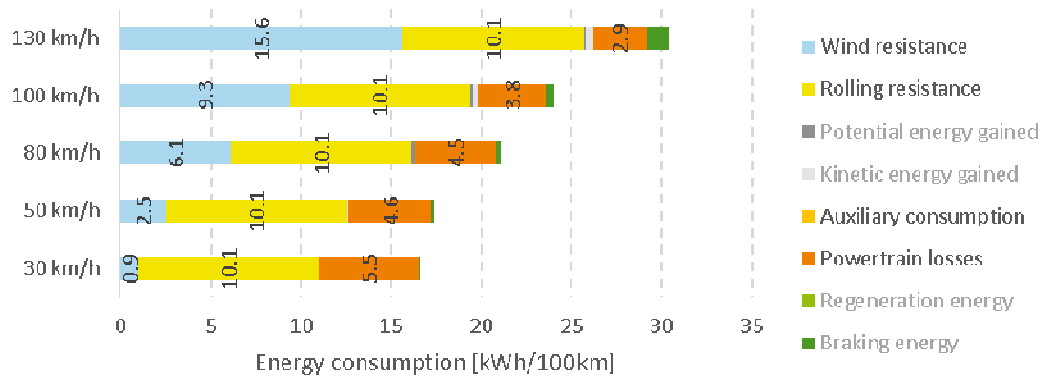


Figure 4.4.5: Energy consumption from driving steady with a large size EV at different target speeds, illustrated by the Tesla Model S

The large size EVs in Figure 4.4.5 are surprisingly similar to the smaller EVs.

4.4.2 Dynamic driving

Dynamic driving means driving the SORDS test scheme. The energy consumption for dynamic driving is shown as the consumption for total SORDS combined with the consumption for the individual SORDS speed sections. The SORDS may be viewed as five individual sections with target speeds 30, 50, 80, 100 and 130 km/h, see Figure 4.1.1 for the detailed SORDS scheme, but by computing the energy balances of each section, the influence of acceleration, braking, etc., are revealed.

Again, the test track presents small variations in height, which introduces marginal gain of potential energy. The potential energy is zero for the total SORDS, because the geographic end point is the same as the starting point. The individual speed sections have minor gain in potential energy, as the test track has some small variations in height. Each individual speed in the SORDS testing is performed at a different part of the test track. Therefore, the slope is different, but can be compared throughout the different speeds. The potential energy is included.

When driving SORDS, the test starts and ends at 0 km/h and therefore the kinetic energy should be zero.

As the SORDS includes deceleration, the regeneration and braking energy appear significantly.

The regeneration energy depends on the speed, the driver's capabilities and the vehicle parameters. The maximum regeneration energy varies with the vehicle.

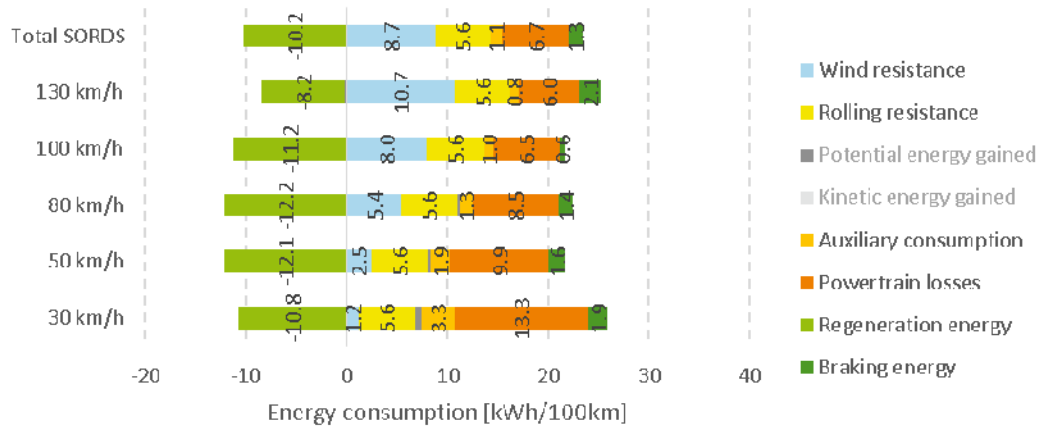


Figure 4.4.6: Energy consumption from driving dynamically with a small EV at different target speeds, illustrated by Mitsubishi i-MiEV

The powertrain losses are more significant at low speeds with the small size EV, as shown in Figure 4.4.6. The regeneration has its optimum near 80 km/h, because the regeneration power hits the maximum limit around this speed. A large part of the braking energy is regenerated.

Overall the dynamic driving does not raise the energy consumption drastically.

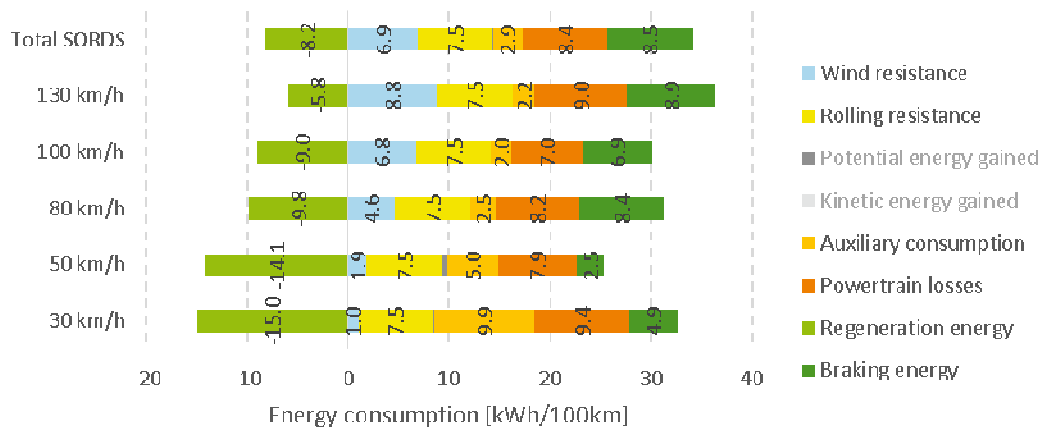


Figure 4.4.7: Energy consumption from driving dynamically with a medium size EV at different target speeds, illustrated by the Nissan Leaf

The medium size EV in Figure 4.4.7 has relatively constant powertrain losses, but it also has a significant amount of braking energy not regenerated. This is caused by the regeneration power limit in combination with the weight of the vehicle.

The impact of driving dynamically with the larger EV is significant greater than for the smaller, lighter EV.

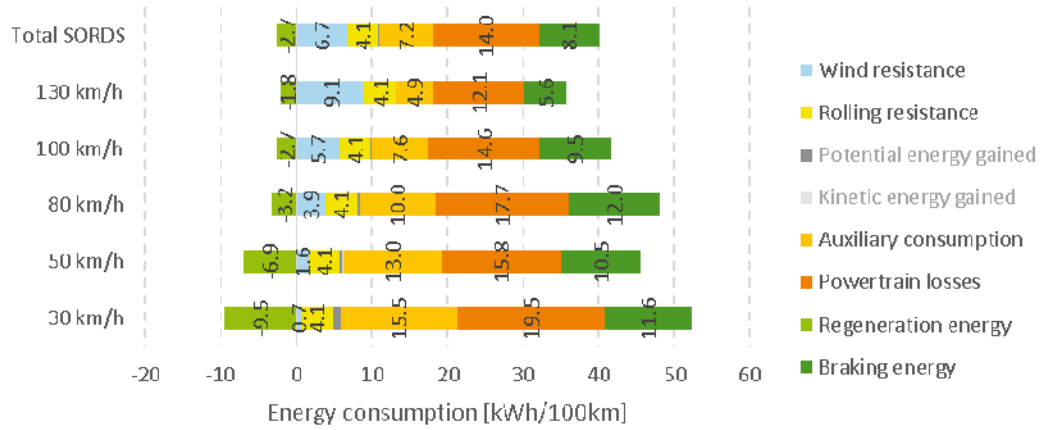


Figure 4.4.8: Energy consumption from driving dynamically with a medium size EV at different target speeds, illustrated by the Fiat Fiorino Micro-Vett Micro-Vett

In Figure 4.4.8 a medium size converted EV with low capability of regeneration is shown. The clutch and gearbox are retained while converting, which, in combination with the desire of a long range, results in choosing a relatively small motor. This results in a dramatic increase in consumption.

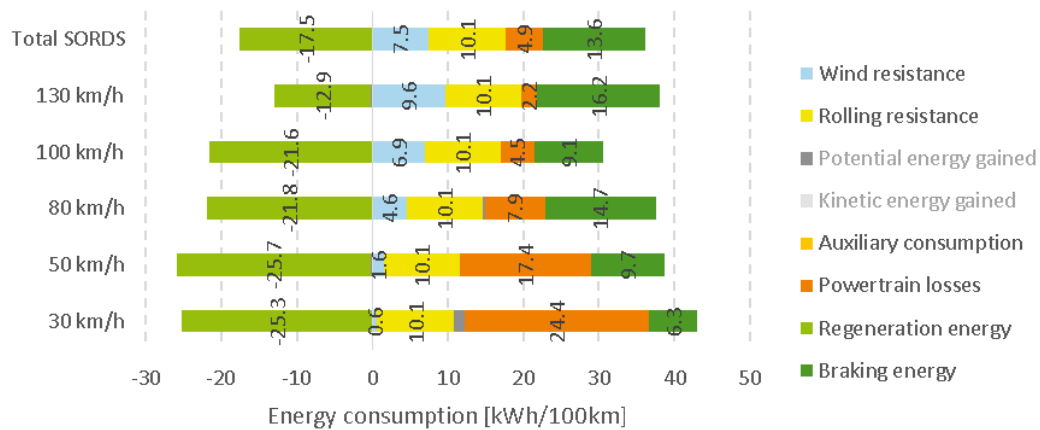


Figure 4.4.9: Energy consumption from driving dynamically with a large size EV at different target speeds, illustrated by the Tesla Model S

While driving dynamically with the large size EV, the energy consumption is lower than expected. The consumption seems not to be proportional to weight and motor size of the EV, but looking at the total energy balance, including the regeneration energy, it actually explains the case. Even though the heavier

vehicle uses more energy, it is able to regenerate a larger part of the energy, reducing the net energy consumption.

So in this case, a larger motor actually saves energy!

4.4.3 Full acceleration

The acceleration test has been performed on a straight line with the throttle pedal fully depressed.

Using full acceleration is known to consume a lot of energy, partly because conventional vehicles need high engine RPM to achieve maximum power. Taking a conventional engine to high RPM creates high losses due to mechanical friction and exponentially growing gas flow resistances. However on electric motors the efficiency might still be relatively high.

When full acceleration starts from 0 km/h the electric torque is usually restricted in order to ensure a smooth start and to save the motor from thermal overload (sometimes on small motors the level of torque is allowed to peak higher than usual) until the speed is 30-40 km/h. From here the traction torque is typically held at the highest continuous value allowed by the motor until the maximum electrical power is reached. When maximum speed is approaching the power is then gradually turned down even if the driver keeps the pedal fully depressed. This entire process can be seen in Figure 4.13.4 - Figure 4.13.5 on page 89. In reality no vehicle can keep on accelerating forever. Electric vehicles are top speed restricted mainly to avoid excessive use of battery energy.

The above mentioned, combined with the fact that the speed increases, results in a decrease in the energy consumption per travelled distance.

Wind and rolling resistances still exert influence, but in minor percentage compared to steady speed and dynamic driving.

Potential energy is gained during full acceleration, if there is a slope, but the values are very small. In contrast to driving at steady speed or dynamic, the full acceleration testing, while driving in a straight line, shows a gain in kinetic energy, because this test actually ends at high speed.

As mentioned in section 4.3 the kinetic energy is not actually lost in the process of acceleration, but rather stored for later use. Therefore kinetic energy is shown separately with a dotted line in the following 3 figures. The efficiency of the acceleration process is illustrated by the relation between kinetic energy gained and total energy lost in the process.

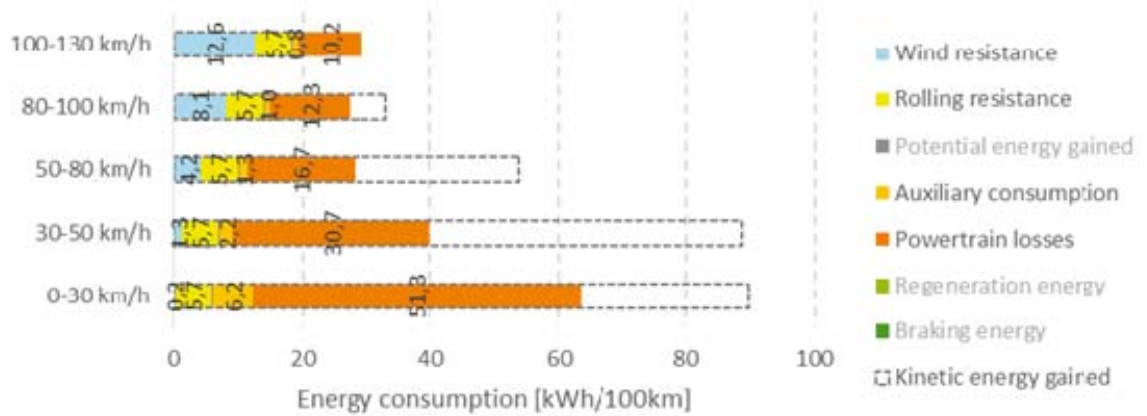


Figure 4.4.10: Energy consumption from driving with full acceleration with a small size EV at different speed intervals, illustrated by the Mitsubishi i-MiEV

Figure 4.4.10 illustrates the lesser importance of wind and rolling resistances at small size EVs during full acceleration. The powertrain losses are significant at lower speeds. The total energy consumption is relatively low due to the light weight of the small size EV.

The medium size EV, see Figure 4.4.11, shows the same characteristics regarding the resistances, but the powertrain losses at low speeds are even higher. The total energy consumption is higher than those from the small size EV according to the heavier weight.

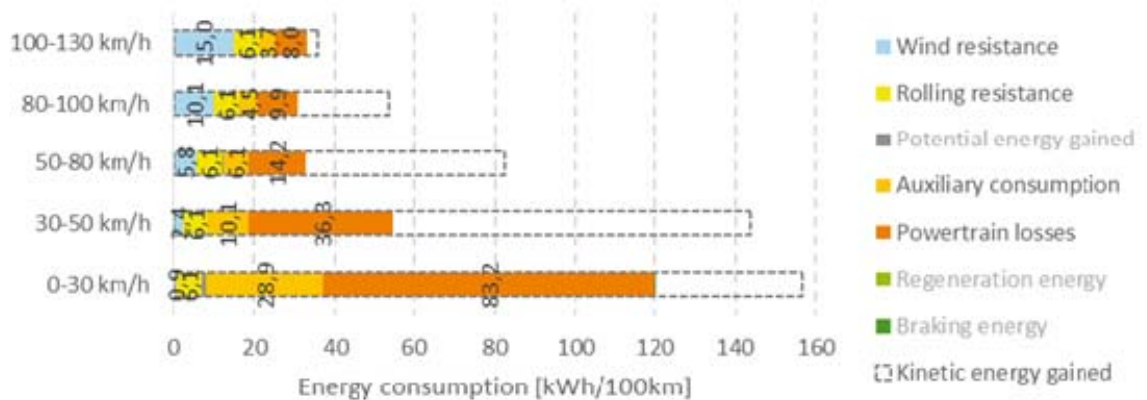


Figure 4.4.11: Energy consumption from driving with full acceleration with a medium size EV at different speed intervals, illustrated by the Renault Fluence

Still the efficiency is quite good from 50 km/h and above. The kinetic energy is not lost, but accumulated, so accelerating from 50 km/h and upwards is actually quite economic. This is seen more clearly in Figure 4.4.13 on page 57 where the efficiency at full acceleration is actually 75 - 80 %.

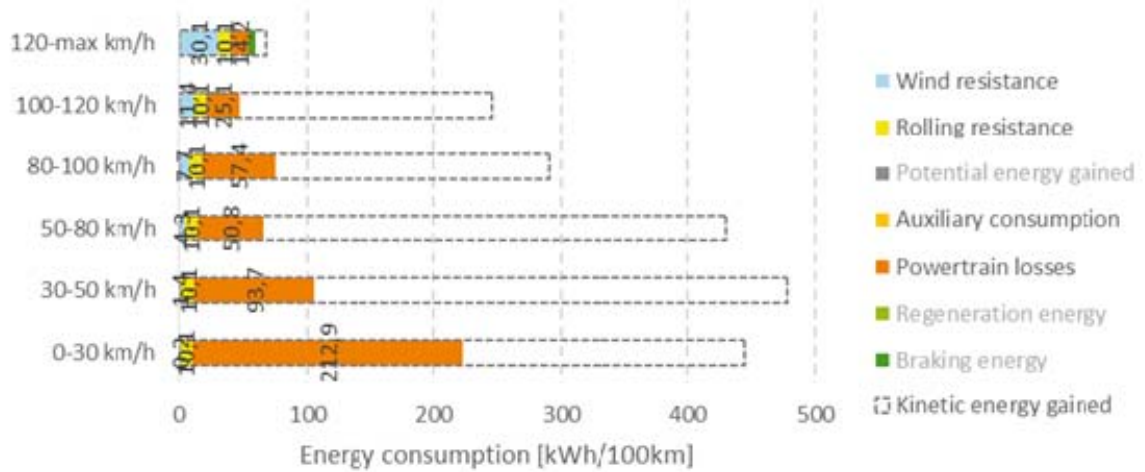


Figure 4.4.12: Energy consumption from driving with full acceleration with a large size EV at different speed intervals, illustrated by the Tesla Model S

The fact that the large size EV has a huge motor power and high weight is clearly shown in Figure 4.4.12. This results in high total energy consumption, but a very large part of the energy is accumulated in kinetic energy. The powertrain losses are high at low speeds, but at higher speeds the losses seem to be the same as those from other EVs. This is because the highest powertrain losses occur when starting from stand-still and in the low speed regions, which is identical for all vehicles in general.

4.4.4 Combinations of dynamic and steady driving

To predict the ideal combination in the drive pattern for a vehicle, the energy consumption and the PABE need to be compared. The total energy consumption and PABE, for each EV, are compared between full acceleration, dynamic and steady driving.

In general, the highest energy consumption per driven distance is found during full acceleration in the low speed region, though it decreases with increasing speed. This is combined with the overall highest PABE, though also increasing with the speed to show that the highest energy flow is not equal to low efficiency (coast and burn).

The energy consumption for acceleration and steady driving converge, because when the maximum speed is achieved during acceleration, the vehicle cannot continue accelerating, hence the speed becomes steady.

The lowest energy consumption can be seen during steady driving, which actually doubles followed by the dynamic driving.

The poorest PABE is typically seen at the low speed dynamic driving, but increasing with the speed. In the lowest speed of the SORDS (30 km/h), the acceleration power is highest and the driver needs to use the friction brakes to be able to decelerate the vehicle in the required distance. Dissipating the kinetic energy as heat in the braking discs decreases the PABE of the low speed SORDS, which happens a lot during dynamic driving.

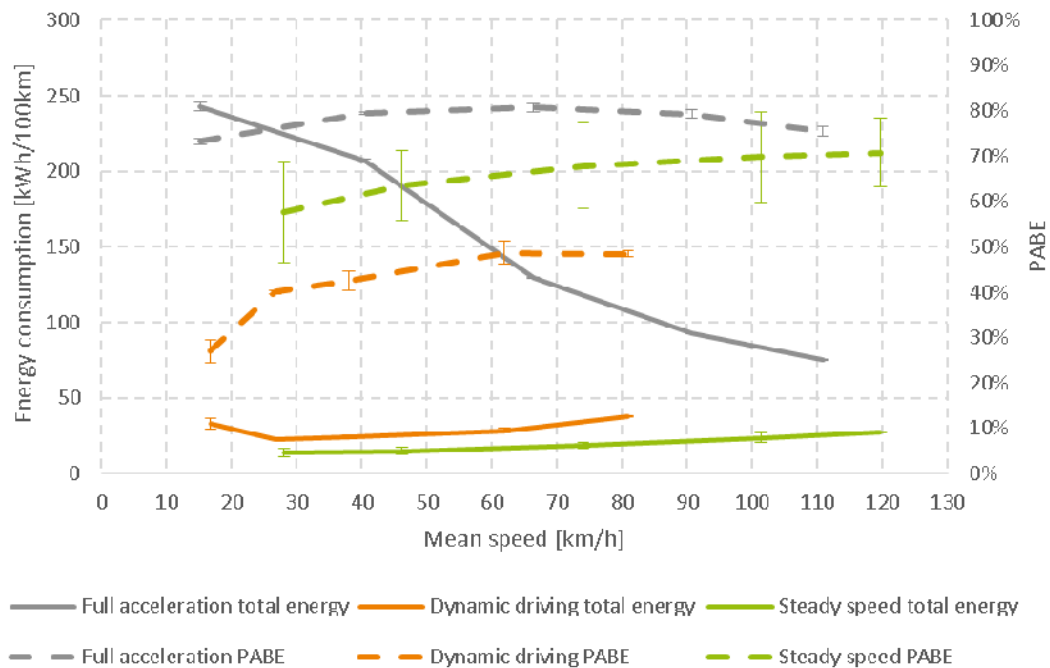


Figure 4.4.13: Total energy consumption and PABE, illustrated by the Nissan Leaf

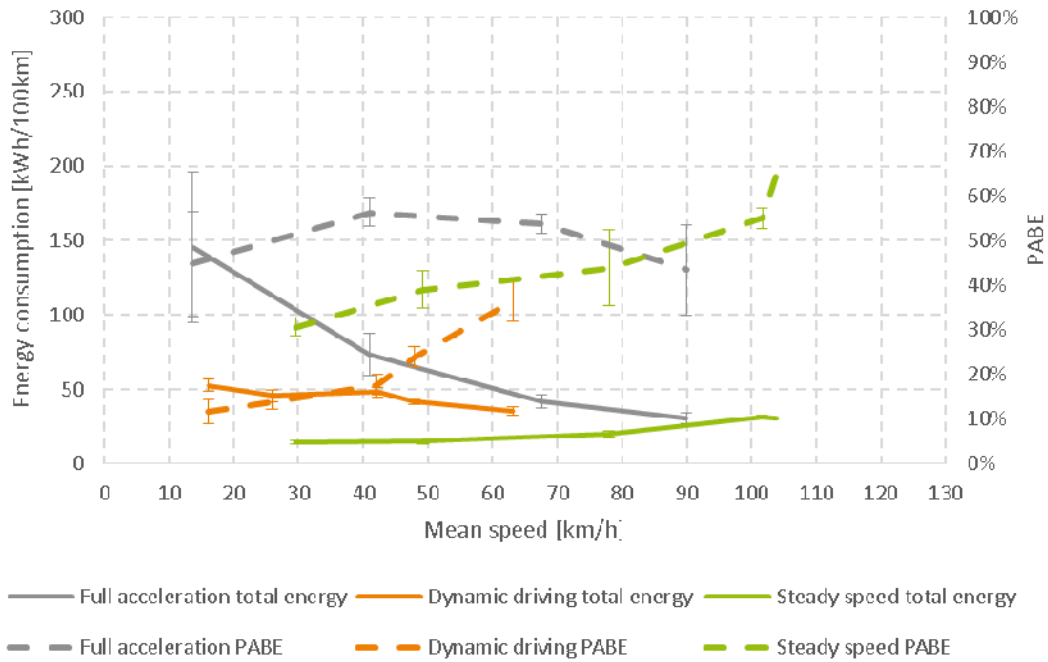


Figure 4.4.14: Total energy consumption and PABE, illustrated by the Fiat Fiorino Micro-Vett

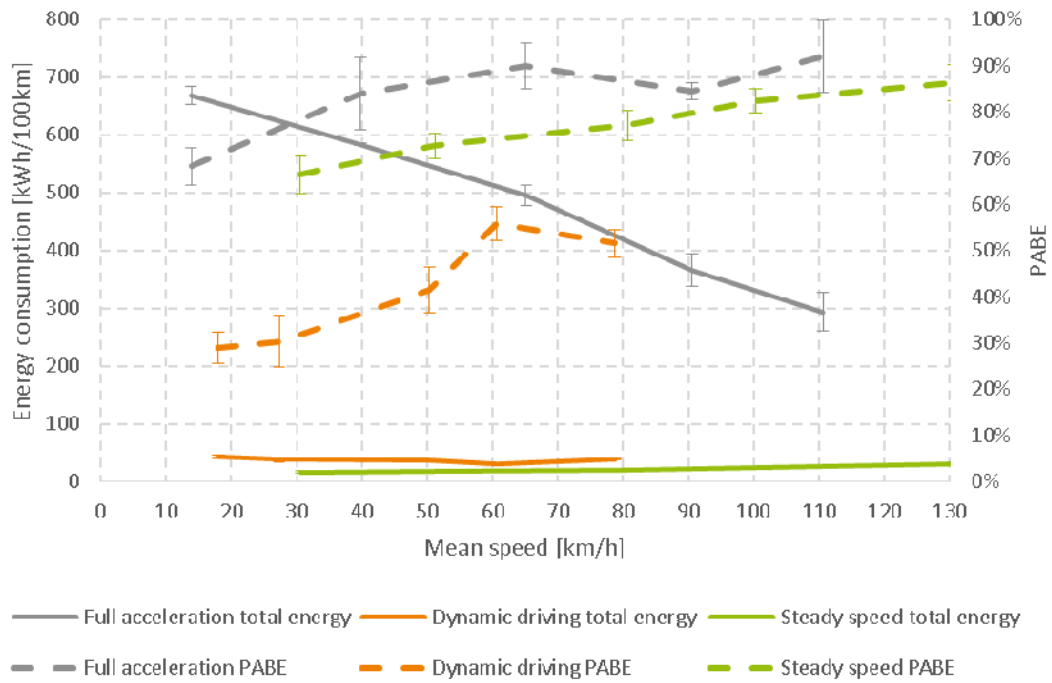


Figure 4.4.15: Total energy consumption and PABE, illustrated by the Tesla Model S

4.4.5 Aggressive driving

It is known from ICE vehicles that aggressive driving consumes more energy, because the efficiency of the powertrain drops. But how is the aggressiveness of a certain drive pattern measured?

This section attempts to predict consumption as a simple function of driver behaviour.

The relation between the energy consumption and the efficiency of the powertrain (PABE) has been compared to different functions (indicators) of aggressiveness. A high aggressiveness includes hard acceleration and hard braking. There is a minimum theoretic consumption, which does not rely on aggressiveness. The two most accurate indicators found are the speed variance and the mean absolute acceleration, which are shown in Figure 4.4.16 and Figure 4.4.17.

Variance shows the diffusion of data with respect to the mean value. The formula for variance is:

$$Var(x) = \frac{1}{n} \sum_{i=1}^k f_i (x_i - \bar{x})^2 \quad (3)$$

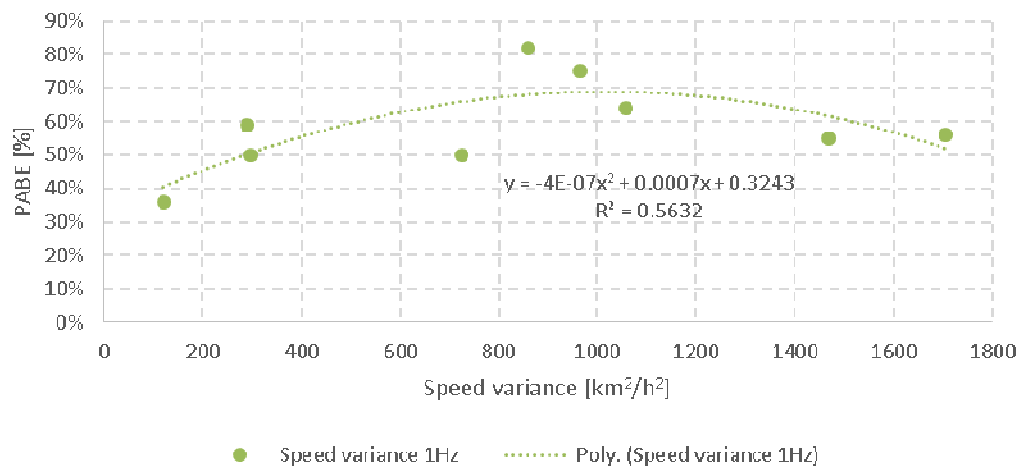


Figure 4.4.16: PABE versus speed variance, illustrated by the Renault Fluence ZE

Mean absolute acceleration is calculated as followed:

$$a(x) = \frac{1}{n} \sum_{i=1}^k f_i |a_i| \quad (4)$$

Even though the apparent accuracy with the mean absolute acceleration seems highest in Figure 4.4.17, it has a gap in the data in the middle, but the speed variance in Figure 4.4.16 covers more of the spectrum, which yields better continuity. Therefore, the speed variance is used here to indicate aggressiveness.

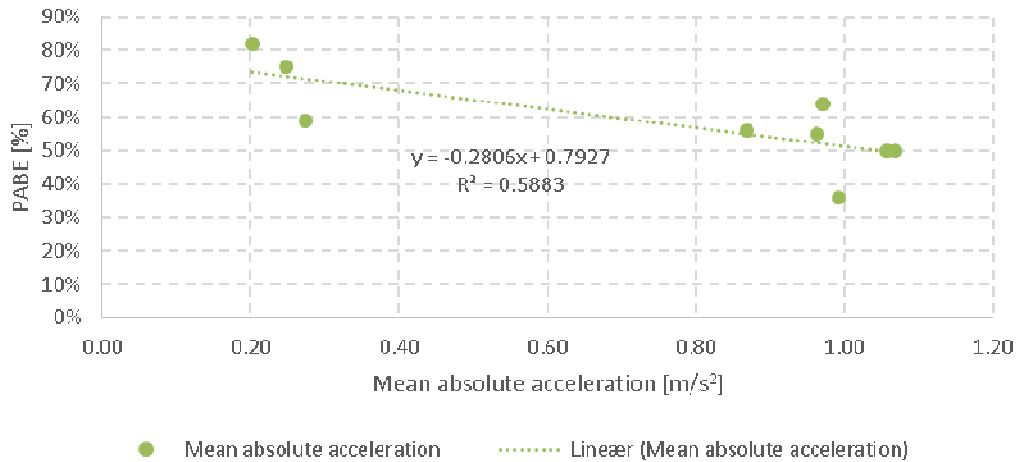


Figure 4.4.17: PABE versus mean absolute acceleration, illustrated by the Renault Fluence ZE

Figure 4.4.18 shows the speed variance of real on-road driving measurements (note the secondary x- and y-axis). The tendency is quite logical, as the dynamic driving scores unmatchable the highest with its fluctuating speed. The steady speed appears at the bottom as expected and the full acceleration is about ten times the steady speed, but still below 1% of the dynamic driving.

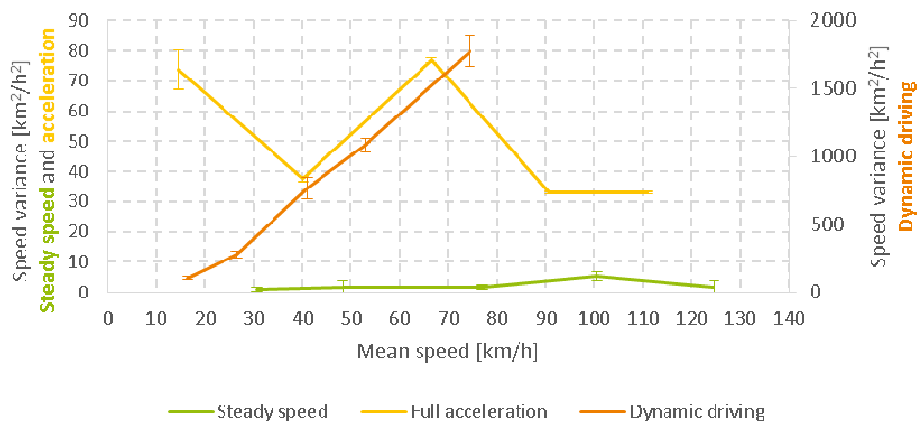


Figure 4.4.18: Speed variance versus speed in different driving styles, illustrated by the Mitsubishi i-MiEV

Comparing speed variance to energy consumption, see Figure 4.4.19, the dynamic driving scores highest as expected, closely followed by the full acceleration (note the secondary x- and y-axis). The steady speed is still playing around at the bottom left corner.

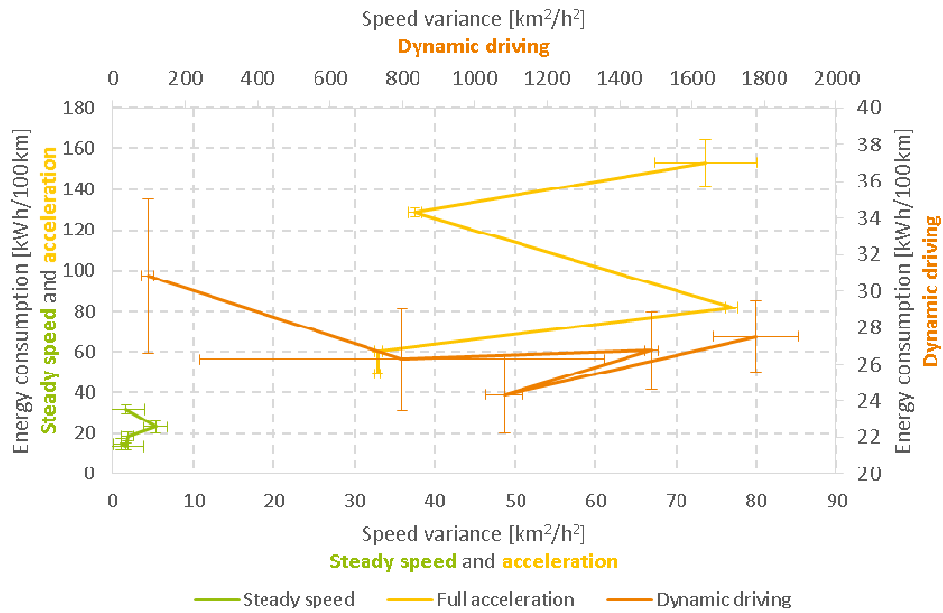


Figure 4.4.19: Impact of aggressive driving on energy consumption, illustrated by the Mitsubishi i-MiEV

This leads to a suggested range correction formula. For further details about this, please see D6.3.

4.4.6 Drive train comparison - ICE vs. EV

When comparing vehicles with ICE to EVs, two types of vehicles can clearly be identified. For both types, the power consumption depends on the drive pattern, but in different ways.

As stated earlier, typical for every vehicle – the higher the speed, the higher the consumption. This is simply a law of physics and counts for the energy needed for propulsion, particularly air resistance.

At heavy urban (low speed) driving the idle consumption of ICE vehicles is significant, because the propulsion energy here is low, but the relative large idle consumption is constant. Therefore, with increasing speed the total consumption for ICE vehicles is then decreasing, until a certain point where it levels out. Figure 4.4.20 and Figure 4.4.21 show the ICE vehicles, which are Mazda 6, Ford C-max and the Opel Ampera in ICE mode. Typical idle consumption for an ICE vehicle is 5 - 7 kW (0.6 - 0.8 litres of fuel per hour), which at the same time sets the minimum power consumption, unless a newer ICE vehicle with start/stop functionality is used.

For EVs, the actual idle consumption is relatively low (excluding the heating consumption) and the total consumption is therefore rising with increasing speed. Nevertheless, the heavy urban where the EV idle consumption is also significant. Furthermore, EVs have the ability to recover some power when braking, which yields another advantage at lower speeds. Figure 4.4.20 and Figure 4.4.21 show also the results for a Mitsubishi i-MiEV, Nissan Leaf, Renault Fluence ZE, Fiat Fiorino Micro-Vett Micro-Vett and the Opel Ampera in EV mode.

The energy consumptions shown in Figure 4.4.20 and Figure 4.4.21 are so-called tank-to-road measurements and the two figures do in principle show the same information in different ways.

Note that the consumption cannot be compared directly between the different vehicles types, because of changes in drive and/or wind conditions. The purpose is to give a general view of the consumption levels of EVs versus ICE vehicles.

To sum up, ICE vehicles are more efficient at long distance highway driving while EVs are best at urban driving. As EVs have lower range this fits well with the lower operation radius in the cities.

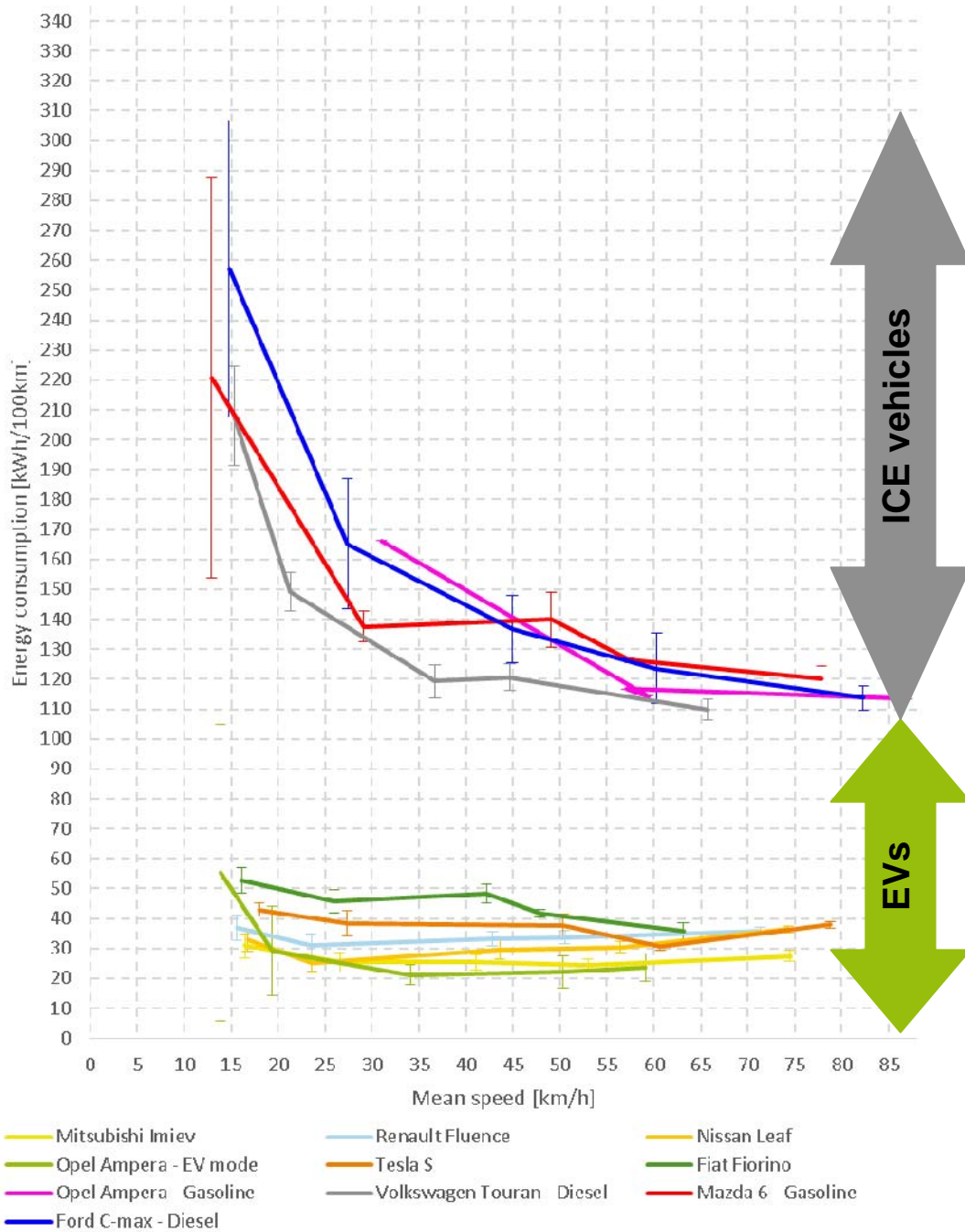


Figure 4.4.20: Energy consumption during dynamic driving, comparison of all vehicles used in the tests

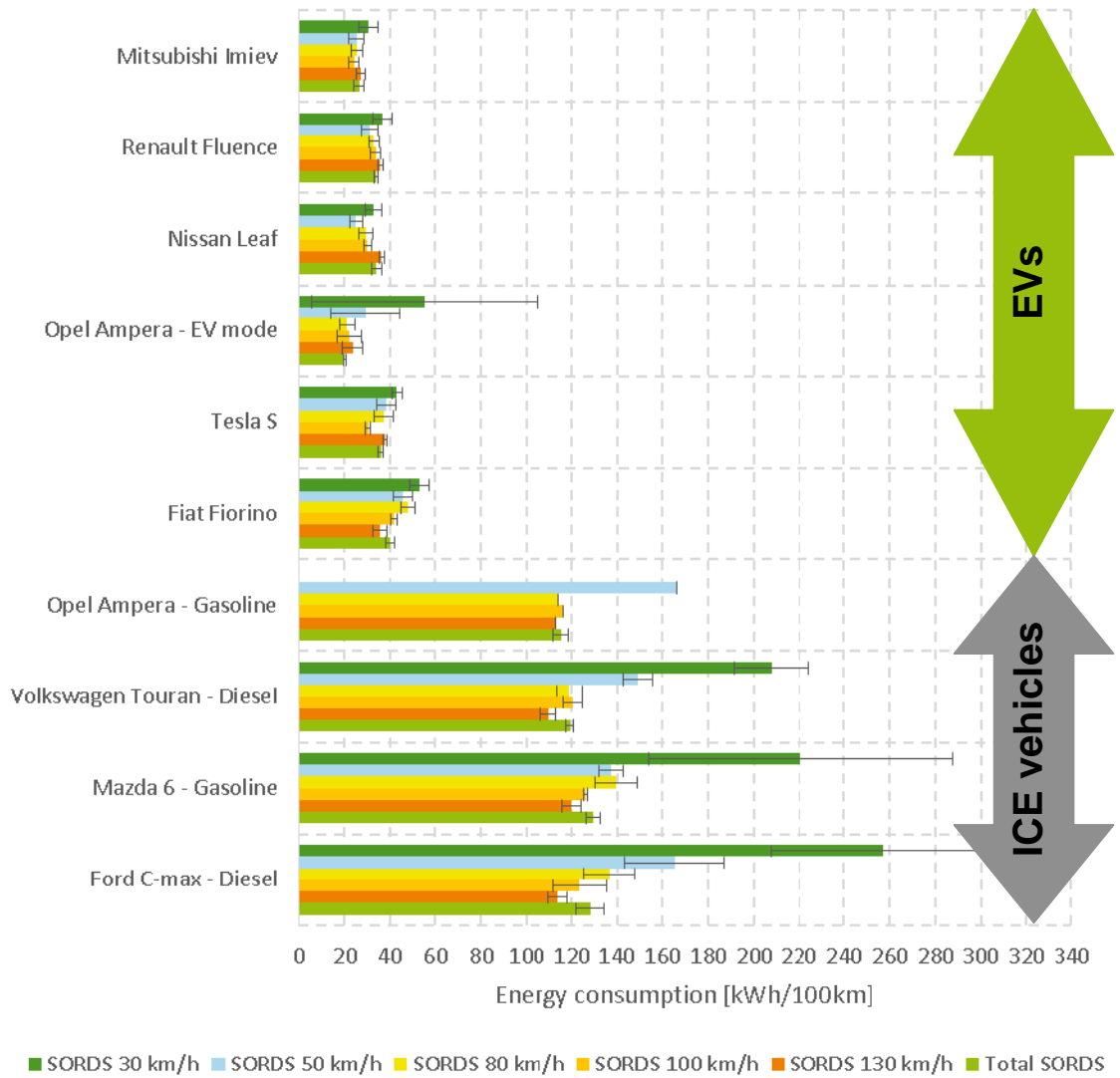


Figure 4.4.21: SORDS energy consumption comparison (all vehicles used in the test)

4.5 Hypothesis 2: Range and consumption depend strongly on the use of auxiliaries

In EVs the heater is part of the auxiliaries, contrary to ICE vehicles, where lots of waste heat can be transferred to the cabin. An EV heater is typically electric and powered from the high voltage battery, but it is also possible to have a heat pump or a fuel-fired heater (diesel or gasoline) in an EV.

The battery performance is highly inflicted by the electric heater in terms of energy available for propulsion, hence the range of the vehicle. Bringing a cold EV to comfort temperature electrically is expected to consume the most energy compared to just maintaining comfort temperature.

In all the EVs, we observed lower auxiliary consumption during the relatively warmer hours in the middle of the day compared to the cold hours at the start of the day. This can be seen in Figure 4.5.1, which show hourly mean values.

The variation between the different curves in Figure 4.5.1 correlates with the weather. If the sun is present, where the EV is parked, the cabin temperature will increase even though the ambient temperature is relatively low. The curves show a slightly lower auxiliary power in the middle of the day as expected. The two curves showing the highest power fit well with the available defrosting power.

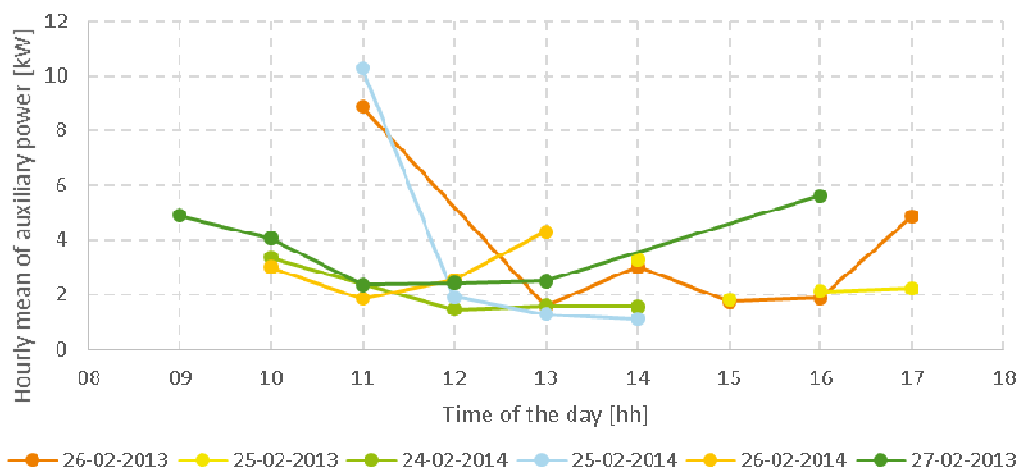


Figure 4.5.1: Auxiliary consumption during the day, illustrated by the Renault Fluence ZE

The two curves in Figure 4.5.2 indicate a quite low auxiliary power, but the measurements are spread within a large interval. The curves illustrate an EV with a diesel-furnace replacing the electric heater, which gives a significant reduction in the demand for auxiliary power. Unfortunately, these are the only data showing the auxiliary consumption for this vehicle. But comparing the demand for auxiliary power with electrical heater of the Renault Fluence ZE in Figure 4.5.1 to those without electrical heater of the

Micro-Vett Fiorino in Figure 4.5.2, the dimension of energy consumed in the electrical heating process can be guessed.

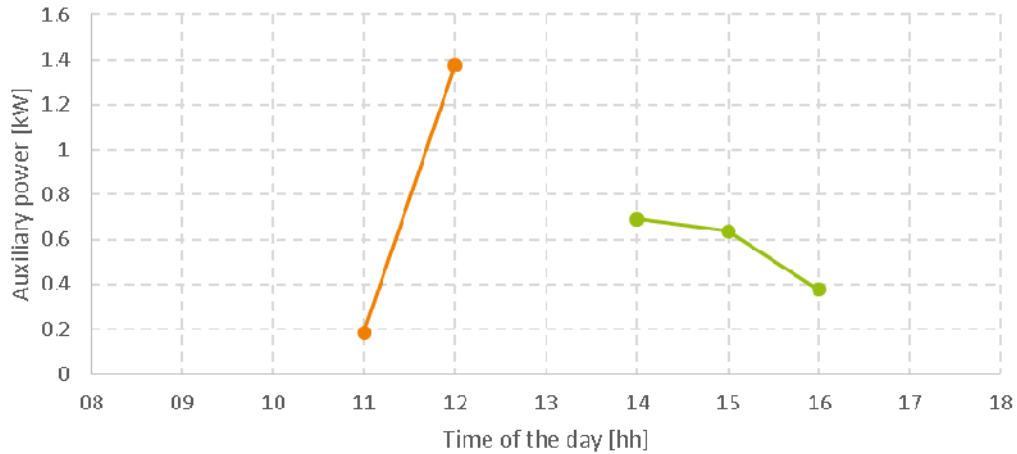


Figure 4.5.2: Auxiliary consumption during the day with no electric heater, illustrated by the Fiat Fiorino Micro-Vett

In Figure 4.5.3 examples of measured auxiliary power of three EVs are shown. The base consumption to standby of the vehicles is almost equal. The Fiat Fiorino Micro-Vett illustrates an EV with a diesel-furnace replacing the electric heater, which gives a significant reduction in the demand for auxiliary power.

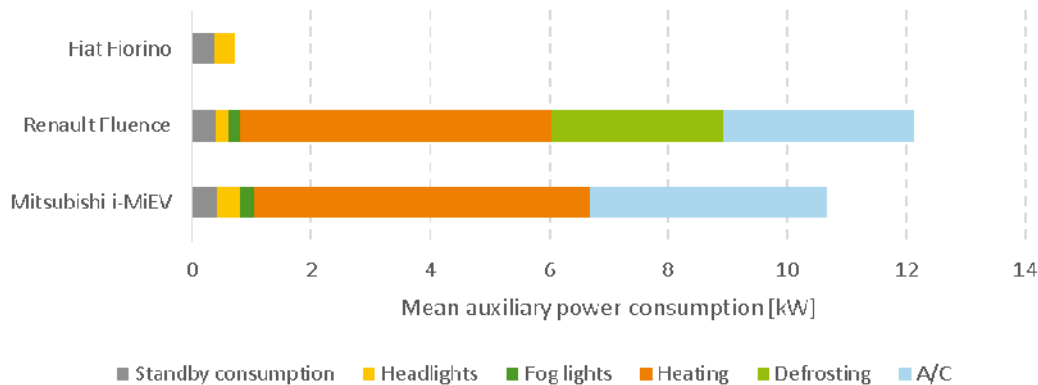


Figure 4.5.3: Distribution of available auxiliary consumption in different kinds of EVs

Energy consumption with a cold vehicle is depicted in Figure 4.5.4, showing how high percentages of the total energy are actually spent for heating up the vehicle. The auxiliary power does not depend on the speed, but per travelled distance the almost constant auxiliary energy consumption becomes lower simply because the vehicle travels further for the same amount of energy.

The data in Figure 4.5.4 are from the heating and defrosting test, meaning a cold start of the vehicle followed by driving SORDS. The target of the test was to reach comfort temperature in the cabin (20°C). For more details about this test please see section 4.9.

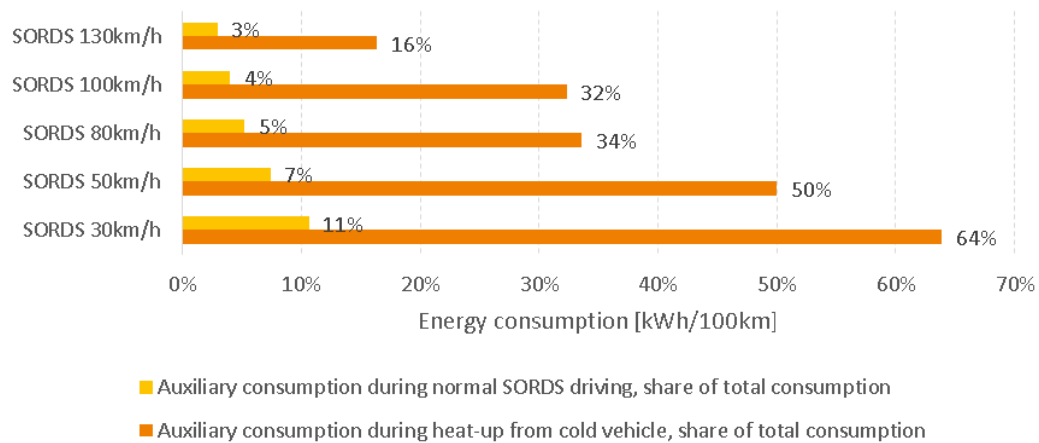


Figure 4.5.4: SORDS driving during heating at 3°C ambient temperature, illustrated by the Mitsubishi i-MiEV with a water-borne electric heater

Figure 4.5.5 show that the auxiliary consumption decreases under acceleration, with respect to driven distance, as the speed increases. The power consumed by auxiliary systems is typically constant, but as the speed increases the car travels faster which yields the smaller kWh/100km value.

Since regular on-road driving does not require full acceleration all the time, the figure also shows the percentage of energy spent on auxiliaries during steady speeds. These figures are significantly higher than the ones on full acceleration, but show more realistic point of view.

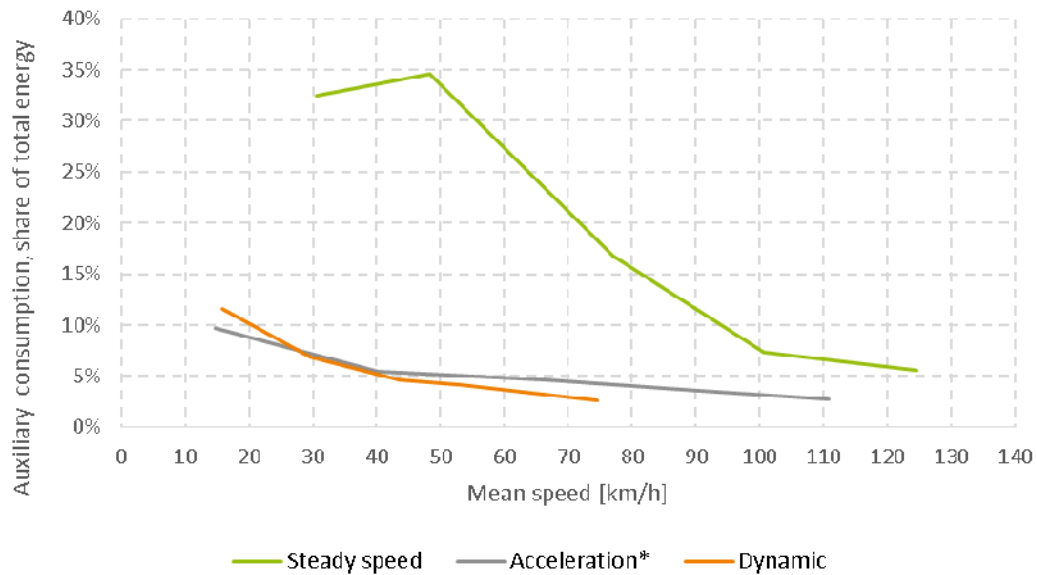


Figure 4.5.5: Auxiliary consumption at different driving styles at 2-11°C ambient temperature, illustrated by the Mitsubishi i-MiEV with a water-borne electric heater

The Fiat Fiorino Micro-Vett does not have an electric heater installed, thus greatly reducing auxiliaries consumption in cold weather, but this vehicle still have a relatively high auxiliary consumption. The share of energy consumed by auxiliaries is marginally less for the Fiat Fiorino Micro-Vett compared to the other EVs in Figure 4.5.6.

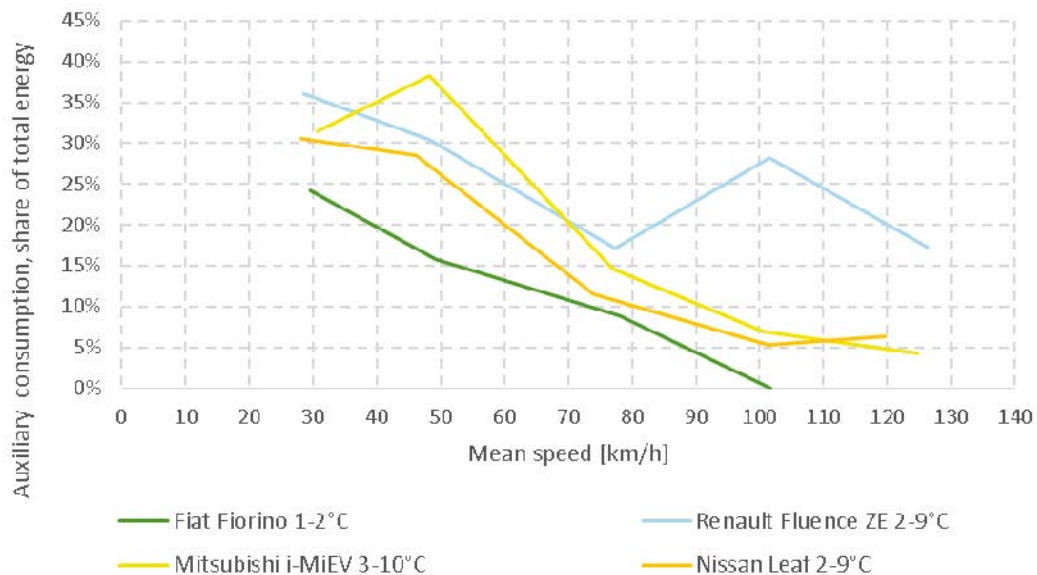


Figure 4.5.6: Comparison between auxiliary consumption in several vehicles at steady speeds, illustrated by all EVs used in the on-road tests at given conditions

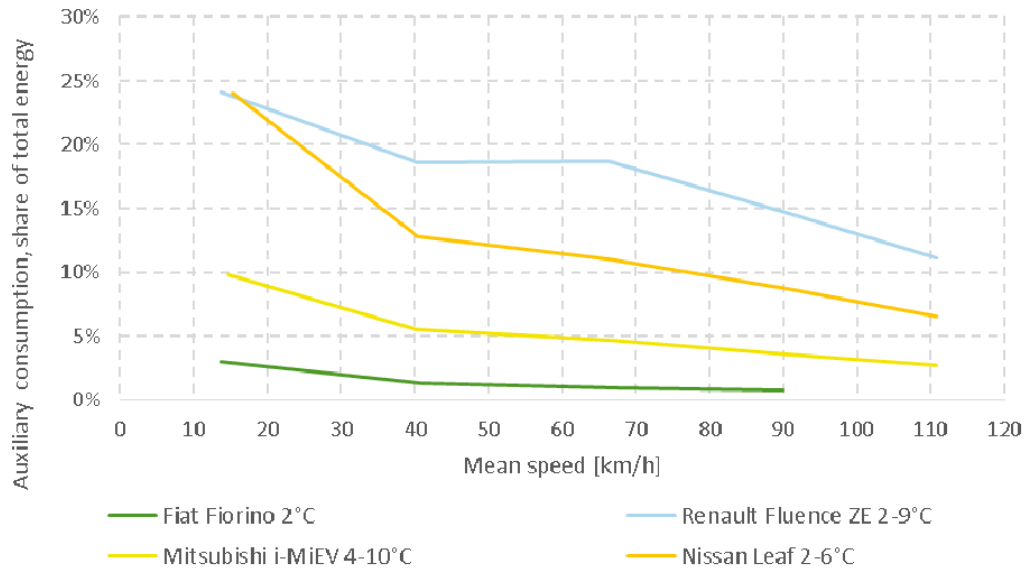


Figure 4.5.7: Comparison between auxiliary consumption in several vehicles at full acceleration, illustrated by all EVs used in the on-road tests at given conditions

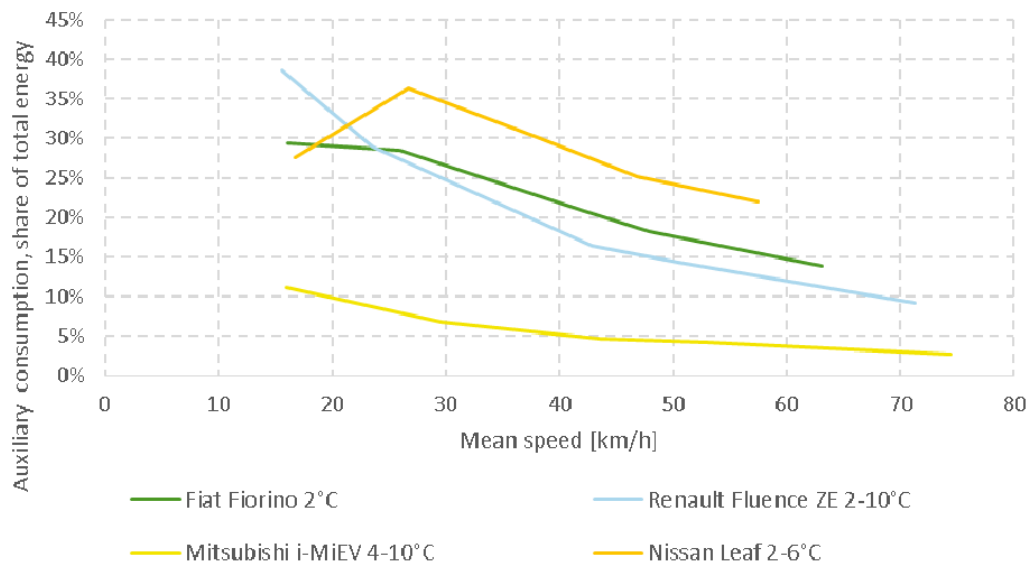


Figure 4.5.8: Comparison between auxiliary consumption in different vehicles at dynamic speeds, illustrated by all EVs used in the on-road tests at given conditions

Auxiliaries are also dealt with in further detail in section 5.2.

4.6 Hypothesis 3: SOH is predictable by step response testing

The step response testing was performed by accelerating the EV fully until 110 km/h, then decelerating down to 0 km/h by using regenerative braking. Please see Figure 4.6.1.

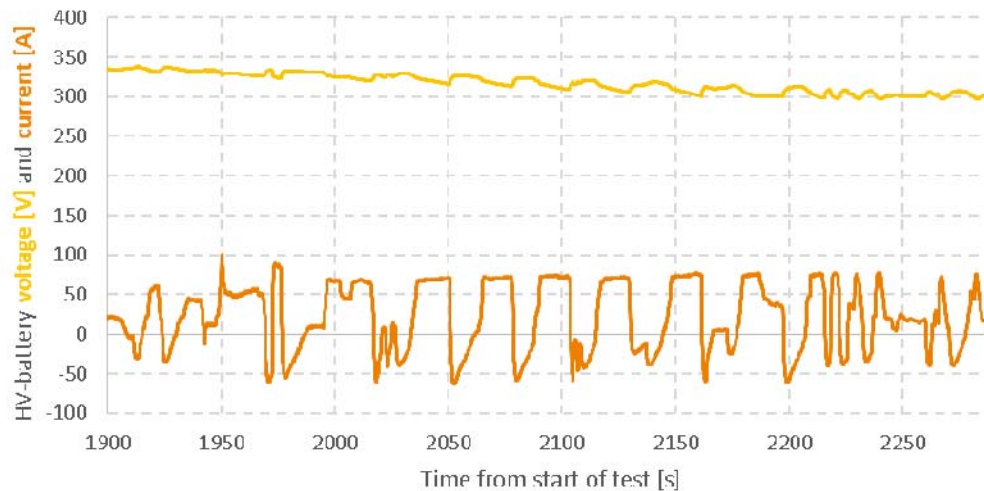


Figure 4.6.1: Exemplary data showing the step response test, illustrated by the Renault Fluence ZE

It is known that a battery's internal resistance can be measured by a simple step response test. This is not wrong, but does it really reveal everything about the battery's SOH?

The answer is no, because a resistance does not include any time-dependent response. Therefore, the battery's insides need to be modelled with an equivalent circuit containing both resistive and reactive elements – the so-called impedance, which seems to change with time and temperature.

Impedance consist of two parts; a real part (the resistance), which is time independent, and a complex part (the reactance), which is time dependent.

Impedance can be plotted as a Nyquist curve and such a curve shows the internal impedance of a battery. Following the progress of a battery's Nyquist curve will reveal the progress of the battery SOH.

For a more thorough investigation of SOH via step response testing and Nyquist curves please refer to D9.8⁶.

⁶ Available spring 2015 at <http://www.greenemotion-project.eu/dissemination/deliverables-evaluations-demonstrations.php>

4.7 Hypothesis 4: Climate has significant impact on battery performance

What is battery performance?

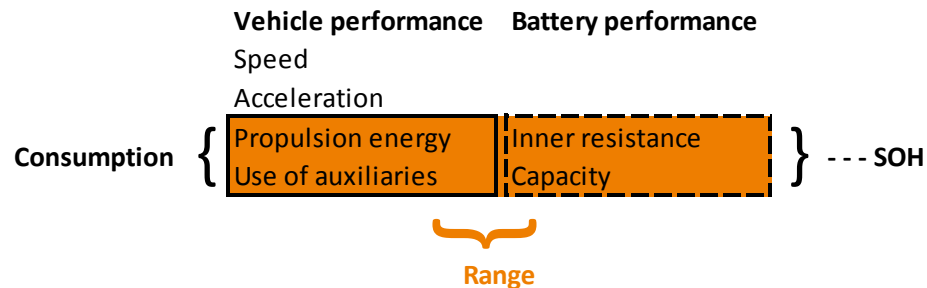


Figure 4.7.1: Vehicle Performance and Battery Performance as defined in D6.1, Figure 3.1

Battery performance is typically given by a combination of energy capacity and internal resistance as shown in Figure 4.7.1. With age a battery loses capacity and the internal resistance rises, hence the battery gets poorer performance.

To test the impact from the climate on the battery performance, the EVs were subjected to conditions of lower temperatures combined with data from other projects.

The values shown in Figure 4.7.2 are actual discharge measurements. The Renault Fluence ZE data were read in the real world via the on-board computer. The Mitsubishi i-MiEV/Citroën C-Zero data were done in a climate chamber and more details about this can be seen in Figure 5.1.4. The reproduced Waterloo data are discharge capacities from battery cells tested in a thermally controlled chamber.

Battery capacity should be given in energy (kWh), because charge (Ah) does not include any voltage information. Power is what the electric motor needs and power equals current times voltage, hence voltage is required. Ampere-hours may be almost constant in many situations, but a modern Lithium ion battery is operated within a certain voltage window and the electric motor controller is compensating for the voltage drop by increasing the load current. All these properties would make the capacity dependent of the voltage.

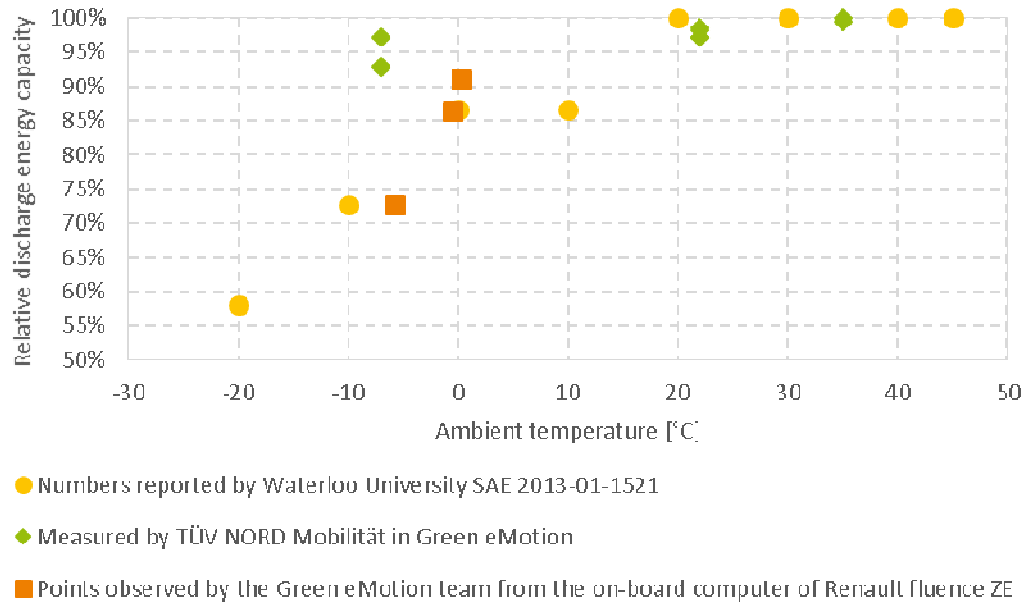


Figure 4.7.2: Total energy delivered of Renault Fluence ZE, Mitsubishi i-MiEV, Citroën C-Zero and results from Waterloo University

The measurements show a significant impact of temperature on battery performance. For grid-to-road efficiencies please see D9.8.

4.7.1 Charging losses

When converting AC power from the grid to DC power to the battery the charging losses occur within the battery charger. A battery charger converts power with modern power electronics, so-called switch-mode technology, with high efficiency (typically >85%), but the losses in the power electronics are still significant.

The charging losses can be calculated as the difference between the energy drawn from the grid and the energy fed into the HV-battery on an EV.

The battery efficiency, which is the loss in the actual battery – from the energy charged to the battery to the energy discharged from the battery – is not included in charging losses.

The numbers in Figure 4.7.3 are from the tests done by TÜV NORD Mobilität in Green eMotion, which are shown in Figure 5.1.2 and Figure 5.1.4.

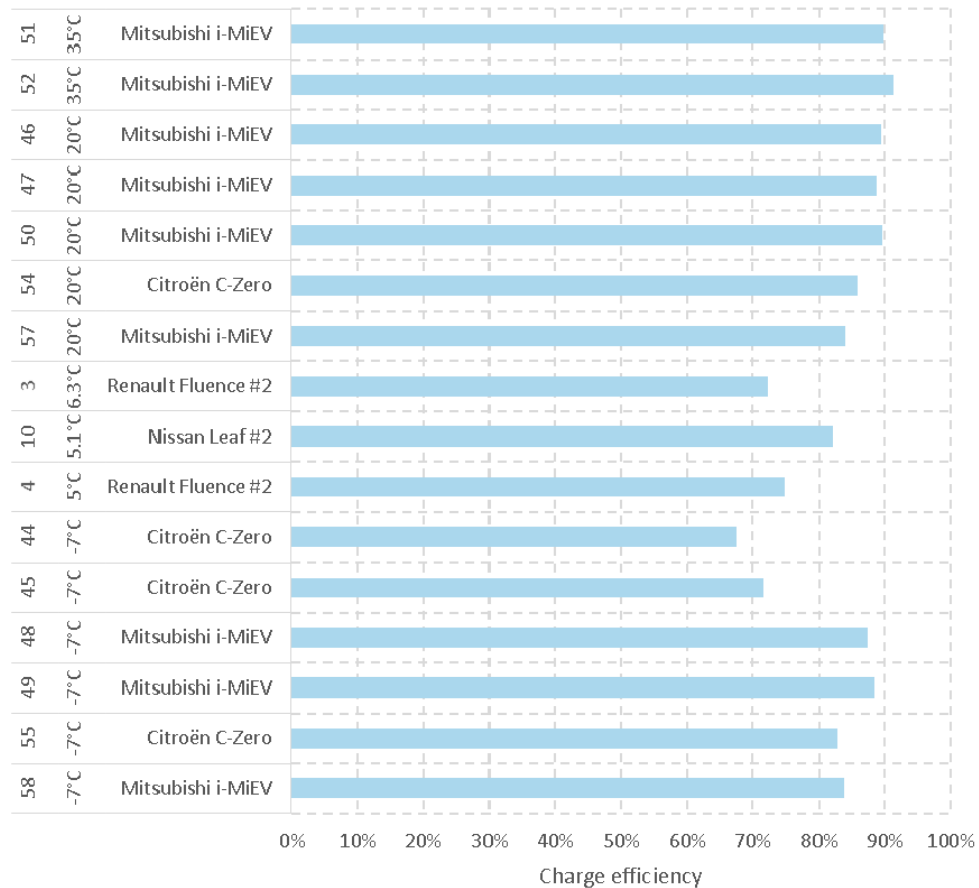


Figure 4.7.3: Mode 2 charging efficiency versus temperature

An estimate of 1.2 kW was lost during CHAdeMO quick charge (Level 3 Mode 4) with an output charge power of 8 kW. The loss of 15% power in the charger is a common loss level for modern power electronics including a transformer. In Figure 4.7.4 quick charging losses were estimated by means of the on board SOC indicator. As seen this gave varying results and thus apparently is an uncertain method.

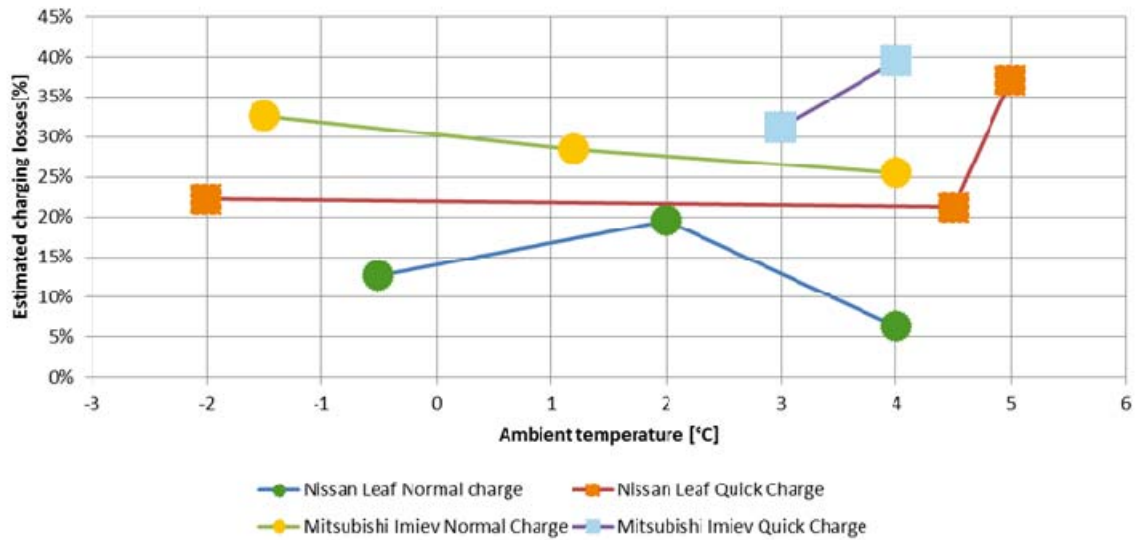


Figure 4.7.4: Apparent charging losses estimated from on board SOC indicators at different charging levels, illustrated by the Mitsubishi i-MiEV and the Nissan Leaf

4.8 Hypothesis 5: Battery performance is almost unaffected by battery charge rate

The primary factor to reduce the battery performance (and life) by the rate of charging would be increase of the battery internal temperature due to charging at high C-rates. Heat is known to reduce battery life. The C-rate is the rate of electric current in the battery compared to the battery's design capacity in Ampere-hours. The C-rate relates to the capabilities of the battery, where the maximum C-rates are normally given by the manufacturer for charging and discharging.

A given example could be a 100 Ah battery specified at C/10. The C-rate defines the condition in which the capacity can be expected. Therefore, the new battery should be able of delivering 10 A in 10 hours rather than 100 A in one hour. The last situation would include higher, hence the delivered charge would be less than expected. The internal loss in the battery can be calculated via the expression below:

$$P_{loss} = R_i \cdot I^2 \quad (5)$$

A situation where an EV is driven aggressively directly after a full quick charge should give the optimum conditions for thermal over load to develop from battery self-heating. The loss during quick charge should be 10 times higher than for standard charge, if the charge current is 10 times larger:

$$\frac{Q_{loss,100A}}{Q_{loss,10A}} = \frac{R \cdot (100[A])^2 \cdot 1[h]}{R \cdot (10[A])^2 \cdot 10[h]} = \frac{10^2}{1^2 \cdot 10} = 10 \quad (6)$$

The WP6 team tried to stress the battery into over temperature by performing the step response test with the EV directly after quick charging. Please see Figure 4.6.1. No indications of over temperature were observed with the EVs used – the Mitsubishi i-MiEV and the Nissan Leaf, as these were the only EVs present capable of quick charging.

The battery temperature indicator in the Nissan Leaf dashboard did not even move during the step response test. Nissan says⁷: “Sustained high battery temperatures (caused, for example, by exposure to very high ambient temperatures or extending highway driving with multiple quick charges)”. These conditions were not tested by WP6 team.

So we can conclude that battery performance is not seriously affected by charge rate.

Self-heating during the charge

An HV-battery’s internal resistance at DC is in the interval 120-600 mΩ giving an estimated maximum resistive power loss at 8 kW quick charging as shown in (7):

$$P_{loss,qchg} = R_i \cdot \left(\frac{P_{q,chg}}{U_{bat}} \right)^2 = 600[m\Omega] \cdot \left(\frac{8[kW]}{360[V]} \right)^2 \cong 300[W] \quad (7)$$

In one hour of quick charging of the Nissan Leaf as example⁸, this would yield a temperature rise in the thermally isolated EV battery as expressed in (8):

$$\Delta T = \frac{Q}{C_p \cdot m} = \frac{300[W] \cdot 60^2}{1100 \left[\frac{J}{kg \cdot K} \right] \cdot 3.8[kg] \cdot 48[pcs.]} = \frac{1080[kJ]}{200[kJ/K]} = 5.38[K] \quad (8)$$

Different C_p values for the battery specific heat capacity were found in several references. Tsinghua University⁹ used $925 \left[\frac{J}{kg \cdot K} \right]$ and Pesaran A. and Keyser M. (2001)¹⁰ used $795 \left[\frac{J}{kg \cdot K} \right]$ for Lithium-Ion batteries.

EV batteries are normally equipped with some kind of cooling and EV batteries are certainly not thermal isolated. Furthermore, quick charging at 8 kW is equal to C/3 for the battery and less than 10% of the

⁷ <https://owners.nissanusa.com/content/techpub/ManualsAndGuides/NissanLEAF/2013/2013-NissanLEAF-Customer-Disclosure-Form.pdf>

⁸ Ikezoe M. et al. Development of High Capacity Lithium-Ion Battery for NISSAN LEAF. 2012. SAE International.

⁹ http://www.transportation.anl.gov/batteries/us_china_conference/docs/battery%20testing%20roundtable/Test_of_battery_tsinghua.pdf

¹⁰ http://www.nrel.gov/vehiclesandfuels/energystorage/pdfs/long_beach_btm.pdf

propulsion power, which means that the temperature during highway driving would be larger than for quick charging.

Therefore, with the quick charging conditions presented here, the self-heating of the EV battery during quick charging are considered less significant.

CHAdeMO has the ability to charge at up to 50 kW, which would of course give a higher temperature rise. Approx. $\frac{50[kW]}{8[kW]} \cdot 5.38[K] \cong 34[K]$, but considering battery cooling and the relatively low ambient temperature during the tests in Karup, this is still not worrying.

Tesla Model S P85 has an 85 kWh battery and Tesla's supercharger charges with 120 kW, which is equal to 1.41 C. Compared to propulsion power, the Tesla Model S P85 has 350 kW and the new Tesla Model S P85 D has almost 508 kW. Then the supercharging is respectively 34% and 24% of the propulsion power.

4.9 Hypothesis 6: Heating and defrosting capacity is adequate

To validate the heating and defrosting capacity, each EV was submitted to SORDS testing starting with a cold vehicle. Please see Figure 4.9.1.

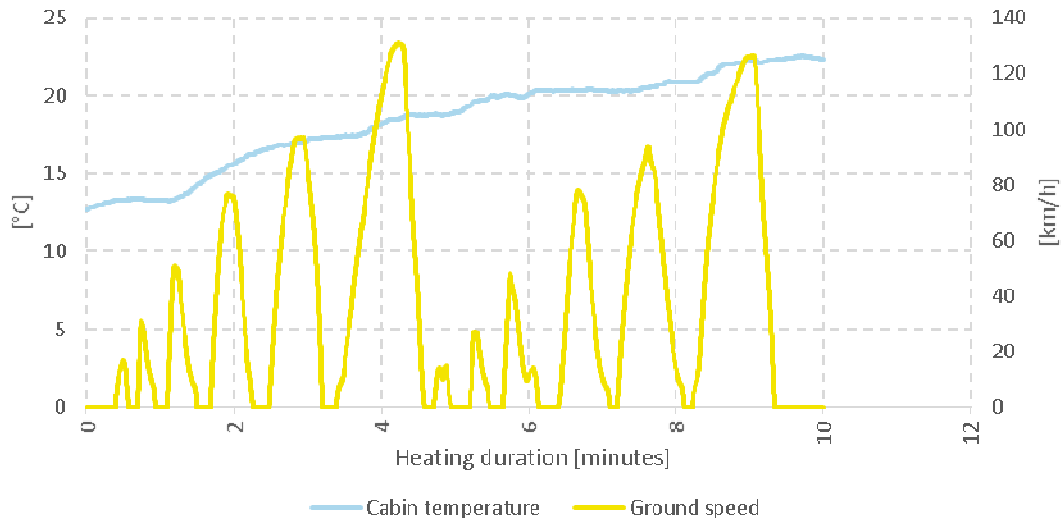


Figure 4.9.1: Heating capacity during SORDS driving, illustrated by the Renault Fluence

The electric heating unit in an EV can produce heat either as water-accumulated or direct-air, like a normal heat blaster. The capacities of these types of heaters are compared in Table 4.3, where Figure 4.9.2 shows how the cabin temperature progresses while driving.

| Heater type | Water-borne | Water-borne | Direct-air |
|------------------------------|---------------------|---------------------------------|--------------------|
| Vehicle | Mitsubishi i-MiEV | Nissan Leaf | Renault Fluence ZE |
| Settings of the heating unit | Maximum temperature | Maximum temperature, defrosting | Defrosting |
| Start temperature | 3.0 °C | 5.5 °C | 7.0 °C |
| End temperature | 21.1 °C | 20.7 °C | 20.9 °C |
| Rise time | 4.5 min | 9 min | 2 min |
| Temperature gradient | 3.8 °C/min | 1.6 °C/min | 6.5 °C/min |

Table 4.3: Consumed time and gradient during cabin heating and defrosting

Figure 4.9.2 compares the behaviour of different types of heaters in different EVs. It also indicates that a climatic control system can regulate differently dependent on the starting temperature. The direct-air heater in the Renault Fluence was very fast in 2013 starting from 7 °C, it took only about 2 min to reach 20 °C, where in 2014 it took almost 6 min (without defrosting) to heat up to the cabin comfort temperature from 13 °C. The water-borne heater types are typically slower than direct-air, but the water holds the temperature more stable.

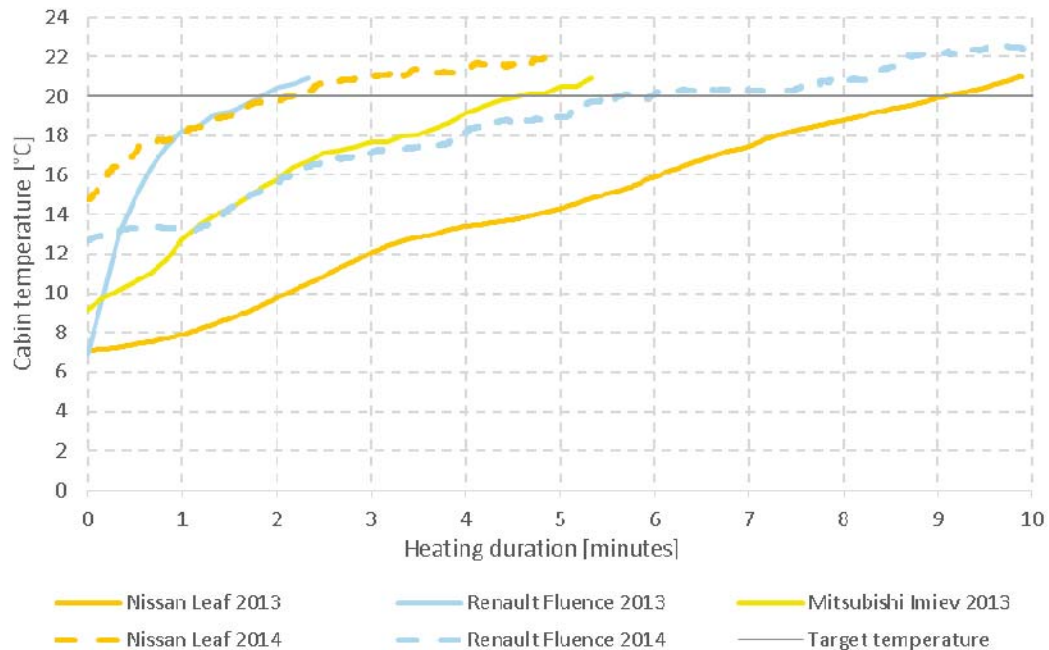


Figure 4.9.2: Comparison of heating capacity during SORDS driving, illustrated by the Mitsubishi i-MiEV, the Nissan Leaf and the Renault Fluence ZE

4.10 Hypothesis 7: Regenerative braking adds significantly to vehicle range

When propelling a vehicle, this vehicle – of course – consumes energy. When stopping a given vehicle, its accumulated energy is normally dissipated as heat in the braking discs during friction braking. However, EVs have the ability to regenerate a part of the braking energy, because the electric motor is able to work as a power generator if the driver of the vehicle brakes with the motor – motor-braking as a term is known from vehicles with ICE. Some EVs have several settings for regeneration.

The regenerated energy does not appear directly, when measuring the total consumed power from the HV-battery. The share can be estimated by adding the negative power to the usage of auxiliaries in kW. The SORDS is repeated with and without regeneration for comparison. Practically, this can be done by shifting the EV into neutral gear mode (N), when decelerating.

The actual efficiency of the electric motor is not improved by the regenerative braking, but the total energy consumption is lowered, because the share of the braking energy, which is regenerated, does not have to be drawn from the battery. The regeneration energy is free, because it is “recycled” energy not dissipated in the braking discs.

Figure 4.10.1 shows the ability of each EV to regenerate the braking energy. If done properly, this energy can produce a significant decrease in the energy consumption, hence an increase in the range of the vehicle.

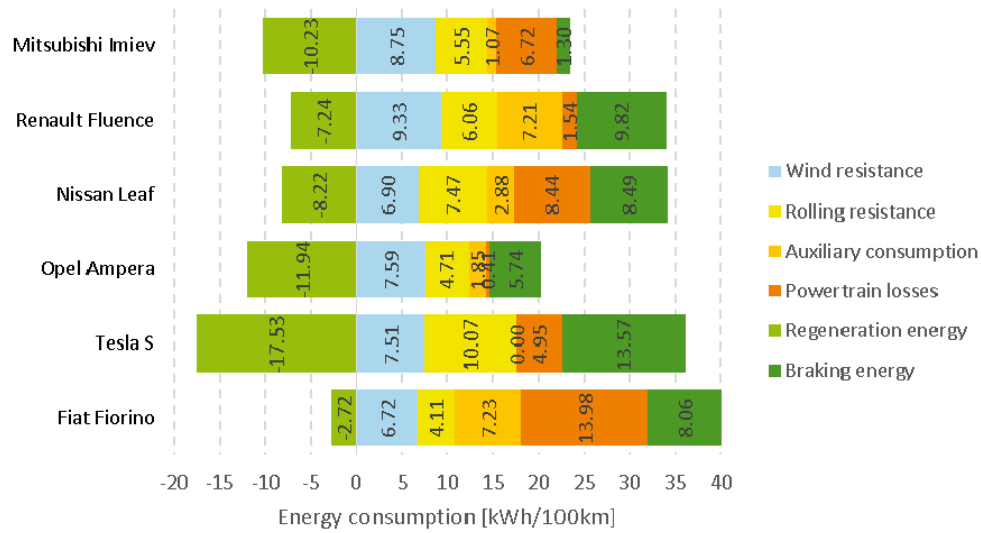


Figure 4.10.1: Distribution of energy during SORDS driving (All EVs, including the Opel Ampera in EV mode)

Even though the energy drawn from the battery is the total amount of energy added to the vehicle, this share becomes only the apparent total energy consumption, because the actual total energy consumed is really the sum of the energy drawn from the battery and the regeneration energy.

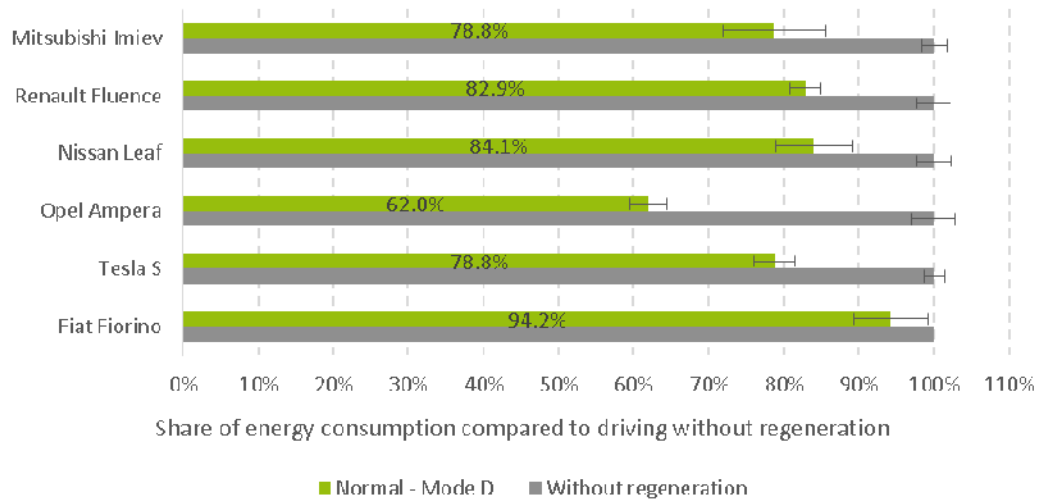


Figure 4.10.2: Comparison of total energy drawn from battery in percent of SORDS driving with and without regeneration (All EVs, including the Opel Ampera in EV mode)

Comparing the energy consumption of SORDS with, and without regeneration, Figure 4.10.2 shows a significant cutback in the required energy. Though, the amount of saved energy varies with the vehicle. With a given EV, saving up to 38% of the total energy – when utilising the normal mode of the regenerative braking while driving SORDS – is possible.

To evaluate the efficiency of the regenerative braking system we need to assess the maximum theoretical braking energy available. This consist of the kinetic energy available before braking minus the energy lost to air resistance and rolling resistance during braking. Since the speeds and braking distances in SORDS are all well-defined we can calculate the regeneration potential from basic equations of motion.

Maximum kinetic energy before braking:

$$E_{kin}[kWh] = \frac{(\frac{1}{2} \cdot m \cdot v_{max}^2) [J]}{3.600.000 \left[\frac{J}{kWh} \right]} \quad (9)$$

Vehicle rolling resistance during braking:

$$E_{roll}[kWh] = \frac{(m \cdot g \cdot f_R \cdot s_{max}) [J]}{3.600.000 \left[\frac{J}{kWh} \right]} \quad (10)$$

Vehicle air resistance during braking:

$$E_{wind}[kWh] = \frac{\frac{1}{2} \cdot \rho \cdot A \cdot C_w \cdot v_{max}(s) [J]}{3.600.000 \left[\frac{J}{kWh} \right]} \quad (11)$$

Theoretical maximum braking energy:

$$E_{max.brake}[kWh] = E_{kin}[kWh] - E_{wind}[kWh] - E_{roll}[kWh] \quad (12)$$

Rewriting:

$$E_{max.brake}[kWh] = \frac{\frac{1}{2} \cdot m \cdot v_{max}^2 [J]}{3.600.000 \left[\frac{J}{kWh} \right]} - \int F_{air}(s) ds [kWh] - \int F_{roll} ds [kWh] \quad (13)$$

Rewriting:

$$E_{max.brake}[kWh] = \frac{(\frac{1}{2} \cdot m \cdot v_{max}^2) [J]}{3.600.000 \left[\frac{J}{kWh} \right]} - \int_0^{s_{max}} \frac{(\frac{1}{2} \cdot \rho \cdot A \cdot C_w \cdot v_{max}(s)) [J]}{3.600.000 \left[\frac{J}{kWh} \right]} ds - \frac{(m \cdot g \cdot f_R \cdot s_{max}) [J]}{3.600.000 \left[\frac{J}{kWh} \right]} \quad (14)$$

Speed versus distance assuming constant deceleration:

$$v_{max}(s) = 2 \cdot a \cdot s [m/s] \quad (15)$$

Using above:

$$E_{max.brake}[kWh] = \frac{\frac{1}{2} \cdot m \cdot v_{max}^2}{3.600.000 \left[\frac{J}{kWh} \right]} - \frac{\frac{1}{2} \cdot \rho \cdot A \cdot C_w \cdot a \cdot s_{max}^2}{3.600.000 \left[\frac{J}{kWh} \right]} - \frac{m \cdot g \cdot f_R \cdot s_{max}}{3.600.000 \left[\frac{J}{kWh} \right]} \quad (16)$$

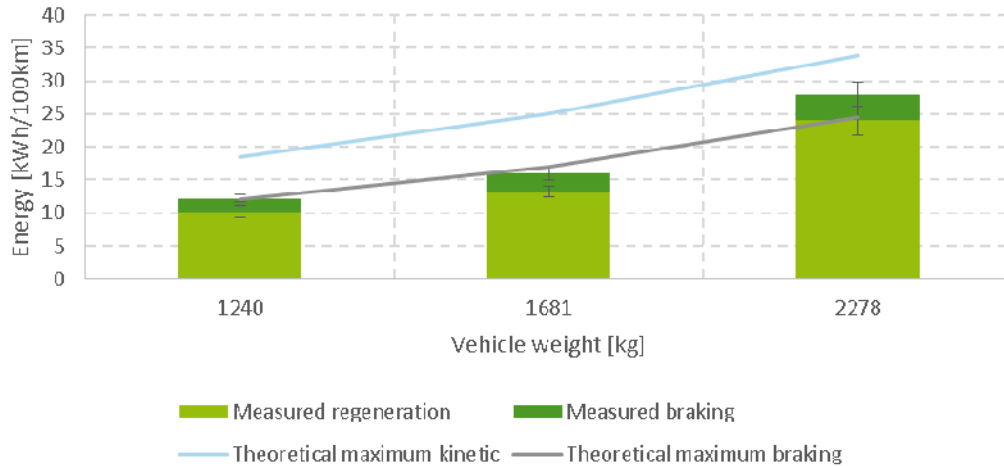


Figure 4.10.3: Theoretical maximum kinetic and maximum braking energy compared to measured braking and regeneration energy in EVs with different weights during SORDS 50 km/h.

Moreover, as depicted in Figure 4.10.3, required braking energy increases with higher vehicle weight. But the growth of weight also has a benefit – the energy that can be regenerated also increases. However, the increase of energy regeneration with higher weight is lower than the overall energy consumption growth, resulting in higher total consumption.

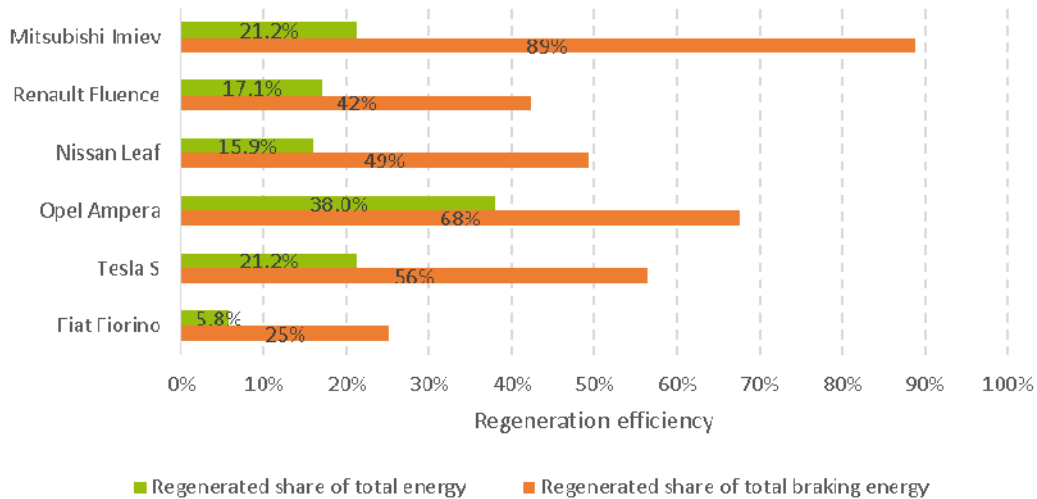


Figure 4.10.4: Total energy saved during SORDS driving with use of regeneration compared to total theoretical braking energy calculated and total energy drawn from battery, illustrated by all EVs used in the tests, including the Opel Ampera in EV mode.

In Figure 4.10.4, the saved energy share is shown compared with the regenerated share of the total braking energy available for regeneration. This indicates the default regeneration setting with the particular EV, which should not be mistakenly understood as the regeneration capability. The regeneration capability of an EV depends on the drivetrain and the battery, where the setting is a typically conservative and a matter of preference.

The total available braking energy was calculated from the maximum available kinetic energy after subtracting the resistance from wind and rolling as seen in (12).

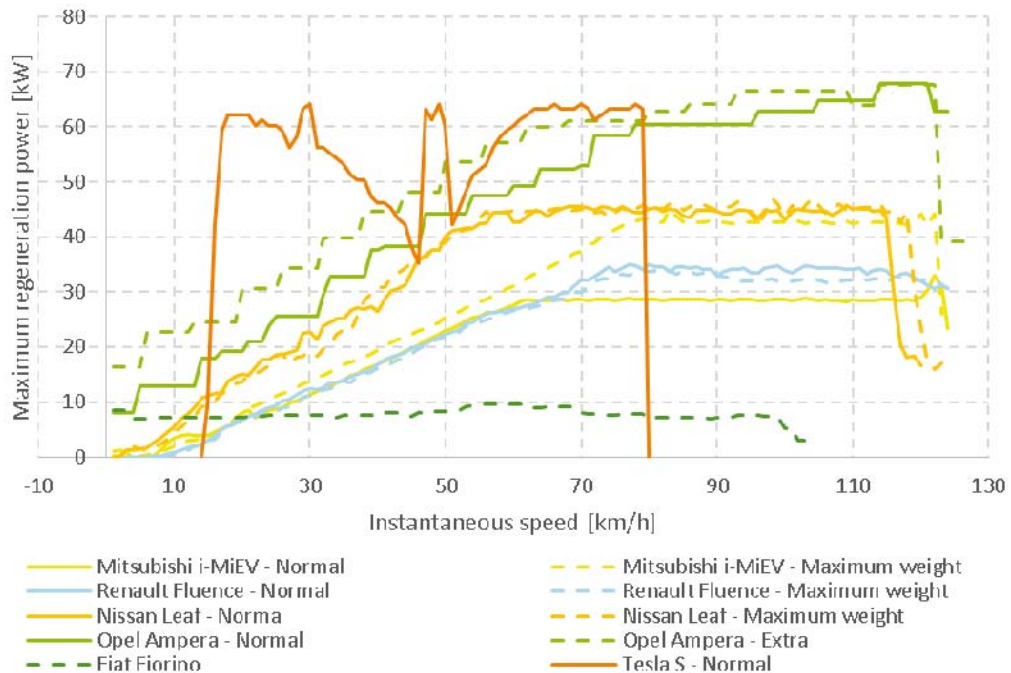


Figure 4.10.5: Comparison of regeneration power versus instantaneous speed, illustrated by all EVs used in the tests.

Figure 4.10.5 indicates a general tendency of regeneration power rising with the speed, except for the Tesla Model S, which seems to have a rather high, but constant, regeneration power limit. It seems like the Mitsubishi i-MiEV has a more complex control of the regeneration power than just a maximum power limit.

This is consistent with the characteristics of electric motors. It also respects the fact that there is not unlimited friction available on the driving wheels. In general the highest possible brake force is the weight on all four wheels in kilo-Newton. Tesla Model S touches the limit of physics with a regeneration force of 16 kN corresponding to almost 80% of the vehicle weight!

As mentioned, this is matter of drivetrain combined with preferences. The average driver would expect any vehicle to feel alike, independent of the type of drivetrain – of course within a certain tolerance, which is for the vehicle designers to interpret, hence the variations in the results.

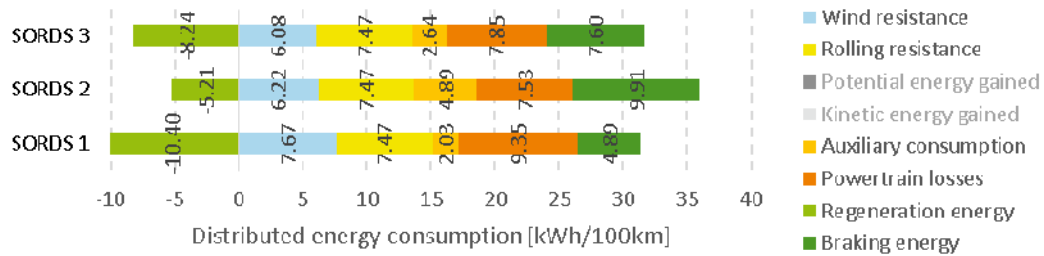


Figure 4.10.6: Regeneration comparison of different through-runs of SORDS, illustrated by the Nissan Leaf

In Figure 4.10.6 it is clear, how the driver can influence the regeneration with either an increase or a decrease in the regeneration energy – with up to 200% ± 30%. Furthermore, an automatic climate control system can make sudden changes in the need for auxiliary power, which doubled the entry in this case.

In conclusion regeneration adds significantly to vehicle range.

Regeneration will be further dealt with in section 5.3.

4.11 Hypothesis 8: Safety functions are maintained in the event of empty battery

This is verified by driving the vehicles until empty battery. The following shutdown sequences of all functions were observed. All the EVs used in the on-road tests do shutdown in a controlled and safe manner. Most importantly brakes and locks remained functional and timely warnings are given to the driver before shutdown.

Even though the same type of EVs were retested, the SOC levels and range indications varied. Historical vehicle data are applied to estimate SOC and range indication. As these historical data are unique for each concerned vehicle, this would partly explain the variations.

Furthermore, the day temperatures were different from 2013 to 2014. In 2013 the day temperatures were around 1-3 °C, while the temperatures in 2014 were 6-8 °C. This could also take part in the explanation of the higher indicated range in 2014 for the Renault Fluence and the Nissan Leaf.

| SOC indicated: | Renault Fluence 2013 | | | Renault Fluence 2014-1 | | Renault Fluence 2014-2 | |
|--------------------------|----------------------|--------|------------------|------------------------|-------|------------------------|------------------|
| | Event: | Trip: | Range indicated: | Event: | Trip: | Event: | Range indicated: |
| 12% | | | | | 0 km | | |
| 5% | Red battery symbol | | 0 km | | | | 2 km |
| 3% | | | | Red battery symbol | 5 km | | |
| 2% | | 0 km | | | 9 km | | 0 km |
| 1% | | | | | | Reduced traction | |
| 0% | | 0.9 km | | Reduced traction | | | |
| | | 3.6 km | | | | | |
| Heater: | Not working | | | Not working | | | |
| Brakes: | Still working | | | | | Still working | |
| Lights: | | | | | | Still working | |
| Power steering: | | | | | | Still working | |
| Ventilation: | | | | | | Still working | |
| Electric windows: | | | | | | Still working | |
| Door locks: | Still working | | | | | Still working | |
| ESP: | Not working | | | Not working | | | |
| Radio: | | | | | | | |

Table 4.4: Empty battery shutdown sequences, illustrated by the Renault Fluence

| SOC indicated: | Nissan Leaf 2013 | | | Nissan Leaf 2014 | |
|--------------------------|--------------------|--------|------------------|--------------------|------------------|
| | Event: | Trip: | Range indicated: | Event: | Range indicated: |
| 15% | | 0 km | 5 km | | |
| 13% | | | 4 km | | |
| 11% | | | 3 km | | |
| 9% | | 3.7 km | --- | | |
| | | | | Red battery symbol | |
| 5% | Turtle symbol | 6.6 km | --- | | 4 km |
| 2% | Red battery symbol | 8.4 km | --- | | |
| 0% | | | | Turtle symbol | --- |
| Heater: | | | | | |
| Brakes: | Still working | | | Still working | |
| Lights: | | | | | |
| Power steering: | | | | | |
| Ventilation: | | | | | |
| Electric windows: | | | | | |
| Door locks: | Still working | | | Still working | |
| ESP: | | | | | |
| Radio: | | | | | |

Table 4.5: Empty battery shutdown sequences, illustrated by the Nissan Leaf

| SOC indicated: | Mitsubishi i-MiEV 2013 | | Mitsubishi i-MiEV 2014 | | |
|--------------------------|------------------------|--------|------------------------|-------|------------------|
| | Event: | Trip: | Event: | Trip: | Indicated range: |
| 15% | Heater off | 0 km | Heater off | 0 km | 1 km |
| 14% | Turtle symbol | 0.6 km | Turtle symbol | 1 km | 0 km |
| 9% | 80% traction | 3.8 km | Reduced traction | 4 km | |
| | 60% traction | 6.4 km | | | |
| 5% | 40% traction | 7.3 km | Traction off | | |
| | 20% traction | 7.6 km | | | |
| | Traction off | 7.9 km | | | |
| 0% | Red battery symbol | | | | |
| Heater: | Not working | | Not working | | |
| Brakes: | Still working | | Still working | | |
| Lights: | Still working | | Still working | | |
| Power steering: | Still working | | Still working | | |
| Ventilation: | Still working | | Still working | | |
| Electric windows: | Still working | | Still working | | |
| Door locks: | Still working | | Still working | | |
| ESP: | | | Still working | | |
| Radio: | | | Not working | | |

Table 4.6: Empty battery shutdown sequences, illustrated by the Mitsubishi i-MiEV

There were no changes in the Mitsubishi i-MiEV's shutdown sequence from 2013 to 2014.

It was not possible to complete this test with all EVs. The Fiat Fiorino Micro-Vett had a malfunction so the remaining tests were discarded. The Tesla Model S battery was too large to discharge completely for practical reasons.

The Opel Ampera is a hybrid EV with a smaller battery than the other EVs. Its battery was typically emptied during the day, where continued driving in the vehicle was carried out on gasoline-produced power without any loss of functions.

4.12 Hypothesis 9: Optimum regenerative braking relies on battery and motor parameters

When an EV battery is fully charged and/or parked on top of a hill, there may be excess regenerative energy (potential energy) to fit into the HV-battery. If the EV has been driving aggressively, the motor or battery temperature may be near its upper limit. In such situations the EV system should limit the regenerative power, hence the ability to regenerate counting on these and perhaps other battery and motor parameters. The grade of influence onto the driving varies with the vehicle.

This test did actually prove that the regenerative energy depend on HV-battery parameters. Though, it was not possible to reach an over temperature state with any of the EVs used in the on-road tests. As seen in Table 4.7, the EVs displayed reactions in situations with a fully charged HV-battery.

| | |
|-------------------------|---|
| Mitsubishi i-MiEV | The vehicle would regenerate normally after a quick charge. |
| Nissan Leaf | The vehicle shows reduced regeneration by turning off the “inner rings” in the power indicator directly after quick charge. |
| Renault Fluence ZE | While driving the vehicle just after battery swap it would not regenerate, but was able to regenerate fully a few seconds after this. |
| Fiat Fiorino Micro-Vett | At 100% SOC the vehicle showed “no regen” on the dashboard, but was able to regenerate a few seconds later. |

Table 4.7: Regeneration status after quick charging or at 100% SOC.

4.13 Hypothesis 10: Vehicle performance is almost unaffected by battery SOH

The SOH of a battery is known to degrade over time. Therefore, in the cases where the exact same EVs were revisited each year, their performance was determined from the test data to reveal any change in acceleration time, motor power or maximum speed.

The measured battery power from the EVs used in the on-road tests was filtered from auxiliary power to show the actual power delivered to the motor.

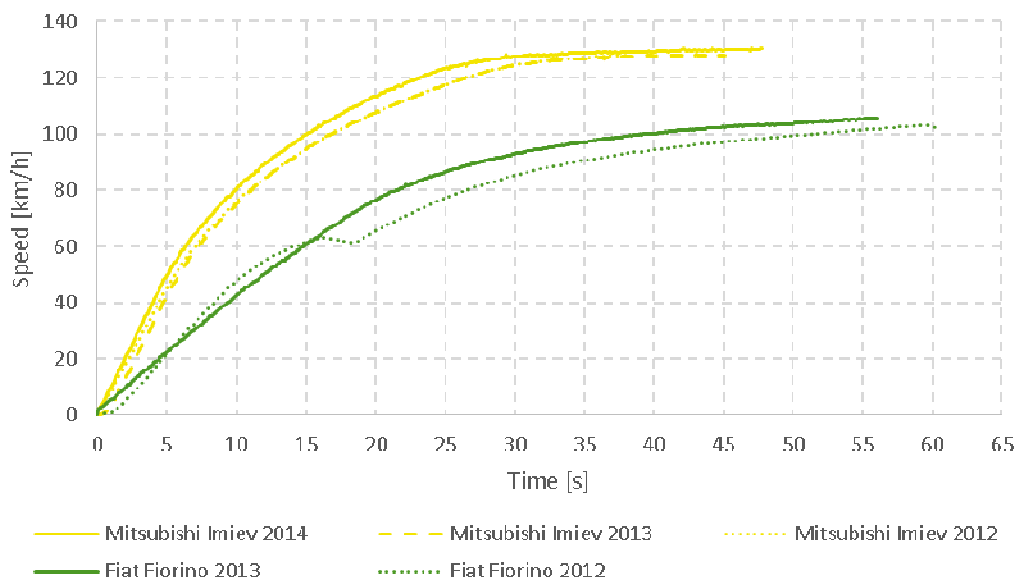


Figure 4.13.1: Acceleration times at straight line, illustrated by the Mitsubishi i-MiEV and the Fiat Fiorino Micro-Vett

The differences are shown in Figure 4.13.1. Regarding the small EV, the Mitsubishi i-MiEV, differences cannot be explained by aging of the vehicle. The fact that the performance did improve can also be due to new tires etc. on the vehicle.

The converted EV, the Fiat Fiorino Micro-Vett, was equipped with a five speed gear box and a clutch that cannot be operated normally while driving. While operating in the 2nd and 3rd gear only in 2012 (until the last day of testing) the vehicle top speed was limited to around 100 km/h. Acceleration times were not improved by shifting gears as seen in Figure 4.13.1.

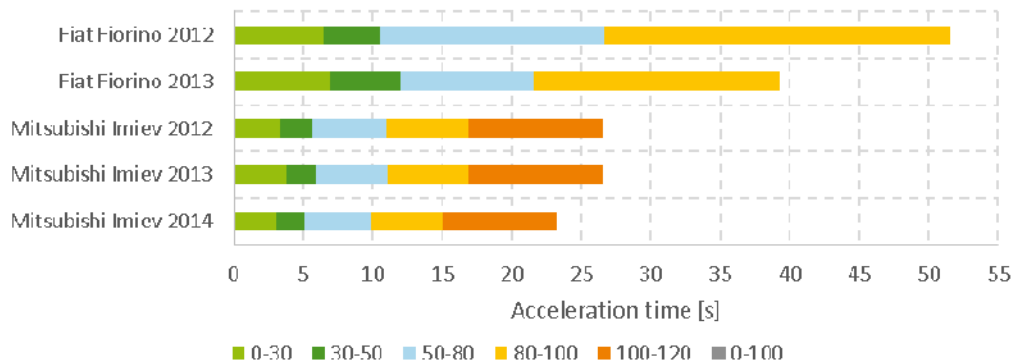


Figure 4.13.2: Acceleration times during straight line testing with the pedal fully depressed, illustrated by the Fiat Fiorino Micro-Vett and the Mitsubishi i-MiEV

Regarding power, the Mitsubishi i-MiEV was available to be revisited all three years. Small variations were observed, but not enough to rule out any influence of the ambient conditions. The dotted curve for the Mitsubishi i-MiEV in Figure 4.13.3 is due to different logging equipment used.

The test personnel learned how to operate the Fiat Fiorino Micro-Vett during the 2012 test (including the 4th and 5th gear). Therefore, a different gear shifting strategy in 2012 and 2013 was developed. A delay is expected when shifting gear during acceleration, which did also occur in 2012, where it prolonged the acceleration time significantly. Please compare Figure 4.13.1 with Figure 4.13.2 and Figure 4.13.3.

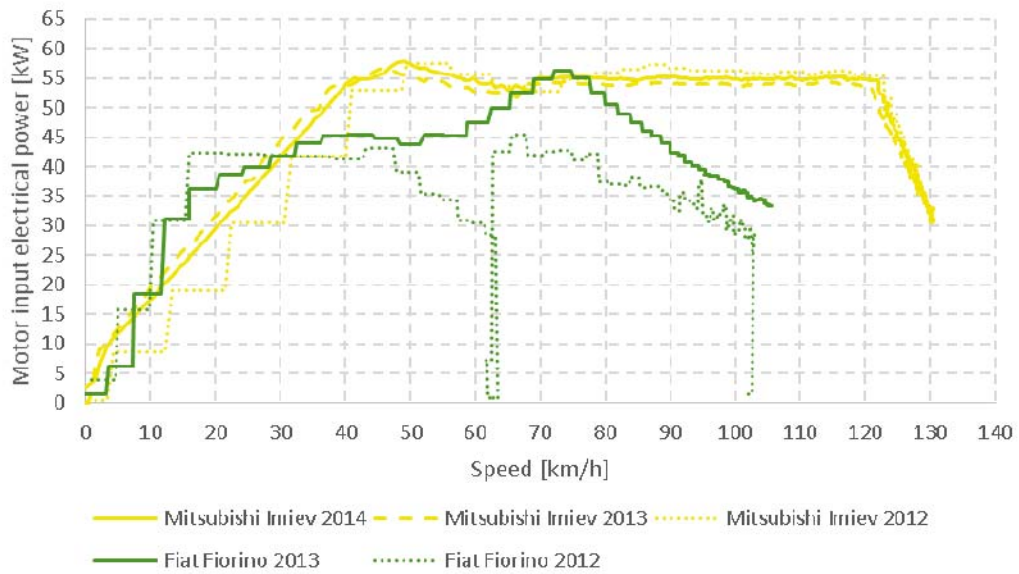


Figure 4.13.3: Power curves at straight line acceleration, illustrated by the Mitsubishi i-MiEV and the Fiat Fiorino Micro-Vett

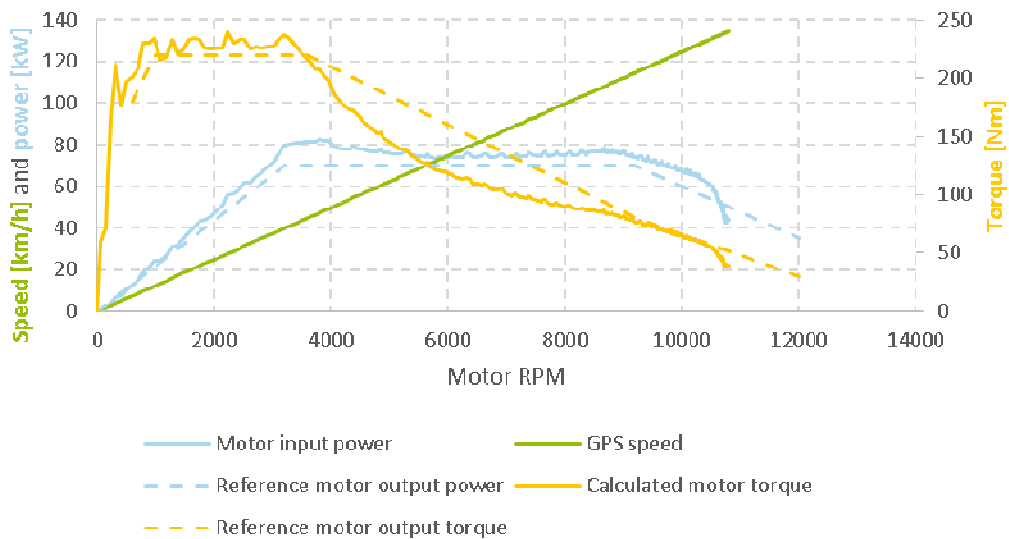


Figure 4.13.4: Motor electrical power and torque versus motor RPM at straight line acceleration, illustrated by the Renault Fluence ZE 2013 (mileage: 500 km) and Renault reference curves¹¹

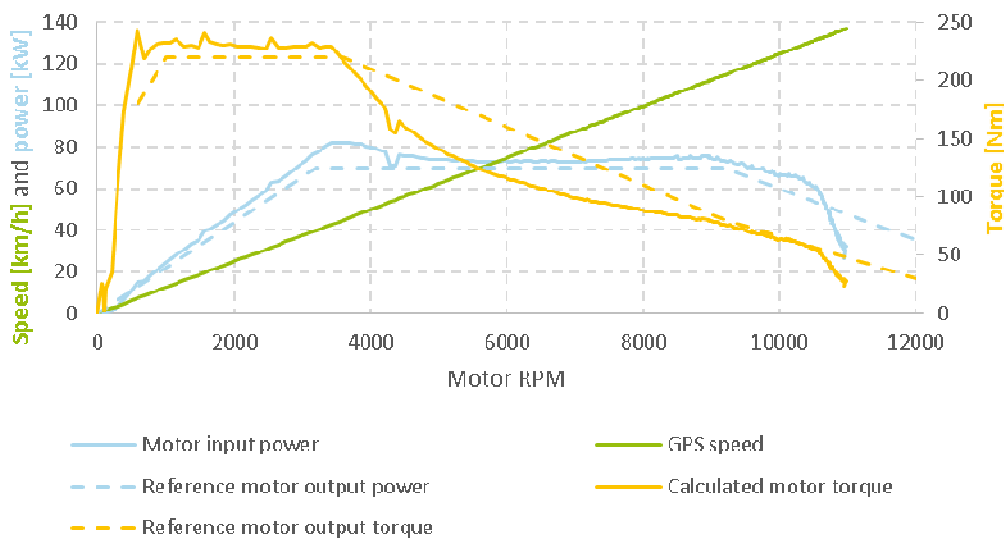


Figure 4.13.5: Motor electrical power and torque versus motor RPM at straight line acceleration, illustrated by the Renault Fluence ZE 2014 (mileage: 25900 km) and Renault reference curves¹¹

The measured motor power and torque at straight line acceleration for the Renault Fluence ZE 2013 (new vehicle) and Renault Fluence ZE 2014 (used vehicle) have been compared to Renault's own reference curves¹¹, which are shown in Figure 4.13.4 and Figure 4.13.5. The EV did not lose any performance expressed in neither motor power nor motor torque.

Please note that the two Renault Fluence ZE vehicles used in the on-road test did drive while HV-battery swap was still available in Denmark. Therefore, each of the vehicles had several HV-batteries installed with different history, hence this test can only tell about the vehicles performance as a whole.

Figure 4.13.6 shows difference in drivetrain efficiency throughout the on-road tests with three years in between. The values shown are the true PABE, which does not include auxiliary consumption.

¹¹ <http://www.powertrain.renault.com/our-range/powertrain-units-of-our-range/5-a-powertrain>

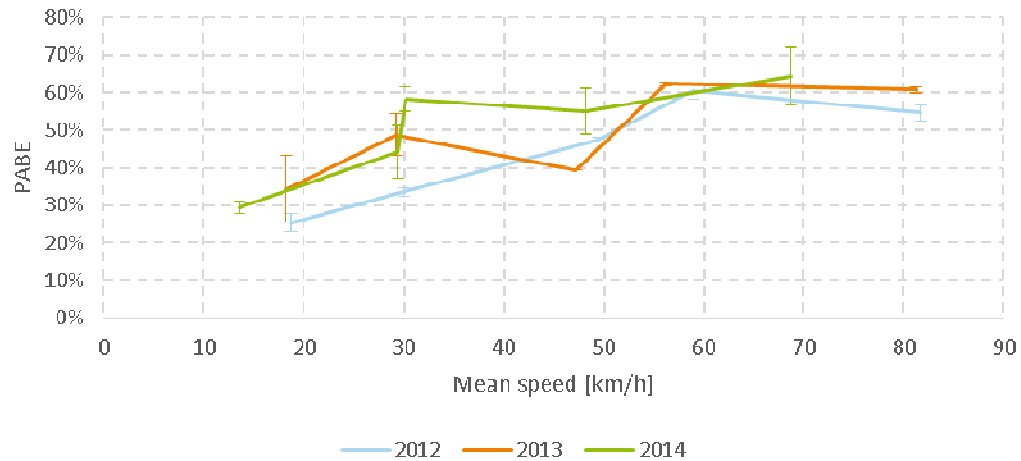


Figure 4.13.6: PABE comparison, illustrated by the Mitsubishi i-MiEV

For more details about SOH please also see D9.8.

4.13.1 Vehicle performance compared to conventional ICE vehicles

Comparing the EVs to similar ICE vehicles, it is possible to find an equivalent to one another.

The small size EVs are typically superior in acceleration than similar ICE vehicles, because of the advantages of the electric drivetrain. As can be seen in Figure 4.13.7, most of the EVs used in the tests lies together within the tolerances just above the rather category D ICE vehicles.

The luxurious Tesla Model S is similar in size and acceleration performance to the Porsche Panamera.

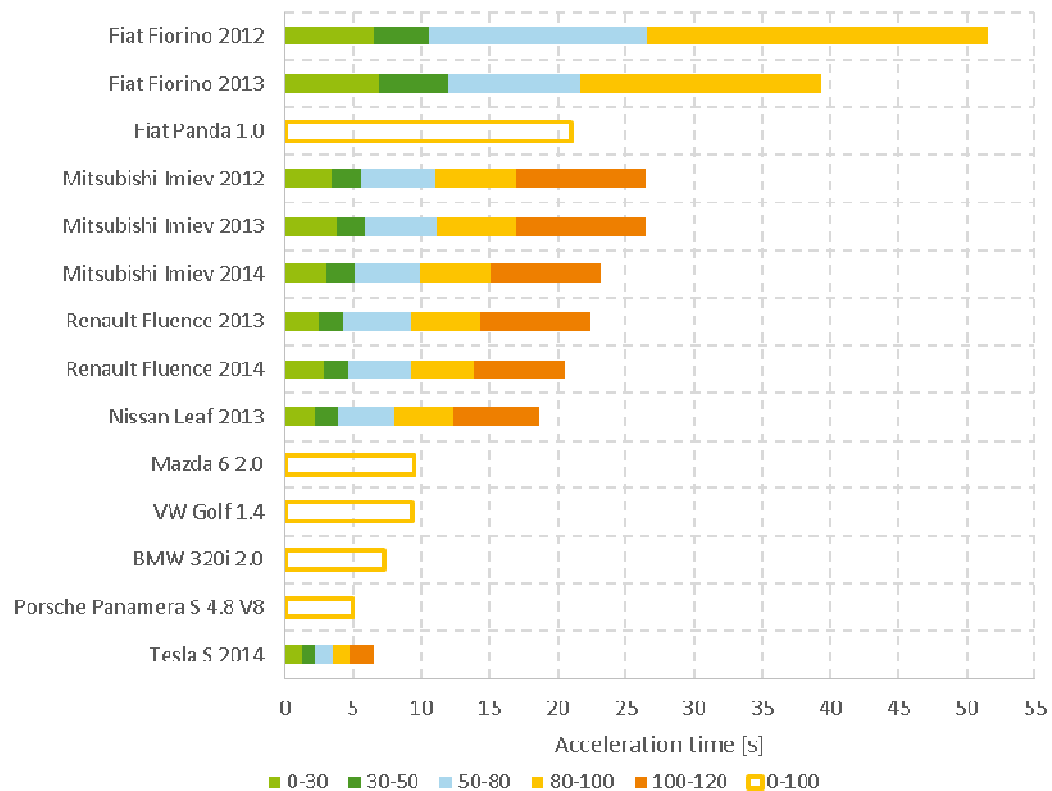


Figure 4.13.7: Acceleration times during straight line testing with the throttle pedal fully depressed

Comparing the performance in motor input power in Figure 4.13.8, the Tesla Model S builds up power superior to the Porsche Panamera, but the Porsche catches up and holds the power level until near 300 km/h, where the Tesla Model S rolls off at around 210 km/h due to the single-gear transmission.

The power curves for the Mazda 6 and the Porsche Panamera have been calculated, based on transmission information, to be able to compare with the EVs.

The Mazda 6 lies just on top of the EVs, it has marginally more power than the Nissan Leaf and the Renault Fluence ZE.

Note, that the acceleration properties of the EVs are more uniform than of the ICE vehicles. Add the absence of noise and the experience becomes even more impressive.

The power curves in Figure 4.13.8 do also reflect the maximum speed of the vehicles respectively.

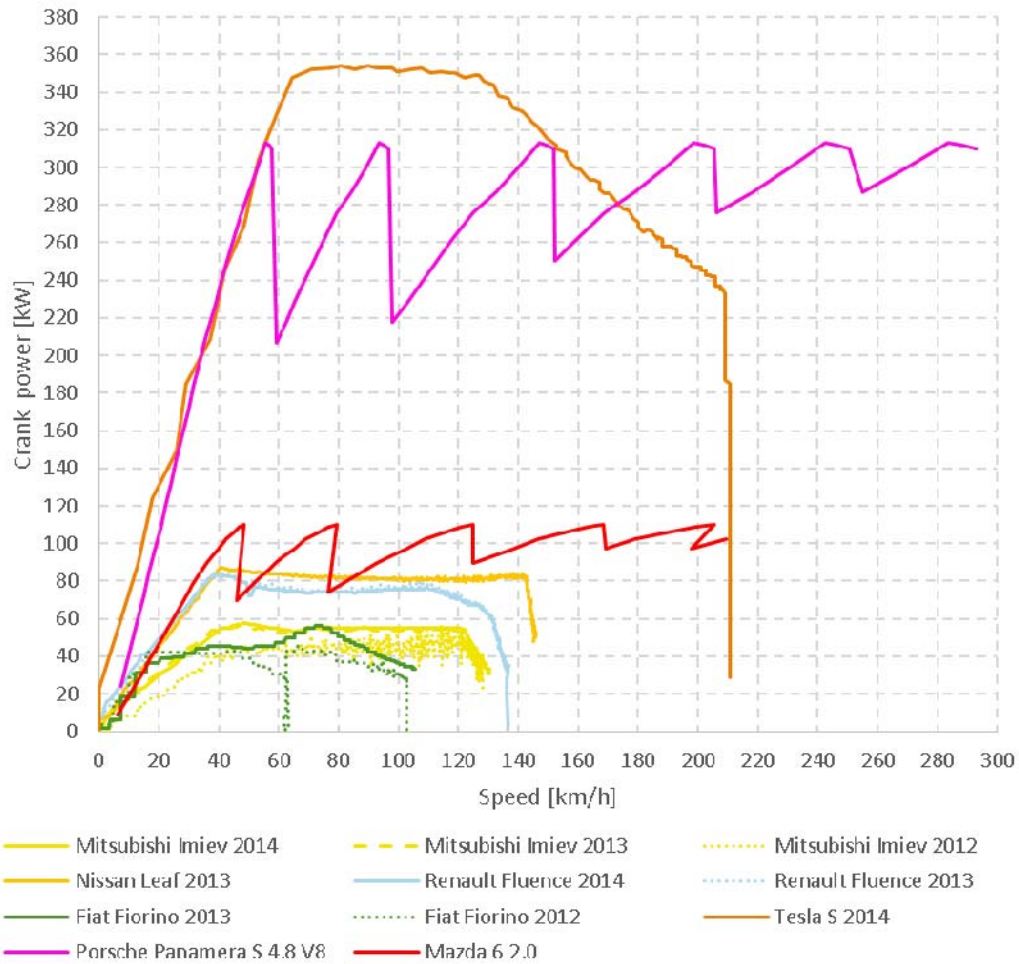


Figure 4.13.8: Power curves at straight line acceleration

4.14 Hypothesis 11: Propulsion energy is largely unaffected by climate conditions

The formulation of this hypothesis comes from conventional ICE vehicles, where climate conditions are not a major factor. On EVs however, there could very well be significant impact of climate. Nevertheless, we cannot assume anything without proof. This chapter seeks proof or disproof of that.

In this section other important factors with impact on the propulsion energy not related to the climate are included. These factors are slope and weight.

4.14.1 The impact of temperature

Please also see section 5.2.

Lower temperature yields generally higher air density, where to the air pressure has a similar influence.

Air density versus air pressure and temperature:

$$\rho \left[\frac{\text{kg}}{\text{m}^3} \right] = \frac{p}{R_{\text{specific}} T} \quad (16)$$

Where:

p = absolute pressure [Pa] [Pa]

R_{specific} = the specific gas constant for dry air = $287.058 \left[\frac{\text{J}}{\text{kg} \cdot \text{K}} \right]$ (17)

T = absolute ambient temperature [K]

The on-road tests included data of air humidity, but the humid air density seemed only to vary on the fourth and fifth decimal, which has no impact on the air density, practically.

Figure 4.14.1 indicates the difference in wind resistance, when the air density changes by the air pressure and air temperature, even though the vehicle and wind speed and direction are held constant. It shows the influence from temperature and pressure onto the air density, hence onto the energy consumption. Just like heavier headwind. At high speed driving the influence would be greater.

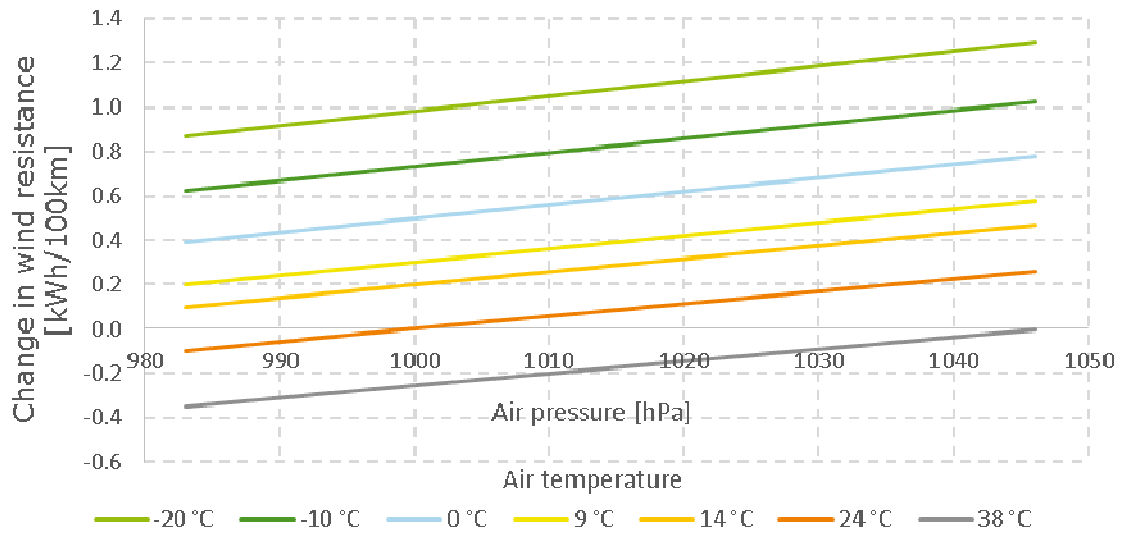


Figure 4.14.1: Calculated change in wind resistance versus air pressure at different temperatures with reference to the wind resistance at 24°C and 1000hPa, illustrated by the Nissan Leaf driving SORDS 2014

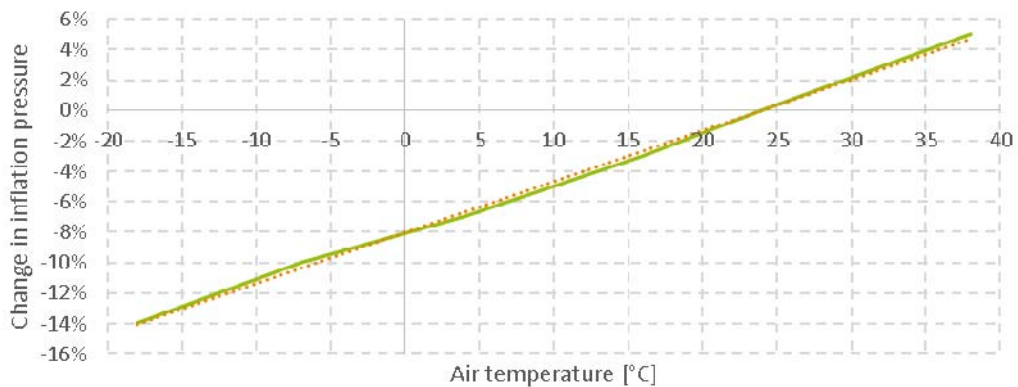


Figure 4.14.2: Tire inflation pressure versus temperature

Figure 4.14.2 and Figure 4.14.3 show the impact of the temperature, if a vehicle's tires are adjusted to the manufacturer-recommended inflation pressure inside a workshop at room temperature. From here the vehicle may drive on into a colder temperature, if it is winter outside, and the tire inflation pressure will decrease (up to 10% at -30°C), hence increase the energy consumption.

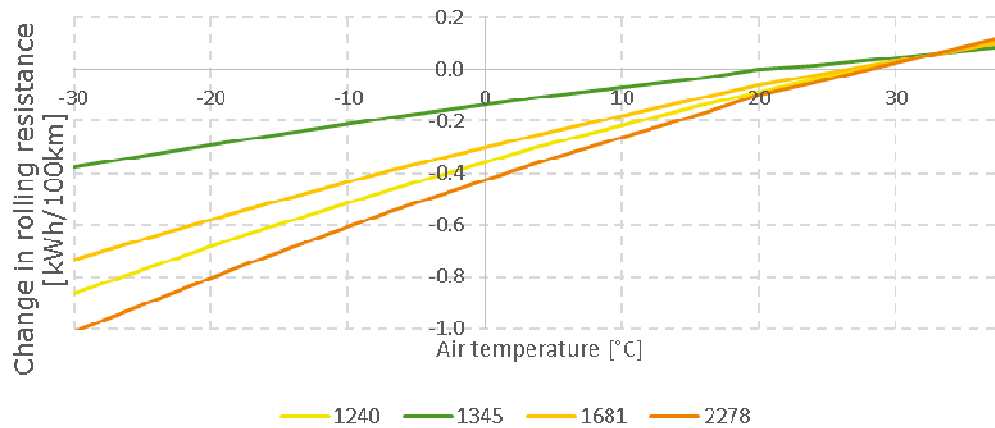


Figure 4.14.3: Calculated change in rolling resistance versus air temperature at several vehicle weights with reference to the rolling resistance adjusted to 36 psi at 20°C, illustrated by the Mitsubishi i-MiEV, Fiat Fiorino Micro-Vett, Nissan Leaf and Tesla Model S driving SORDS¹²

4.14.2 The impact of wind

As stated in D6.1 Section 5.8.1, the wind can have a significant impact on the propulsion energy of a vehicle. A wind speed of 7 m/s would theoretically increase energy consumption by 4-7 %, if the trip consists of equal distances with head- and tail wind. The reason why head and tail winds do not cancel out each other, is, that the power of the wind is not linear but rises with the square of the wind speed relative to the vehicle.

EVs do not take the wind direction into account, when estimating the range required for a given trip, but this could very well be part of future navigation systems. This chapter illustrates how wind data can be used to predict the increased drag and thus the reduction in range of a given trip.

As it is seen in Figure 4.14.4 the wind is definitely a factor at high speeds on our test track.

¹² Gyenes, L. and Mitchell, C.G.B., "The Effect of Vehicle-Road Interaction on Fuel Consumption," Vehicle-Road Interaction, ASTM STP 1225, B.T. Kulakowski, Ed., American Society for Testing and Materials, Philadelphia, 1994, pp. 225-239.

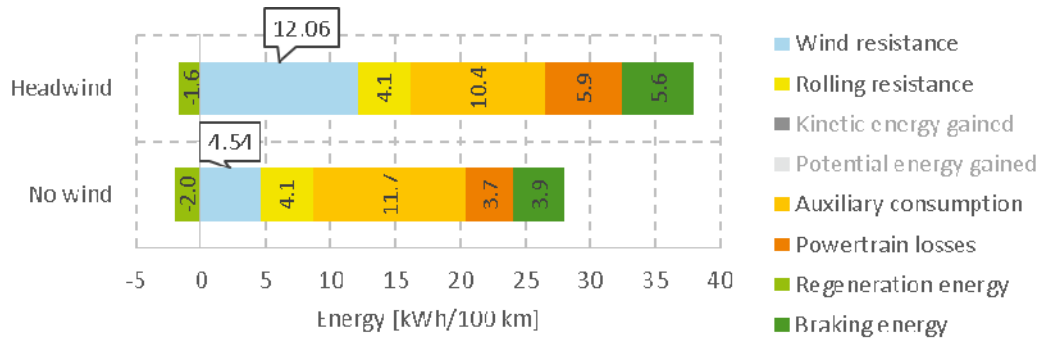


Figure 4.14.4: SORDS high speed part (1500-3000m) in Værløse 2012, illustrated by the Fiat Fiorino Micro-Vett

From trigonometry we can assume that total wind drag can be calculated from the formula below:

$$D_{wind} = v_{vehicle} \cdot \cos \angle_{eff} \cdot \frac{1}{2} \cdot \rho \cdot v_{wind,eff}^2 \cdot A \cdot C_w \quad (17)$$

Where the effective speed (relative to the vehicle) is:

$$v_{wind,eff} = \sqrt{v_{vehicle}^2 + v_{wind}^2 + 2 \cdot v_{vehicle} \cdot v_{wind} \cdot \cos(\angle_{heading} - \angle_{wind})} \quad (18)$$

The effective angle (relative to vehicle's direction of motion) is:

$$\sin \angle_{eff} = \sin(\angle_{heading} - \angle_{wind}) \cdot \frac{v_{wind}}{v_{wind,eff}} \quad (19)$$

The wind speed and wind angle is taken as 10 minute averages from weather data supplied by the Danish Meteorological Institute (DMI). The speed and heading of the vehicle is known from GPS data. Note that all wind drag data in this report have been calculated, not measured. To validate the calculations we need to look at the total propulsion energy and see that it matches to the expectations.

Vehicle wind resistance:

$$E_{wind}[kWh] = \frac{(\int_0^{s_{max}} \frac{1}{2} \cdot \rho \cdot A \cdot C_w \cdot a \cdot s \, ds) [J]}{3.600.000 \left[\frac{J}{kWh} \right]} \quad (20)$$

The wind conditions during the on-road tests of this WP have been rather mild with wind speeds, only reaching about 6 m/s on the days of testing. So there is no data to support the impact of strong winds. However, there is enough evidence that wind influences the vehicle like assumed in D6.1.

The impact of wind will be strongest on high speed, straight line runs. Thus we look at some steady speed runs, which have been performed in both directions on the same day. Please see Figure 4.14.5.

The possible error margin is quantified as the sum of all unexplained losses. This includes some mechanical losses, which are inevitable, so there should be some margin larger than zero. However, if the margin is consistently large, or even negative, it could suggest some over/under estimation of wind drag.

In this case there seems to be good agreement between the calculated wind drag the real world, because the error margin is consistent and probably due to mechanical losses.

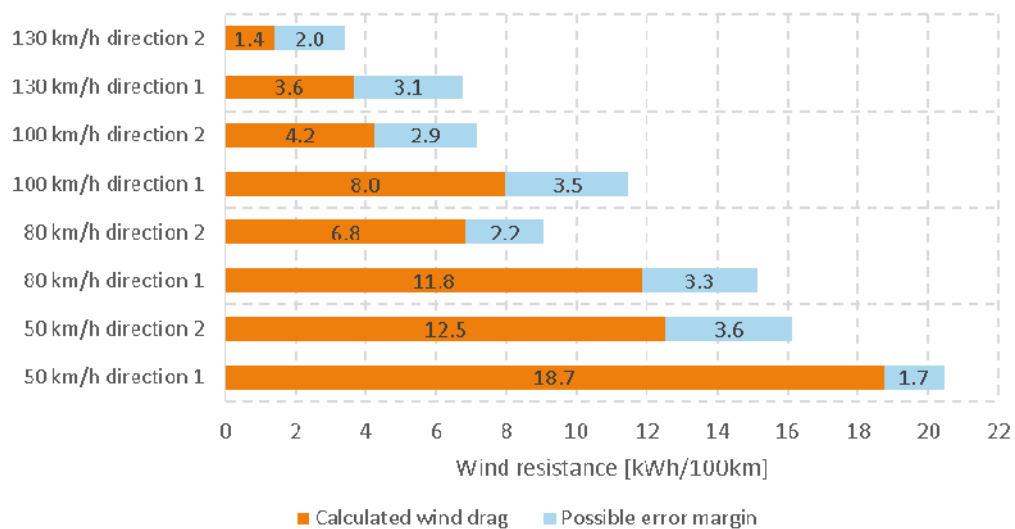


Figure 4.14.5: Calculated wind drag at steady speed with possible error margin shown in blue, illustrated by the Tesla model S

4.14.3 The impact of rain

The effect of rain on the energy consumption of automobiles is rarely discussed. This is probably because the effect is quite small and without practical consequences. People tend to drive slower in the rain, which would immediately lower the consumption. Any physical effects are therefore mostly of academic interest.

In real life it is far more important to talk about the safety effects of wet surface due to lower friction, which impairs the braking and steering ability of the vehicle. However, we will not discuss friction in this chapter, but only deal with possible effects on the wind and rolling resistance of the vehicle. Contrary to popular beliefs, friction is not the same as rolling resistance.

In bicycle racing, it is said that a wet surface marginally decreases the tire rolling resistance, thus enhancing the performance of a bicycle racer.

To test the impact of rain on a car it is mandatory to have a substantial amount of data both in the wet and in the dry. However the team did not see any substantial rain during the test weeks. Only in Værløse 2012 were short periods with moisture on the track, thus comparing the moist and the dry track. As shown in Figure 4.14.6 there was a much smaller energy consumption on the damp track compared to the dry. However, after analysis this turned out to be caused by the difference in regenerated braking energy and auxiliary consumption, which have nothing directly to do with the moist. There remains only a 2 % drop in rolling resistance, which **could** be caused by the damp road. But at this point there just isn't enough data to say if this was actually caused by the damp road or by something else.

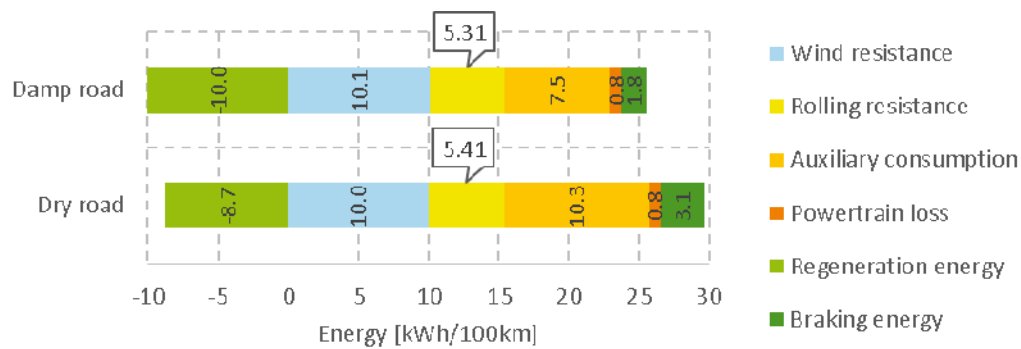


Figure 4.14.6: Apparent impact of surface humidity, illustrated by the Mitsubishi i-MiEV (SORDS in Værløse 2012)

To try and justify observations, taking a look at the possible ways in which rain may influence energy consumption of a vehicle is crucial:

1. Smoothing of the surface by a water layer (up to 7.5%)
2. Increased air mass due to the presence of rain drops (<1%)
3. Energy required for water expulsion from surface (up to 34 %)
4. Increased cooling of tires due to water splash (<1%)
5. Auxiliary energy needed to drive windshield wipers (<1%)

4.14.3.1

moothing the surface

If the observation in Figure 4.14.6 is exact, then there must be a smoothing effect of the water layer lessening the effective roughness of the surface.

It can't be determined whether the surface in Værløse was actually smoothed by the rain. But assuming this was the case, rolling resistance would also drop. According to literature ("Measuring road

roughness and its effect on user cost and comfort”, ASTM 1985) rolling resistance as a function of roughness can vary by up to 23 % on roads of different roughness.

This means that the 2 % drop in rolling resistance observed in Figure 4.14.6 could very well be within the possible effects of surface smoothing.

4.14.3.2 Increase in air mass due to the presence of rain drops

In

When it rains, the air contains rain drops, which have a certain mass. Therefore, the rain must have some kind of impact on a vehicle passing through it. But is this impact significant?

The possible effect of rain drops is not included in Figure 4.14.6 or in any other calculations shown in this report. To justify this simplification we will consider a condition with hard rain described as following:

- 30 mm of rain per hour is considered very hard rain.
- In this case 30 litres of rain hit one square meter every hour.
- Rain drops fall at a terminal velocity of about 5.5 m/s.

This amounts to a rain mass of:

$$M_{rain} \left[\frac{g}{m^3} \right] = \frac{30 \left[\frac{kg}{m^2 \cdot h} \right] \cdot 1000 \left[\frac{g}{kg} \right]}{5.5 \left[\frac{m}{s} \right] \cdot 3600 \left[\frac{s}{h} \right]} = 1.5 \left[\frac{g}{m^3} \right] \quad (22)$$

Since the density of dry air is approximately 1200 g/m³ this increase in air mass due to rain drops even in hard rain is **only about 0.1 %**.

Assuming that the vehicle body scoops up every rain drop and accelerates this to 60 km/h (16.7 m/s). the rain then removes kinetic energy from the vehicle, which will demand for extra consumption to keep the speed, hence rain resistance. The rain resistance is divided into impact onto the roof, and onto the front of the vehicle.

On a vehicle roof with a given area of 7.2 m², the rain resistance will be:

$$P_{rain,roof} [W] = \frac{1}{2} \cdot 7.2 [m^2] \cdot 30 \left[\frac{kg}{m^2 \cdot h} \right] \cdot \frac{\left(16.7 \left[\frac{m}{s} \right] \right)^2}{3600 \left[\frac{s}{h} \right]} = 8.4 W \quad (23)$$

And rain resistance onto a vehicle front with a given area of 2.2 m²:

$$P_{rain,front} = \frac{1}{2} \cdot 2.7[m^2] \cdot 60 \left[\frac{km}{h} \right] \cdot 1000 \left[\frac{m}{km} \right] \cdot 0.0015 \left[\frac{kg}{m^3} \right] \cdot \frac{\left(16.7 \left[\frac{m}{s} \right] \right)^2}{3600 \left[\frac{s}{h} \right]} = 9.4W \quad (24)$$

To make a quick assessment of the significance of the rain drop presence, these numbers are compared to the ordinary aero dynamic drag to which the vehicle is exposed. The aero dynamic drag is expressed as following:

$$D_{aero} = \frac{1}{2} \cdot 2.7[m^2] \cdot 1.2 \left[\frac{kg}{m^3} \right] \cdot \left(16.7 \left[\frac{m}{s} \right] \right)^3 \cdot 0.3 = 2263.5W \quad (21)$$

The sum of the rain resistances calculated in (23)-(24), hence the contribution from rain, is then **less than 1%** of the normal aero dynamic drag. This means that the presence of rain drops in the air has a **minimal influence** on the energy consumption of a vehicle.

4.14.3.3

In

creased cooling of tires

As a wet person will easier be cold outside in the wind, because the increased transfer rate of heat, so will the tires of a vehicle. The normal operating temperature of road vehicle tires is about 40 °C at 15 °C ambient. Assuming that all rolling resistance is converted into heat, then each tire shall dissipate about 650 W at 60 km/h. The external surface area of one tire is about 0.6 m². Together these would create an equilibrium at $45 \frac{W}{m^2 \cdot K}$, which is the approximate heat transfer coefficient in air at 17.6 m/s.

Water would increase the coefficient of heat transfer to the surroundings by several folds. Let us assume a quadrupling in heat transfer coefficient. This would bring the equilibrium tire temperature to:

$$T_{tire} = \frac{40^{\circ}C - 15^{\circ}C}{4} + 15 = 21^{\circ}C \quad (22)$$

The tire pressure thus will then be reduced by:

$$\Delta p_{tire} = \frac{273.15 + 40}{273.15 + 21} - 1 = 6\% \quad (23)$$

The resulting increases in rolling resistance will be about 4/10 of that, approximately 2.4 %. Total energy would change **less than 1 %**. Thus cooling of tires in the wet has a **minimal influence**.

4.14.3.4

A

uxiliary energy needed to work the wind shield wipers.

A standard set of wipers uses about 30 W to operate. At 60 km/h this is roughly $\frac{30W}{8kW} = 0.4\%$ of the total energy consumption. This also has **minimal influence**

4.14.3.5

E

energy required for water expulsion on surface

What if the rain did leave puddles on the streets?

Driving through puddles creates an enormous water splash which effect can be felt clearly inside the vehicle. The picture shows how the vehicle effectively creates a path of dry road as it pushes the water aside. There is no doubt that this slows down the vehicle significantly.



Figure 4.14.7: Example of water expulsion from a flooded road (Picture from the [Internet](#))

However, puddles like the one on the picture are rare. On a well-drained road there should be less than 1 mm of water on the surface. Let us assume that the vehicle pushes aside all water that comes under the wheels and shoots it off with a pressure equal to the internal tire pressure.

The vehicle has four tires of 185 mm width and travels at 16.7 m/s.

The energy spent on water expulsion can then be estimated by:

$$P_{water} = 4 \cdot 0.185[m] \cdot 1[mm] \cdot 16.7 \left[\frac{m}{s} \right] \cdot 220kPa = 2718.8W \quad (24)$$

This is a quite coarse assumption. But it shows, at least in principle, that water expulsion could add as much as 34 % to the consumption, which is significant. Since this is far more than the other factors investigated here, and since there does not seem to be any other noticeable factors causing effects of rain, we will conclude that rain on the road and on the car has **minimal influence unless there is actual splashing from water expulsion under the tires**.

Conclusively rain should have minute influence unless there is actual splashing from water expulsion.

4.14.4 The impact of slope

Travelling uphill consumes more energy because of the accumulated potential energy due to the gravity. In addition to this, an EV can be allowed to exceed its nominal power for a short period during acceleration, in a state which the particular EV could be held erroneously when travelling up-hill. Though, this is not confirmed by the on-road tests.

To visualise this, the potential energy accumulated is compared to the total electric energy drawn from the HV-battery.

The potential energy accumulated:

$$E_{pot} \left[\frac{kWh}{100km} \right] = \frac{(m \cdot g \cdot h_1 - m \cdot g \cdot h_2) \cdot 100[km]}{s[km] \cdot 3600000 \left[\frac{J}{kWh} \right]} \quad (25)$$

Figure 4.14.8 illustrates the potential energy gain in case of travelling uphill or energy release in case of travelling downhill. Potential energy is depending on the objects mass and the difference in height between two positions, e.g. a vehicle with a mass of 2278 kg gains about 2 kWh/100km of potential energy, if travelling uphill with a slope of 0.3%.

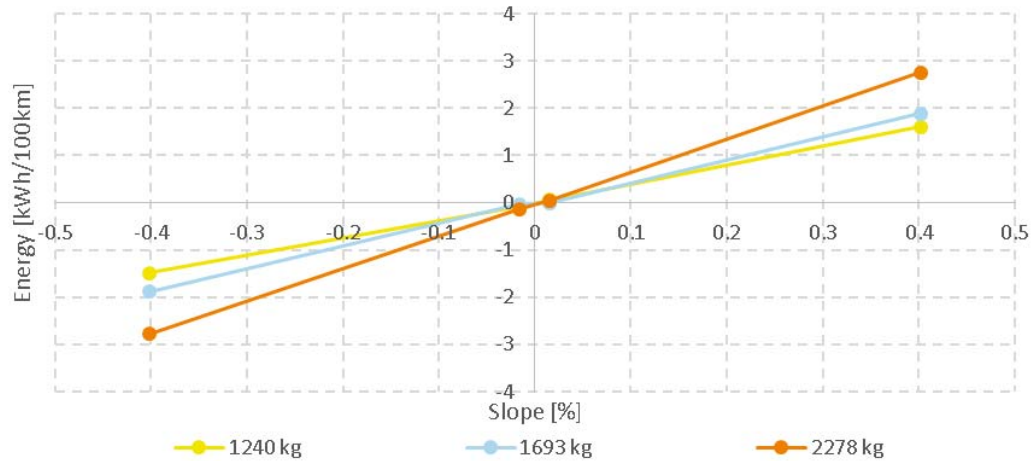


Figure 4.14.8: Potential energy versus slope of road for different vehicle weights, illustrated by the Mitsubishi i-MiEV, Renault Fluence ZE and Tesla Model S

This potential energy gain of the EV must be provided by the HV-battery. Figure 4.14.9 shows the total energy drawn from the HV-battery packs depending on the vehicles weight and the slope.

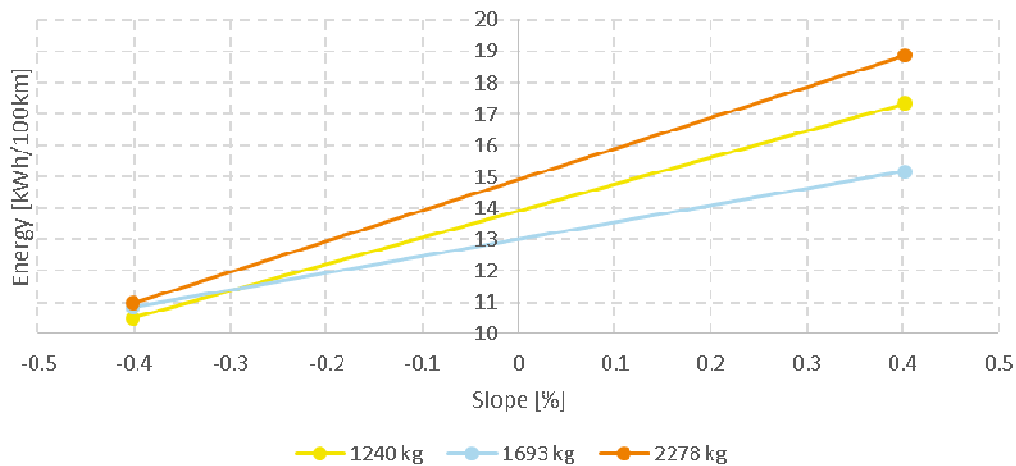


Figure 4.14.9: Total energy drawn from battery versus slope of road for different vehicle weights, illustrated by the Mitsubishi i-MiEV, Renault Fluence ZE and Tesla Model S

4.14.5 The impact of weight

Vehicles of different classes tend to have different weights. Therefore, the weight's influence onto the energy consumption of EVs with different weights is analysed in this section.

The influence of weight can be divided into two categories; the influence from the curb weight of the vehicle and the influence of luggage and passengers.

The theoretic consumption only limited by the vehicle, the VLFC, excluding powertrain losses and auxiliary consumption, is shown in Figure 4.14.10.

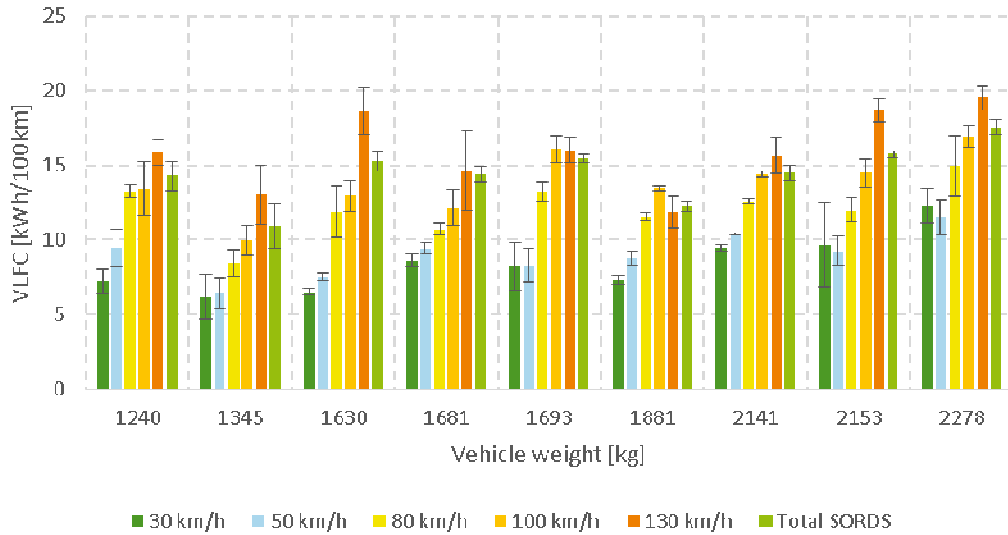


Figure 4.14.10: VLFC during dynamic driving from EVs with different weight

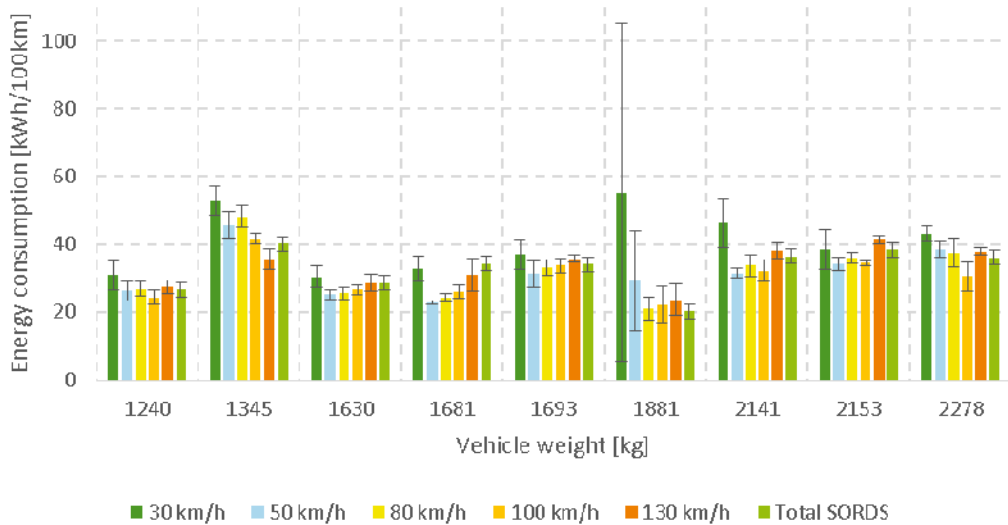


Figure 4.14.11: Total measured energy consumption during dynamic driving from EVs with different weight

However, the general trend is much weaker for the EVs than it is expected from ICE vehicles, where the weight has a vital influence. This is due to the regeneration.

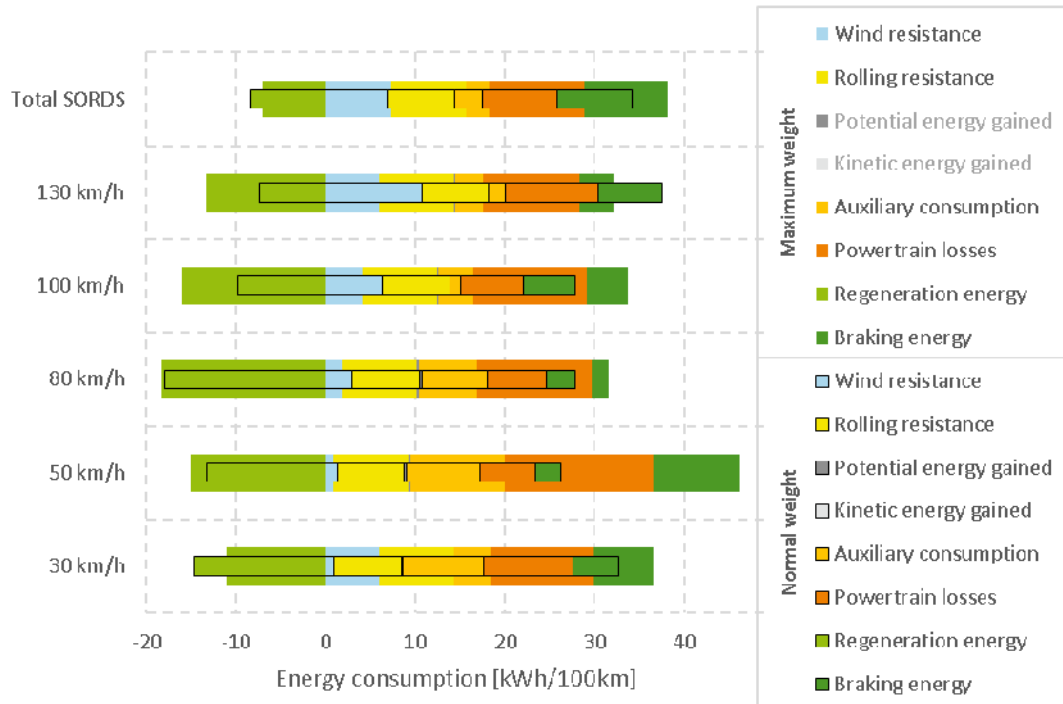


Figure 4.14.12: Comparison of energy consumption at dynamic driving with the same EV at maximum weight and normal weight, illustrated by the Nissan Leaf

The trend is verified by tests shown in Figure 4.14.12. Nissan Leaf's total consumption results driving SORDS with two persons inside (normal weight – narrow graph) are quite lower compared to SORDS consumption results with the EV at maximum loaded weight (maximum weight – wide graph). Note also the higher regeneration energy.

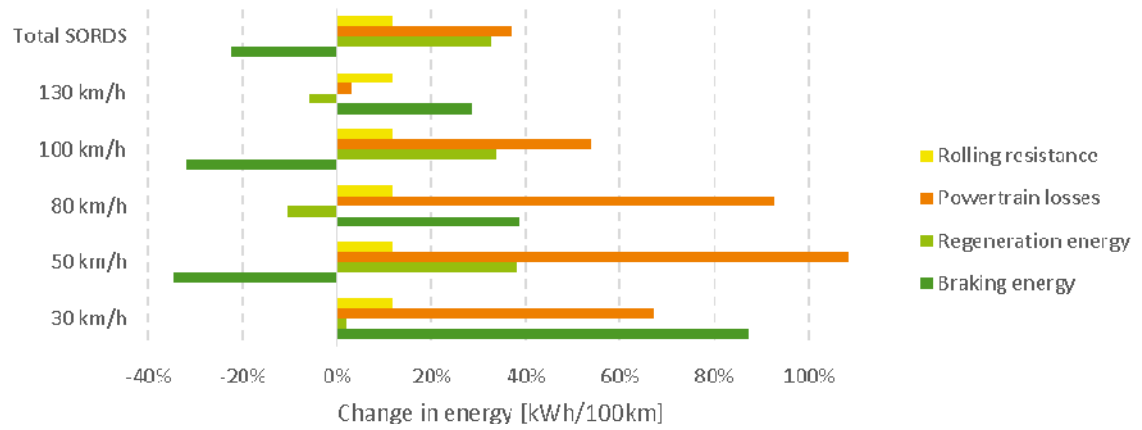


Figure 4.14.13: Change in the energies at maximum weight compared to normal weight, when driving dynamically with the same EV, illustrated by the Nissan Leaf

5 Validation and analysis of climatic impact

As a supplement to the on-road testing, measurements of the behaviour of electric vehicles under different environmental temperatures were also procured on a dynamometer in a climate chamber. Main objective of the measurements was an assessment of the temperature impact on the vehicle performance. An overview of the methodology used is given in paragraph 3.1.2 and it is described in more detail in deliverable D6.1. Two small vehicles (Mitsubishi i-MiEV and Citroën C-Zero) and one mini (Renault Twizy) were used for the tests. Citroën C-Zero and Mitsubishi i-MiEV are based on the same technical platform and it is expected that the results are comparable. Vehicles are shown in Figure 5.1.1.

5.1 Analysis of influence of temperature and aging on charging efficiency and battery capacity

5.1.1 Charging behaviour

The analysis is based on full charging cycles of two vehicles: Mitsubishi i-MiEV and Citroën C-Zero. A full charging cycle is defined as charging the HV-battery from a SOC of 0% to a SOC of 100%. Because no fast charger was available for the measurements slow charging with a power below 3 kW was used. While both vehicles are technically very similar, they exhibited some differences in their charging behaviour.



Figure 5.1.1: Vehicles used on the dynamometer: Mitsubishi i-MiEV, Citroën C-Zero, Renault Twizy

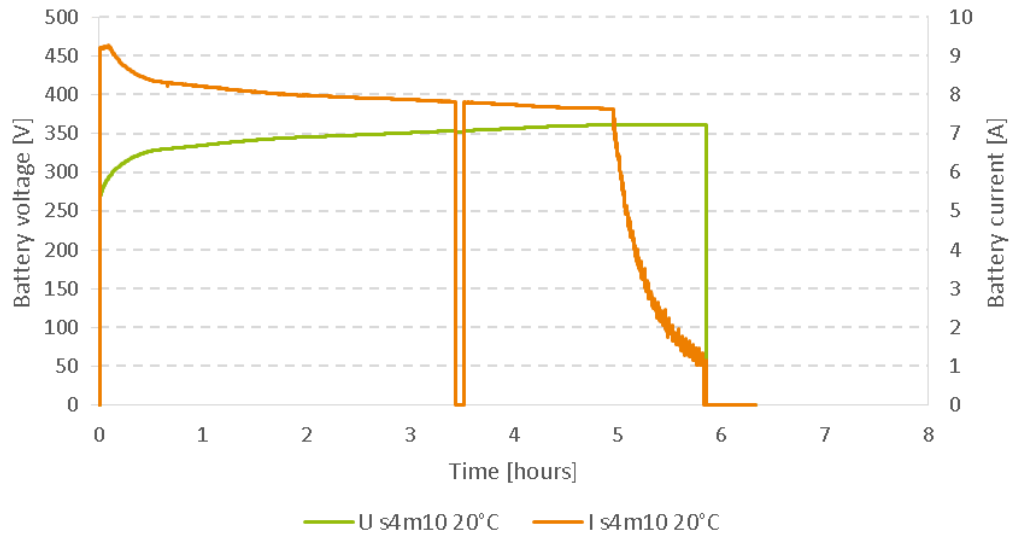


Figure 5.1.2: Exemplary HV-battery current and voltage of Mitsubishi i-MiEV during full charge (s4m10)

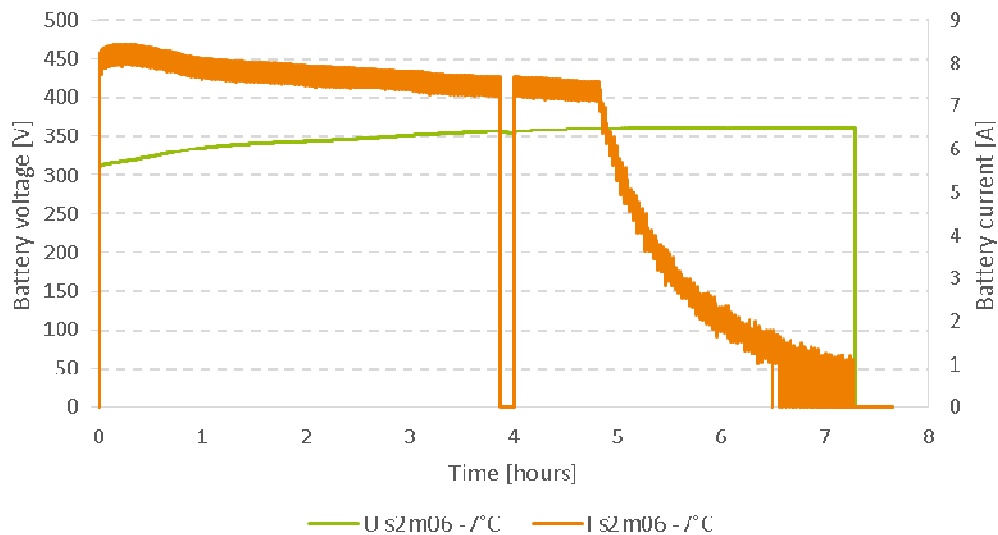


Figure 5.1.3: Exemplary HV-battery current and voltage of Citroën C-Zero during full charge (s2m06)

As seen in Figure 5.1.2, the Mitsubishi i-MiEV starts its charging procedure at a voltage of approx. 280 V and with a current peak of approx. 9 A. In contrast, the Citroën C-Zero, as depicted in Figure 5.1.3, starts at a higher voltage of approx. 300 V and with a slow ramp up of the current. After approx. 30 min of charging the voltage graphs of both vehicles align at approx. 330 V. The charging current of the Citroën C-Zero is pulsing from beginning to end, the charging current of the Mitsubishi i-MiEV is relatively smooth. Both vehicles have a single interruption of 5 to 10 min during each charging cycle. This break typically occurs after 3 to 4 hours of charging, in some cases more early after 1.5 hours of charging. During the

break the charging current drops to 0 A, while the HV-system remains active (i.e. there is still a high voltage measurable, the battery doesn't switch off).

At the end of a full charge the internal battery switches automatically open and voltage and current drop to zero. There is no energy flow after this cut-off point.

The charging behaviour is controlled by the on-board charging system¹³ and the battery management system (BMS)¹⁴. Therefore, different versions of these systems are the most likely reason for the differences in the charging behaviour.

5.1.2 Influence of temperature

The charging cycles of the Mitsubishi i-MiEV and the Citroën C-Zero were measured at three different environmental temperatures¹⁵:

- T = +35 °C
- T = +20 °C
- T = -7 °C

The internal energy distribution of the vehicle during these measurements is shown in Figure 5.1.4, sorted according to environmental temperature. The energy stored in the HV-battery and the LV-battery was measured with a power analyser, the energy at the external charging cable was measured with a power meter¹⁶.

¹³ The on-board charging system converts the alternate voltage of the grid to the direct voltage of the HV-battery.

¹⁴ The BMS is part of the HV-battery and supervises the state (temperature, voltage, etc) of the complete battery as well as the individual cells.

¹⁵ For organisational reasons it was often not possible to pre-condition the vehicle completely to the environmental temperature before start of the measurement. For this reason the internal temperature of the battery might be different than the environmental temperature. Furthermore during a charging cycle the battery may heat up. While the environmental temperature was controlled during measurements by a climate system, the internal battery temperature is not constant during the measurement.

¹⁶ Note: For measurements s1m12 and s2m11 only the external energy at the charging cable was recorded, for measurement s5m21 only the internal energies at the HV- and the LV-battery were recorded.

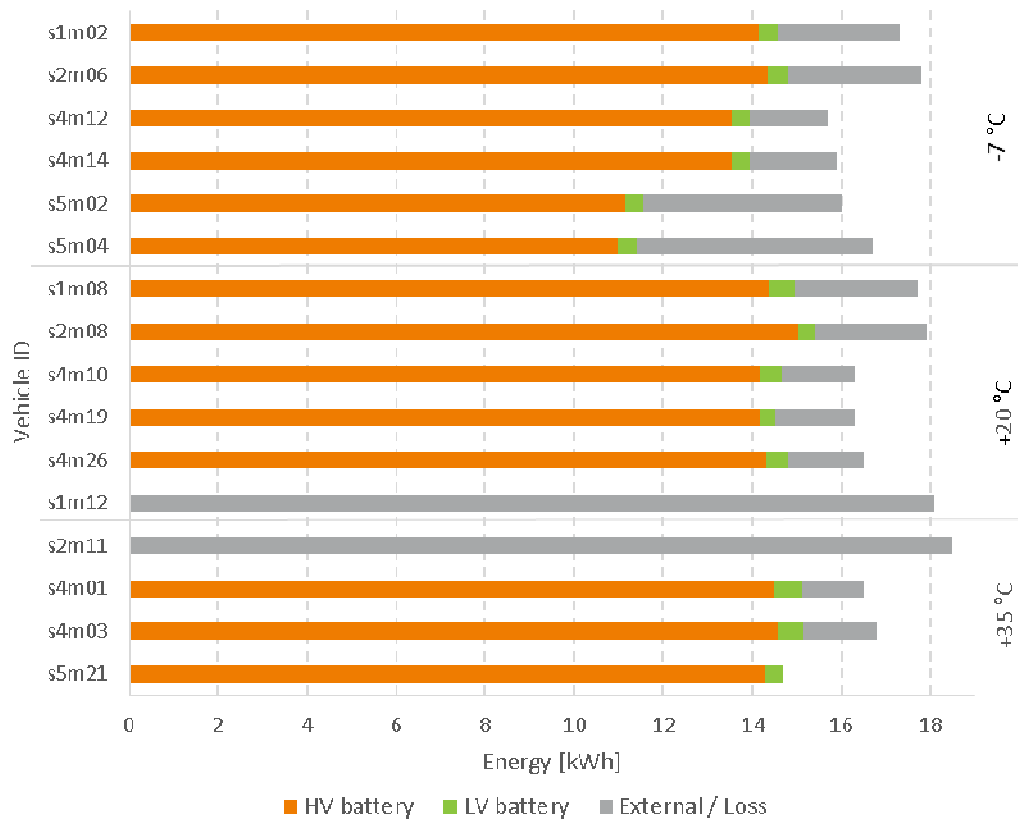


Figure 5.1.4: Total energy during full charge, sorted according to ambient temperature

A comparison of the external energy at the charging cable and the internal energies shows a substantial loss of more than 1 kWh during all measurements¹⁷. These losses occur in the on-board charger (AC/DC), which converts the AC of the grid to the DC of the HV-battery, and to a lesser extent in the DC/DC, which converts the high voltage of the HV-battery to the much lower voltage of the LV-battery.

Two measurements (s5m02 and s5m04) show exceptional high losses. These are measurements at an environmental temperature of -7 °C in 2014. It is possible that these are erroneous results based on a symmetrical measurement offset at the current clamp used to detect the current flowing to the HV-battery. Due to the integration of the results over a period of approximately 6 hours the error can be substantial.

The average results of the energy measurements for each environmental temperature are listed in Table 5.1 along with the average duration of the measurements.

¹⁷ Of course with the exception of measurements s1m12, s2m11 and s5m21, due to incomplete data.

| Measurements | Average energy at charging cable | Average energy at HV-battery | Average energy at LV-battery | Average duration of full charge | Total loss |
|--------------|----------------------------------|------------------------------|------------------------------|---------------------------------|------------|
| T = +35 °C | 17,48 kWh | 14,46 kWh | 0,52 kWh | 05:57:55 | 14.3% |
| T = +20 °C | 16,94 kWh | 14,41 kWh | 0,46 kWh | 05:59:20 | 12.2% |
| T = -7 °C | 16,57 kWh | 12,95 kWh | 0,43 kWh | 06:39:55 | 19.3% |
| all combined | 16,93 kWh | 13,80 kWh | 0,46 kWh | 06:16:26 | 15.8% |

Table 5.1: Average energy and duration of a full charging cycle based on environmental temperature

Comparing the average results for temperatures of +35 °C and +20 °C illustrates that roughly 0.5 kWh more were measured at the charging cable for the higher temperature. But the other results are very similar. This is an indication of a higher loss at the on-board charger, probably due to the necessity of added cooling.

For the measurements at -7 °C it can be seen that these took longer (on average approximately 40 min more than at the higher temperatures) and that less energy was stored by the HV-system. While this is true for the average energy at the charging cable as well as the average energy at the batteries, it is most obvious at the HV-battery: the average energy at -7 °C is 1.46 kWh below the average energy at +20 °C. Of course the average energy at -7 °C is heavily influenced by the two possibly erroneous measurements (s5m02 and s5m04) mentioned above, so it shouldn't be over-interpreted. Still there is an obvious trend to be seen.

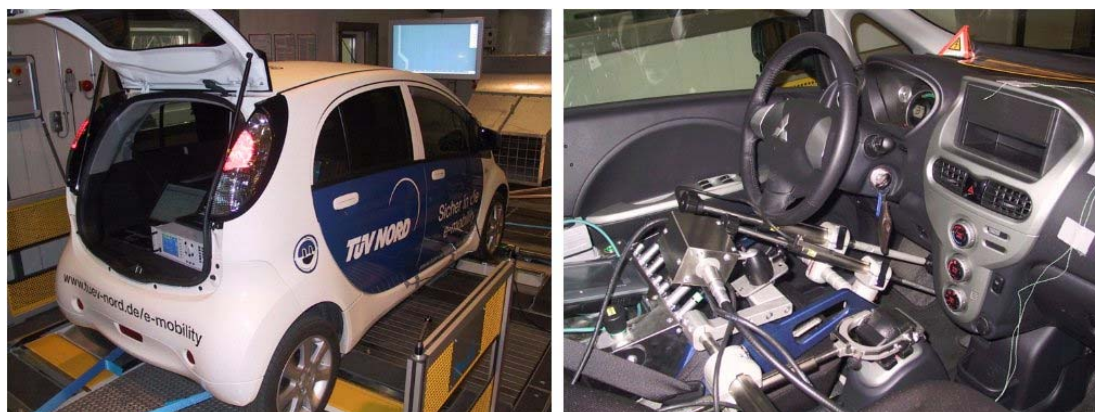


Figure 5.1.5: Mitsubishi i-MiEV on MAHA dynamometer in climate chamber; driving robot in Mitsubishi i-MiEV

5.1.3 Influence of aging

A comparison of the full charge measurement results in March 2012 to the results in November 2013 and March 2014 indicates no clear trend, if the two doubtful measurements are removed. There are some variations in the measurement results, but still Figure 5.1.6 show a clear trend. However, the results of the measurements at the HV-battery are not quite as clear.

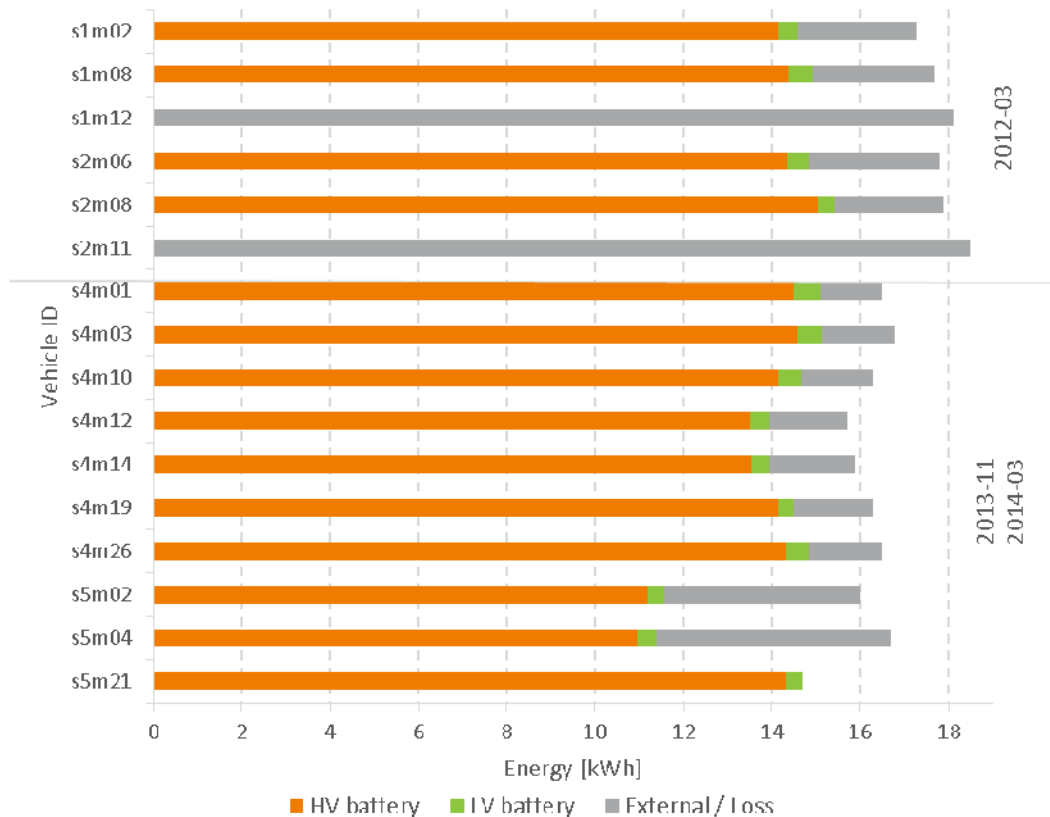


Figure 5.1.6: Total energy during full charge, sorted chronological

The average energies listed in Table 5.2 show a similar trend, but it should be noted that in 2013 and 2014 more full charge measurements at -7 °C were performed than in 2012, therefore the numerical results in the table are a little bit skewed and not quite as meaningful as it seems at first glance¹⁸.

¹⁸ Measurements s5m02 and s5m04 are included in the average for 2013/2014 and have a heavy influence regarding the low results for the HV-battery.

| Measurements | Average energy at charging cable | Average energy at HV-battery | Average energy at LV-battery | Average duration of full charge | Total loss |
|--------------|----------------------------------|------------------------------|------------------------------|---------------------------------|------------|
| in 2012 | 17,88 kWh | 14,48 kWh | 0,46 kWh | 06:39:01 | 16.4% |
| in 2013/2014 | 16,30 kWh | 13,52 kWh | 0,46 kWh | 06:07:24 | 14.2% |
| all combined | 16,93 kWh | 13,80 kWh | 0,46 kWh | 06:16:26 | 15.8% |

Table 5.2: Average energy and duration of a full charging cycle based on year

5.2 Analysis of influence of temperature and auxiliary loads on vehicle performance

The vehicle performance of Mitsubishi i-MiEV and Citroën C-Zero was measured by a couple of reach tests. This was done by driving NEDC cycles until the HV-battery was fully drained. This procedure is based on the official reach certification according to ECE-R 101. For comparison a single reach test (s4m25) using a WLTP variant¹⁹ was performed. The resulting reaches of the vehicles are shown in Figure 5.2.1.

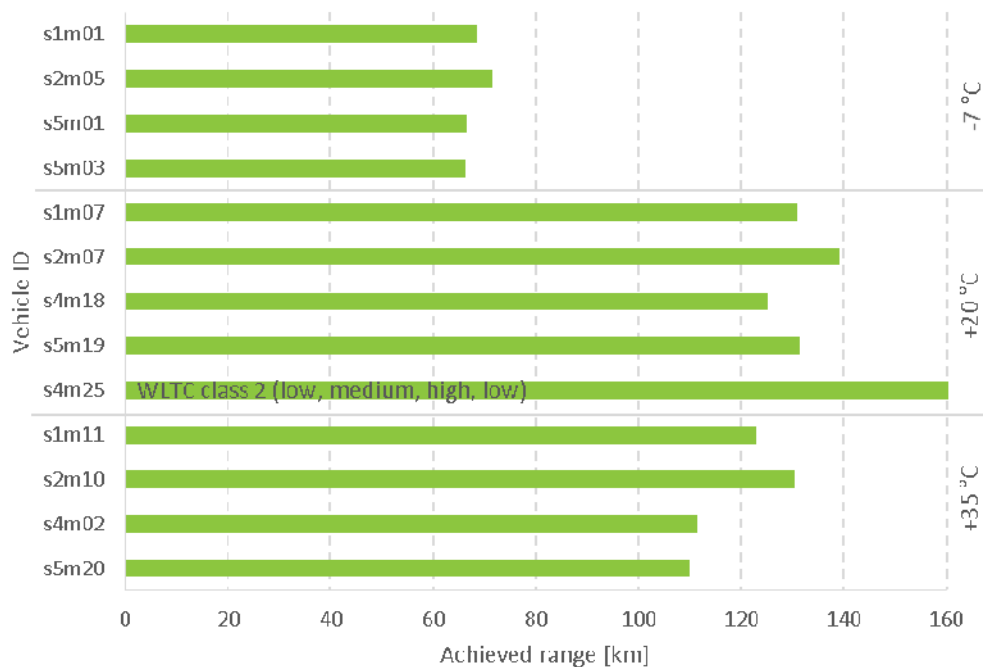


Figure 5.2.1: Range of vehicle starting with full HV-battery

¹⁹ The WLTP variant used a WLTC class 2 with four parts: low, medium, high, low.

The single WLTP measurement (s4m25) showed an obvious boost of more than 20 km to the vehicle reach. This can be explained by the relatively high share of low speed parts in the WLTP variant used.

It can be seen, that the temperature has a major influence on the vehicle performance. Especially at -7 °C the reach was significant lower than at higher temperatures.

A more in depth regard at the energy distribution, as seen in Figure 5.2.2 and Figure 5.2.3, reveals that the main influences regarding these results are the auxiliary loads²⁰, i.e. the heater and the air conditioning system. At -7 °C the heater used up nearly 40% of the available energy.

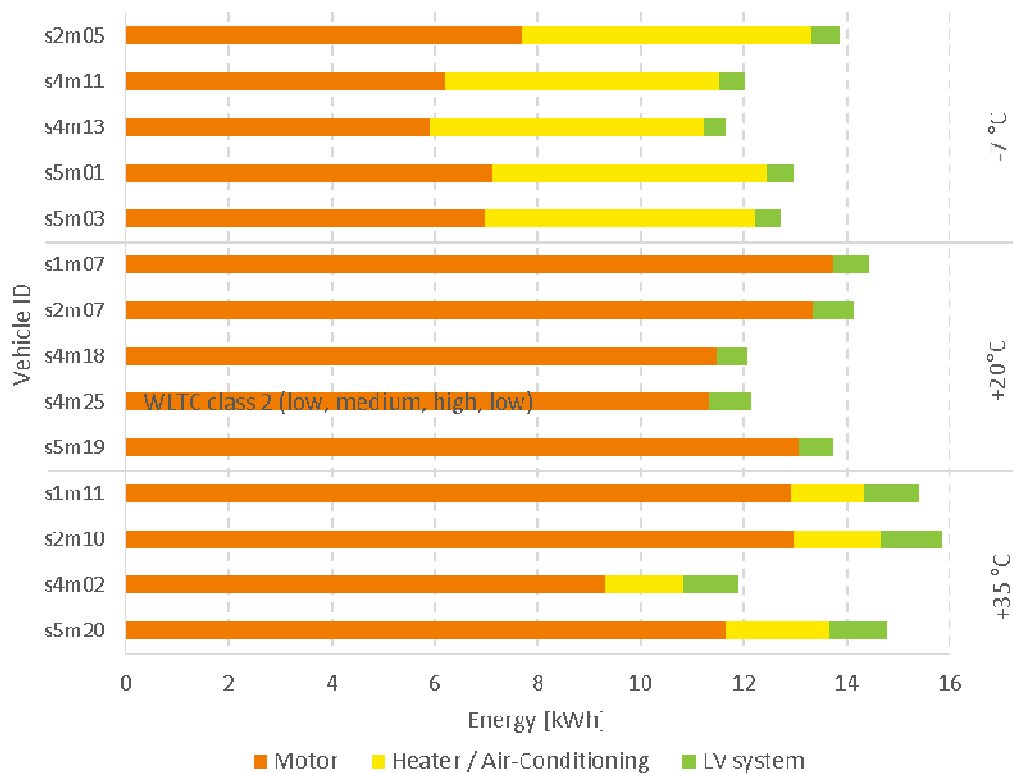


Figure 5.2.2: Energy distribution during range measurements (absolute values)

²⁰ The vehicles used for this test do not have an automatic climate control. The climate system can only be set to a fixed value. At an environmental temperature of -7°C the climate controls were set to maximal Warmth, at +35 °C they were set to minimal Cold, at +20 °C they were switched off. Thus the results represent a worst case scenario.

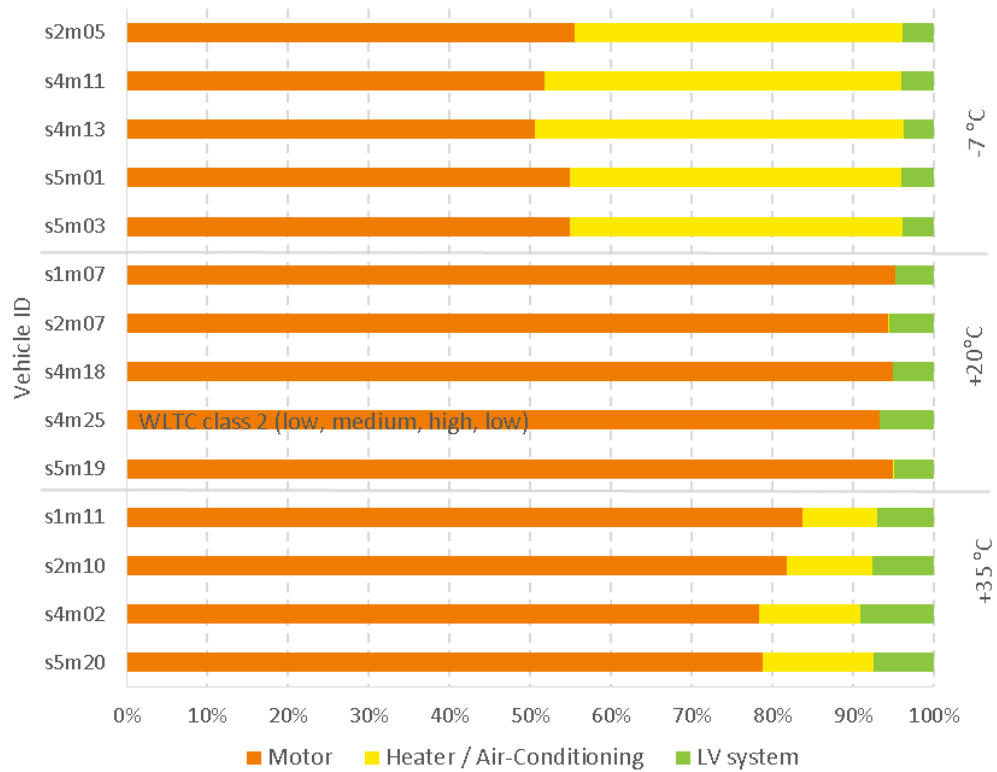


Figure 5.2.3: Energy distribution during range measurements (relative values)

To exclude the influence of the auxiliary loads the average energy consumption of the powertrain per 100 km can be calculated. Results are shown in Figure 5.2.4.

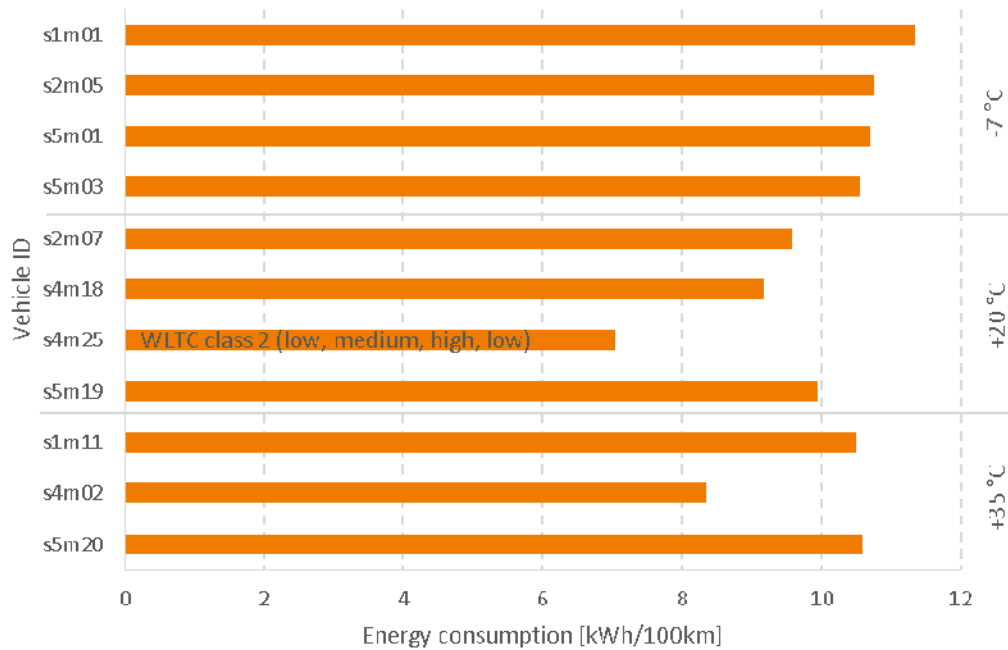


Figure 5.2.4: Average energy consumption during range tests

5.3 Validation of driving cycles

Different driving cycles were used during the measurements: NEDC, WLTC class 2, WLTC class 3 and SORDS. Of these the NEDC is the cycle used during official certification of range and energy consumption according to European regulations. The WLTC cycles are part of the World Light vehicles Test Procedures, currently under development. It is planned to replace the NEDC by the WLTP in the next years. The SORDS cycle was specifically designed for on-road testing and developed by DTI during the Green eMotion project.

In Table 5.3 average values as measured by the dynamometer system for the different driving cycles are listed.

| Cycle | Duration [s] | Distance [km] | Max. Speed [km/h] | Max. Force [N] | Max. Power [kW] |
|-------|--------------|---------------|-------------------|----------------|-----------------|
| NEDC | 1180 | 10,94 | 120,57 | 1469,90 | 31,42 |
| WLTC2 | 1800 | 22,66 | 123,19 | 1323,43 | 31,18 |
| WLTC3 | 1800 | 22,37 | 129,45 | 2165,55 | 37,77 |
| SORDS | 243 | 3,03 | 127,49 | 3465,92 | 46,53 |

Table 5.3: Average values measured by the dynamometer for different driving cycles

The kinetic energy measured by the dynamometer is listed in Table 5.4.

| Cycle | Mechanical energy [kWh/100km] | | |
|-------|-------------------------------|------------------------|-------|
| | Positive propulsion | Regenerative + braking | VLFC |
| NEDC | 10.70 | -2.65 | 8.05 |
| WLTC2 | 11.26 | -2.08 | 9.23 |
| WLTC3 | 13.02 | -2.98 | 10.05 |
| SORDS | 24.67 | -13.00 | 11.67 |

Table 5.4: Average mechanical energy measured by the dynamometer for different driving cycles

The positive propulsion energy shown in Table 5.4 is lowest for the NEDC. The positive propulsion energy is significantly higher during a WLTC (WLTC3 more so than WLTC2) and again much higher during a SORDS cycle.

However, in a SORDS cycle has also by far the highest share of energy used for braking. This energy can theoretically be recovered by electrical braking. The reason for the high energy consumption as well as the high share of braking energy for a SORDS cycle can be found in the dynamic acceleration and deceleration in the SORDS, as shown in Figure 5.3.1.

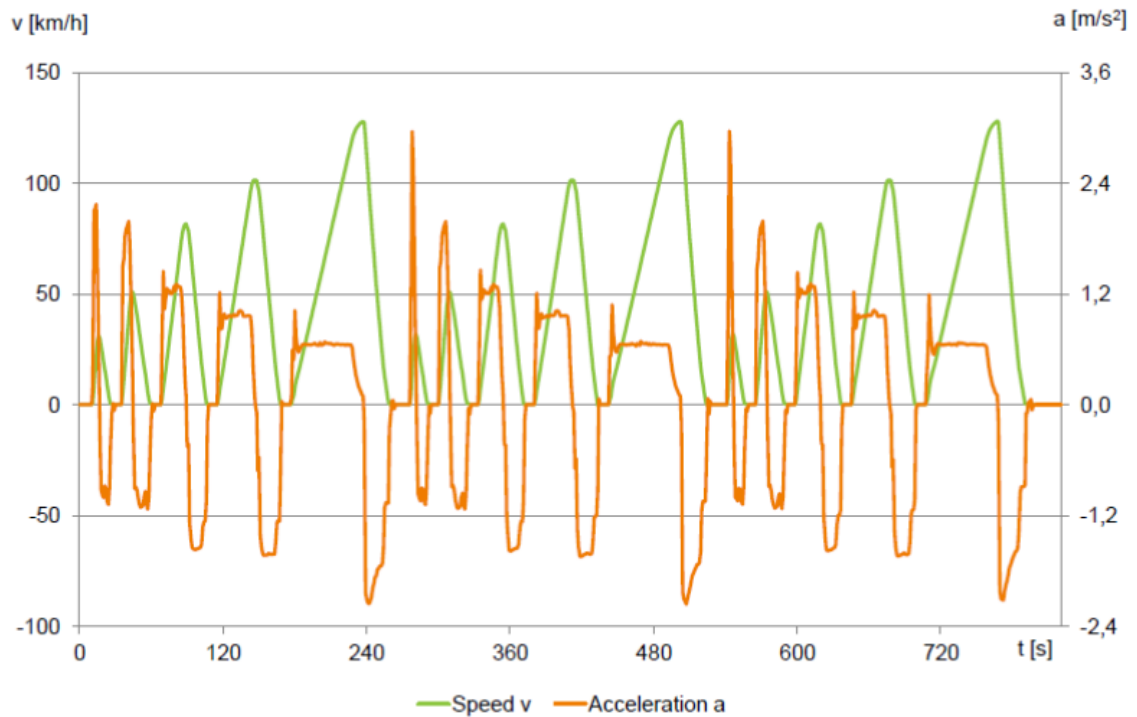


Figure 5.3.1: Speed and acceleration during three SORDS cycles (s1m09)

The high deceleration in a SORDS cycle can be problematic on a dynamometer. If only the rear axle is mounted on the dynamometer rolls, the brakes at this axle can be severely stressed.

5.4 Validation of CAN data

The measurements were performed with external test equipment (power analyser with current clamps) as well as by using internal sensor data transmitted via CAN.

Figure 5.4.1 shows a comparison of the internal and external measurements of the current at the HV-battery for a NEDC. Figure 5.4.2 gives a similar comparison for three SORDS-cycles and Figure 5.4.3 a similar comparison for a WLTC class 2. In Figure 5.4.4 a comparison for a full charge cycle is shown.

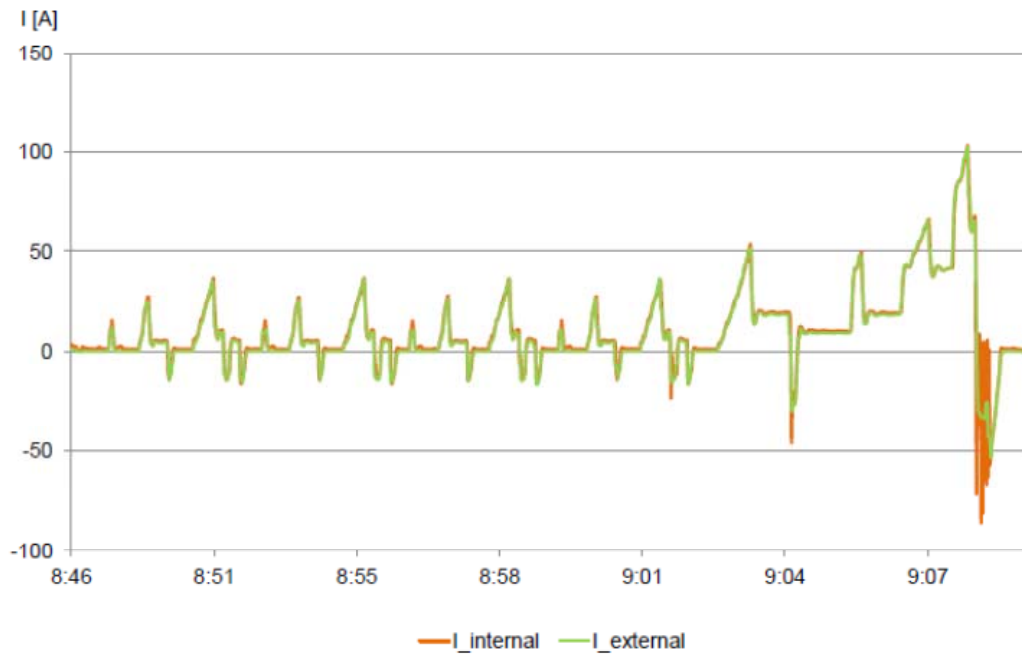


Figure 5.4.1: Comparison of internal and external measurements of current at HV-battery (NEDC, s4m21)

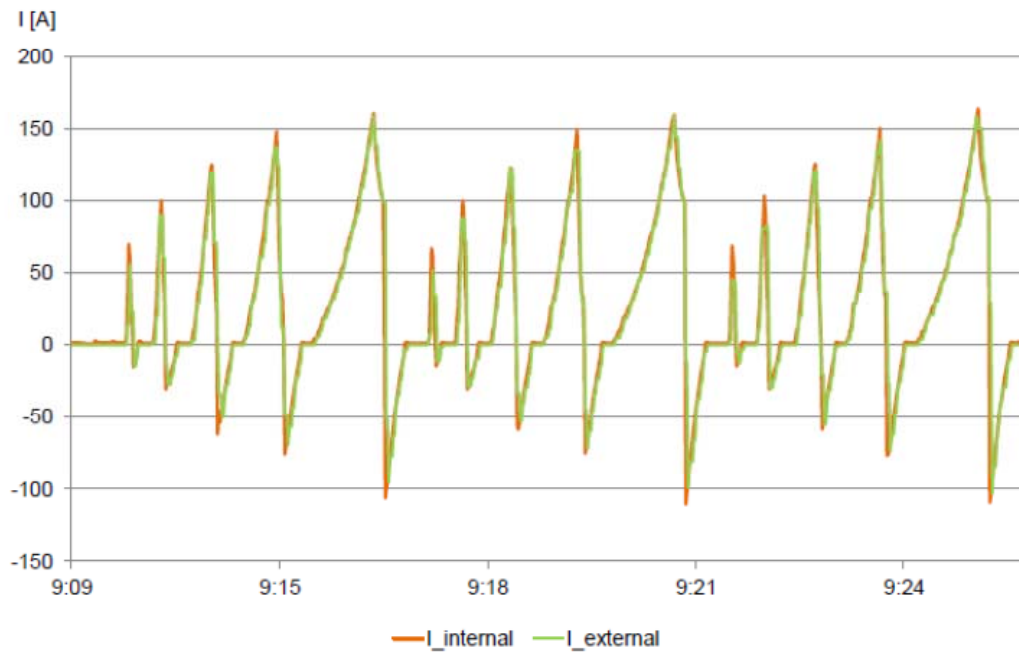


Figure 5.4.2: Comparison of internal and external measurements of current at HV-battery (SORDS, s4m22)

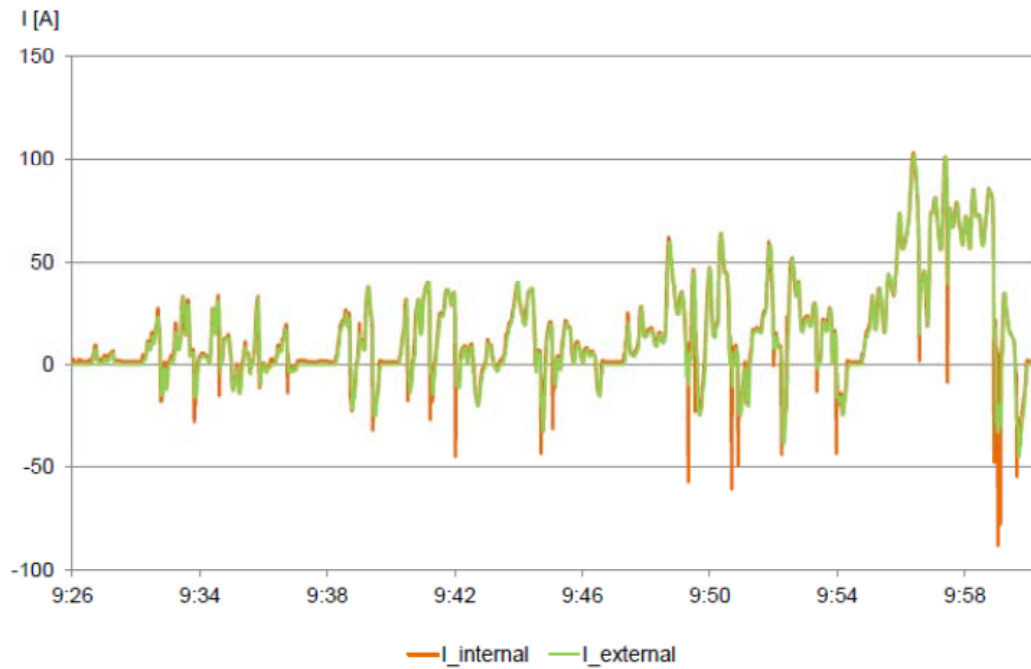


Figure 5.4.3: Comparison of internal and external measurements of current at HV-battery (WLTC2, s4m23)

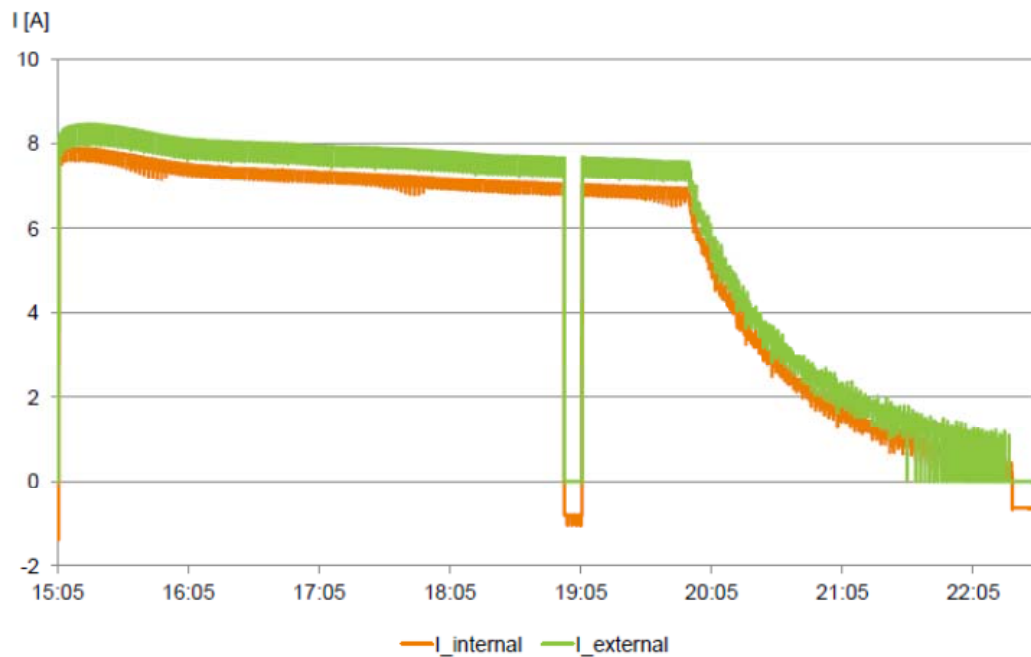


Figure 5.4.4: Comparison of internal and external measurements of current at HV-battery (full charge, s2m06)

The results for the internal and external measurements are very similar, but some differences can be shown:

- The internal data is more dynamic
- The internal data has a constant offset of approximately 0.5 A to 1.5 A (depending on vehicle and individual measurement setup)

The lower dynamic of the measurements with the power analyser can be explained by capacitive effects at the current clamps. They are not able to follow fast changes in the current at higher frequencies, e.g. those shown at the end of the NEDC in Figure 5.4.1.

One possible explanation for the constant offset, are additional internal loads in the HV-battery. For long going measurements (like a full charge) the offset can lead to a significant deviation for integrated values like charging energy. In the example in Figure 5.4.5, the offset results in a difference of approximately 1.5 kWh between internal and external measurements.

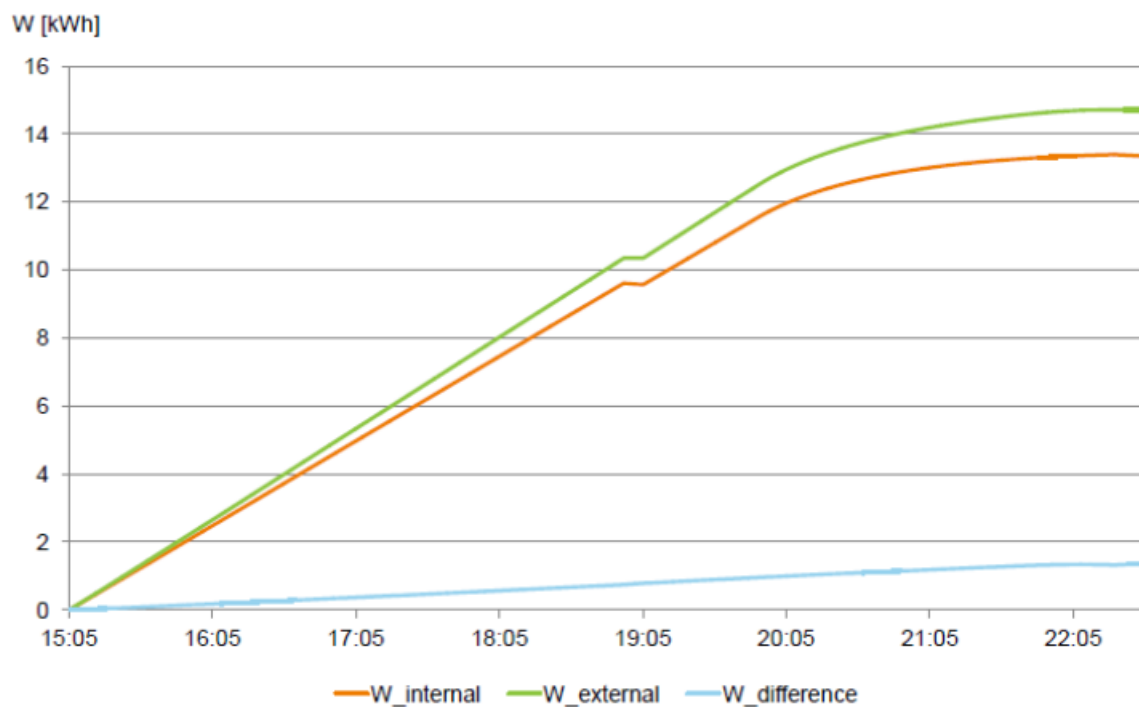


Figure 5.4.5: Integrated energy stored in HV-battery based on internal and external measurement data (full charge, s2m06)

5.5 Validation of SORDS measurements

SORDS measurements were performed in a laboratory on the dynamometer, as well as on-road on test tracks. The latter are already discussed in depth in chapter 0. It should be noted, that some of the basic test premises differ between the setups. The on-road tests are guided by a fixed layout of the test track. The actual acceleration, deceleration and in consequence the speed are variable. On the dynamometer the fixed parameters are the test time and the driving speed. Of course, in both setups there are tolerances for all measured values - in general these are more strictly enforced in a laboratory setup.

The laboratory tests showed that the SORDS cycles can be replicated on the dynamometer. As already discussed in section 5.3, the SORDS cycle requires very fast acceleration and deceleration in comparison to other cycles like NEDC and WLTC. If the dynamometer is configured just for the rear axle there is a real risk of brake damage during the test, because the rear brakes are not designed for the high load.

In Table 5.5 the average energy consumption in kWh/100km during a SORDS cycle in the laboratory on a dynamometer, at different environmental temperatures, is shown.

| Temperature | Average energy consumption in kWh/100km | | | |
|--------------|---|--------------------|-------------------------|--------------------------|
| | Kinetic (Wheels) | Electrical (Motor) | Electrical (HV-Battery) | Electrical (Auxiliaries) |
| T = +35 °C | 11,52 | 20,70 | 24,32 | 2,29 |
| T = +20 °C | 11,51 | 20,18 | 20,95 | 0,04 |
| T = -7 °C | 11,54 | 20,14 | 32,02 | 10,70 |
| all combined | 11,52 | 20,40 | 24,91 | 3,41 |

Table 5.5: Average energy consumption during SORDS at different environmental temperatures

| Temperature | True PABE | PABE (including auxiliaries) |
|-------------|-----------|------------------------------|
| T = +35 °C | 52.3% | 47.3% |
| T = +20 °C | 55.0% | 54.9% |
| T = -7 °C | 54.1% | 36.0% |

Table 5.6: Efficiencies based on the average energy consumptions in Table 5.5

It can be seen that the kinetic energy measured by the dynamometer and the electrical energy at the motor are not much influenced by environmental temperature. Of course the electrical energy used by the auxiliaries (i.e. heater and air conditioning) and in consequence the total electrical energy drawn from the HV-battery is strongly influenced by the settings of the climatic system. A comparison between kinetic (mechanical) energy at the wheels and the electrical energy at the motor shows an efficiency of the powertrain of approximately 57%.

A comparison of the consumption results of the dynamometer tests (Table 5.5) and the on-road tests (Figure 4.4.21) indicates roughly the same results for the Mitsubishi i-MiEV in regard to the electrical energy at the motor. As such the dynamometer tests can validate the on-road tests.

6 Technical conclusions

Hypothesis 1: Range and consumption are mainly dependent on drive pattern

Confirmed!

Driving style and speed explained approx. 80% of the energy consumption measured during the tests. Remaining factors, such as temperature and wind, account for the remaining 20%.

The driving tests show more than a 100% increase in energy consumption when driving the newly developed SORDS driving schedule on real tarmac (road) in cold weather, compared to the indoor NEDC test.

During steady driving the consumption increases significantly with speed, meanwhile during driving dynamically the consumption often decreases with average speed (as it is also known from city busses).

Use of the aggressiveness index shows, that there is linearity between the index and the energy consumption. High aggressiveness means high speeds and fast accelerations/decelerations.

Hypothesis 2: Range and consumption depend strongly on the use of auxiliaries

Confirmed!

Values from 0.4 to 2.5 kW were observed even without use of heat. Using heating would typically increase the auxiliary consumption by an additional 2-5 kW. It was not possible to switch off all power consumers such as steering and braking aids

At heavy urban driving the auxiliaries consume more than 50% of the total power drawn from the battery. When doing high speed highway driving this number is reduced to approximately 25%.

Hypothesis 3: SOH is predictable by step response testing

Confirmed!

Given Randle's circuit battery model (described in D6.1 and D9.8), the inner impedance of the EVs is estimated. The impedance estimate is based on the acquired EV voltage and current data, which makes possible to include EV data from previous years to compare progress in inner impedance throughout the whole vehicle lifecycle. The model can still be developed, but presently it has shown good accuracy in the allowed region of the EV battery voltage.

Hypothesis 4: Climate has significant impact on battery performance

Confirmed!

Both power and capacity of the batteries were up to spec in the weather conditions tested. However, in climate chamber at -7°C the charging losses were a significant part of the input energy. The battery OCV and internal impedance also change with temperature. However the effect is not permanent. Our observations furthermore indicate that some battery management systems have difficulties calculating correct state of charge in cold weather.

Hypothesis 5: Battery performance is almost unaffected by battery charge rate

Confirmed!!

The charge rates, even at fast charging, are small compared to driving. There was no performance loss of any importance after fast charging. Losses in the charger itself however, can be high.

Hypothesis 6: Heating and defrosting capacity is adequate

Confirmed!

The slowest vehicle heater took 8 minutes to heat the cabin up from 0°C until it passes comfort temperature (20 °C). This is within the normal for a traditional vehicle. Most of the vehicles were equipped with water-to-air heaters which are quite slow, but are accumulating heat energy, where direct-air heaters are much faster, but do only accumulate very little heat energy. The fastest heater took only 2 minutes to reach cabin comfort temperature.

Hypothesis 7: Regenerative braking adds significantly to vehicle range

Confirmed!

The vehicles were able to regenerate about 25% of the total propulsion energy exerted in the tests. This cuts the overall energy consumption by approximately 10%. A surprising fact is that larger electric motors actually saves energy by regenerating more strongly than smaller motors.

Hypothesis 8: Safety functions are maintained in the event of empty battery

Confirmed!

All necessary functions were available to the end. However, it was experienced that the battery indicator and warning light were seriously misleading on one older vehicle which died at 9% indicated SOC. This is

consistent with other observations that SOC indications from the dashboard can sometimes be misleading.

Hypothesis 9: Optimum regenerative braking relies on battery and motor parameters

Rejected!

Although some EV dashboards indicate “no regeneration” or similar right after charging no change could be detected in the driving tests. The vehicles seemed to regenerate quite normally after few seconds. We have found that a larger electric motor actually saved energy.

Hypothesis 10: Vehicle performance is almost unaffected by battery SOH

Confirmed!

Speed and acceleration were up to spec on all vehicles with mileages of up to 17,500 km. The marginally visible differences are within the tolerance taking the different drivers into consideration. Some vehicles even improved slightly with time. Even after four years of use no visible loss of capacity had occurred.

Hypothesis 11: Propulsion energy is largely unaffected by climate conditions

Confirmed!

The propulsion energy does only change very little with the climate. Overall the use of energy for heating is what really changes with the climate. It is significant whether a vehicle is driven in headwind or tailwind, headwind consumes more energy, though it is assumed the average wind consumption is a mix of both, but they never cancel each other.

7 Overall conclusions

Chapter 6 describes the technical conclusions as a result of the measurements performed. Within this chapter the more generic conclusions are described. The aim of the work in WP6 was to evaluate and assess the EV technology. With the work described in deliverable 6.1 (Methodology description) and the analysis of the results in this deliverable 6.2 the WP6 team has delivered an overall innovative concept to validate the EV technology. Comparison of dynamometer tests and realistic on road tests are a novelty and have been quite successful.

As overall conclusions we can identify the following major results;

- Development of a realistic outdoor driving cycle for EVs, suitable for both city and highway conditions.
- Development of a quite innovative technical process to get data out of a vehicle.
- Validation of realistic on road data with dynamometer tests.
- Realistic monitoring and analysis of climate impact on EVs
- Driving behaviour influence on EV performance

In addition to the last point, an overall conclusion of the WP6 is that EV technology can be validated on a technical level as performed in this WP6. However, the question if an EV is “good” or “bad” can’t be answered due to the fact that here the end-consumers wishes and boundary conditions are crucial for this statement.

As an overall conclusion, it can be stated that the WP6 has shown that EV technology is a sustainable technology. Component and vehicle development are at a high evolution level and could still make major development steps in the next years. The battery technology will probably reach a higher level in the near future and so have an influence on EV price/range.

The performance of an EV, from a technical point of view can be rated as good under the boundary conditions described for the validation of the different hypothesis.